DEVELOPMENT OF ELECTROSPUN TISSUE ENGINEERING SCAFFOLDS WITH TUNABLE PROPERTIES

A Dissertation

by

ROYA MICHELLE NEZARATI

Submitted to the Office of Graduate and Professional Studies of
Texas A&M University
in partial fulfillment of the requirements for the degree of

DOCTOR OF PHILOSOPHY

Chair of Committee,	Elizabeth Cosgriff-Hernandez
Committee Members,	Melissa Grunlan
	Michael Moreno
	Jun Kameoka
Head of Department,	Gerard Coté

August 2014

Major Subject: Biomedical Engineering

ABSTRACT

Each year millions of Americans receive grafts to replace and repair damaged tissue such as arteries or skin. Autografts are the current gold standard for treatment; however, synthetic grafts are a common alternative due to the limited availability of autografts. A biodegradable synthetic graft that temporarily replaces the function of the damaged tissue while promoting and directing neotissue formation would combine the availability of synthetic grafts with the healing properties of autografts. To achieve functional repair, the graft needs to have appropriate mechanical properties to restore tissue function and possess the necessary bioactivity to support cell growth and direct stem cell differentiation throughout remodeling. Electrospinning, a technique to fabricate fibrous polymer meshes, has the potential to provide the required control of scaffold properties through alteration of fiber morphology. The high tunability of electrospinning presents a facile method for controlling both mechanical properties and bioactivity of tissue engineering scaffolds; however, an improved understanding of fiber formation and modulation of fiber morphology through varying solution, processing, or environmental parameters is necessary for precise control of scaffold properties.

We have developed methods to tune scaffold mechanical properties and bioactivity through modulation of electrospun mesh microarchitecture and *in situ* gelatin crosslinking. First, we developed methods to improve mesh reproducibility by investigating the effects of environmental and solution parameters on fiber morphology. Segmented polyurethanes (SPUs) were utilized because they possess highly tunable

mechanical properties via alteration of segmental chemistry. We have elucidated structure-property relationships of SPUs and the effects of mesh microarchitecture on mechanical properties. This knowledge was used to fabricate a small diameter vascular graft (<4 mm) with mechanical properties similar to native vessels for improved clinical success. Next, we developed *in situ* crosslinked electrospun gelatin that provides bioactivity for enhanced cell viability and adhesion. This methodology was coupled with a biodegradable SPU into a co-electrospun mesh that combines the robust and tunable mechanical properties of synthetic polymers with the bioactivity of natural polymers. Overall, this work provides methodologies for fabricating electrospun scaffolds with tunable mechanical properties and bioactivity for tissue engineering applications.

DEDICATION

To my family and friends, for providing me with the never-ending love, faith, and support that has been instrumental to my success.

ACKNOWLEDGEMENTS

Moving to Texas and beginning the roller coaster ride that is graduate school was a huge step for me. Luckily, I have spent these last four years surrounded by some of the most supportive and encouraging people without whom I would not have been able to accomplish this monumental task. I would first like to thank my advisor, Dr. Elizabeth Cosgriff-Hernandez, for investing the time and effort towards developing my scientific and professional skills. I have grown so much as a researcher because she always pushed me to be better. I must also thank my committee members, Dr. Melissa Grunlan, Dr. Michael Moreno, and Dr. Jun Kameoka for providing a diverse perspective to improve the quality of my research. I would like to additionally thank Dr. Melissa Grunlan for the use of her differential scanning calorimeter.

Graduate school does not only test your knowledge and research ability, it also tests your confidence and perseverance. I have been extremely lucky to share this experience with some fantastic people who have helped through the good and the bad, for without them I would not have been able to complete this dissertation. It's rare to be able to refer to your labmates as first your friends, and I have been privileged with that opportunity. In no particular order, I would like to thank those of you I have had the pleasure of sharing a small office with: Jenny Robinson for all your efforts running cell studies on my materials and always lending your ear when I need to vent; Mary Beth Browning for being the second half of the vascular graft project and establishing the biomechanical testing protocols, and for getting pedicures with me when I need to de-

stress; Bobby Moglia for always be there for me, whether I needed help in the lab or someone to share funny pictures with; Dave Dempsey for establishing electrosinning in the lab and for being a kind and patient mentor since the first day I walked through the door; Tyler Touchet for synthesizing awesome polyurethanes for me to electrospin, and always being down for a beer and a puppy play date; Nick Sears for providing "nickineering" solutions that keep the lab running; and finally Alysha Kishan and Mike Whitely who I have only had the chance to get to know for a short time but have been extremely supportive in the last chapter of my PhD. I have also had the pleasure of mentoring some phenomenal undergraduate students, Michelle Eifert, Chris Radzicki, and Audrey Renfro, who have been an invaluable resource and have devoted significant time and energy towards the completion of these studies. Additionally, Brennan Bailey, Ruochong Fei, and Marc Rufin from the Grunlan lab have been great friends and colleagues.

I must earnestly thank Adam Smith, who despite the distance was always just a phone call away, for keeping me grounded and always providing a positive outlook throughout the challenges I have faced. I thank my immediate and extended family who have helped shape me into the person I am today. It has been a blessing to have aunts, uncles, cousins, and grandparents nearby throughout these past four years. Lastly, thank you to my parents, Moe and Dziep Nezarati and my brother, Amir, for the constant love and encouragement, which consequently has equipped me with the drive and confidence to always strive to achieve more.

TABLE OF CONTENTS

Page

LIST OF FIGURES

Page

LIST OF TABLES

Page

CHAPTER I

INTRODUCTION AND LITERATURE REVIEW

1.1. Tissue Engineering

Tissue engineering utilizes the body's ability to heal itself by implanting a 3-dimensional scaffold with bioactive factors and isolated cells into the site of damaged tissue. The scaffold restores tissue function while enabling neotissue formation. Rational scaffold design is critical to regeneration. First, material selection ensures the necessary mechanical properties of a given tissue can be met. Then, the material must be fabricated in a way that provides the necessary geometry and porosity for the defect. Finally, topographical or chemical bioactive cues can be incorporated to direct and control cell growth for improved healing. In this manner, tissue engineering scaffolds have been fabricated and investigated for a variety of applications.

1.2. Polymeric Biomaterials

1.2.1. Synthetic Polymers

Synthetic polymers are advantageous because they can be prepared with controlled physical and chemical properties. The degradation rate and mechanical properties can be easily tuned by altering the polymer chemistry[1] and they can be prepared in large quantities with less batch-to-batch variability than natural polymers. Common biodegradable synthetic polymers used in tissue engineering scaffolds are poly(L-lactic acid), poly(D,L-lactic acid), poly(L-lactic-co-glycolic acid) copolymers,

poly(glycolic acid), polycaprolactone, polyorthoester, and polyanhydrides. These polymers are biocompatible, degradable by hydrolysis, and are have been used in FDA approved devices.[2] Polyesters have been attractive for tissue engineering applications because of their ease of degradation by hydrolysis of the ester linkage into products that can be resorbed through metabolic pathways. By tuning polymer chemistry, degradation rates from months to years can be achieved.[3,4]

Poly(glycolic acid) (PGA) is a rigid thermoplastic with high crystallinity that is prepared by ring-opening polymerization. PGA is an attractive polymer for tissue engineering applications because its degradation product, glycolic acid, is a natural metabolite. PGA is commonly co-polymerized with poly(lactic acid) (PLA) to tune crystallinity, mechanical properties, and degradation rate. PLA is more hydrophobic and more resistant to hydrolytic attack than PGA.

Polycaprolactone (PCL) is a polyester synthesized by ring-opening polymerization of the cyclic monomer ε-caprolactone. PCL degrades at a rate much slower (2-3 years) than PLA and is useful for devices designed for long-term implantation.

Polyanhydrides are an extensively studied class of biodegradable polymers with excellent biocompatibility. These polymers degrade by surface erosion, making them ideal candidates for drug delivery applications. However, limited mechanical properties of these polymers have restricted their used to non-load bearing applications.

Polyurethanes have historically been used in non-degradable applications; however, polyurethanes that can degrade into nontoxic byproducts have recently been

developed. These polymers are advantageous due to their highly tunable mechanical properties owed to their segmented chemistry.[5-7] Segmented polyurethane elastomers have been utilized in a variety of biomedical applications over the past 40 years, typically long-term implants such as pacemaker leads and vascular grafts.[8-11] Segmented polyurethanes are synthesized by reacting a diol with a diisocyanate and chain extender. This reaction scheme creates a segmented block copolymer with a rigid hard segment and a flexible soft segment. Hydrogen bonding between hard segments acts as rigid net points that contribute to the high elastic recovery of polyurethanes, while strain induced crystallization of the hard segment contributes to their strength. Hard and soft segment chemistry can be rationally selected to further tailor material properties ranging from soft elastomers to rigid thermosets.[9,12-14] Polyurethanes' exceptional tunability has led them to be investigated for use in both soft and hard tissue engineering applications.

1.2.2. Natural Polymers

Protein-based polymers such as collagen, gelatin, silk fibroin, fibrin, and elastin are advantageous because they can mimic many features of the extracellular matrix and thus have the potential to direct the migration, growth, and organization of cells during regeneration. Their polymeric form allows them to be fabricated into many three dimensional scaffolds, including electrospun meshes. Properties of common natural polymers are discussed below.

Collagen is the major protein component of the extracellular matrix to provide support to connective tissues. It consists of three polypeptide chains in a triple helix and

interacts with cells to transduce essential signals for cell attachment, migration, proliferation, and differentiation. Collagen is derived from animal tissues and must be enzymatically treated to prevent immunogenicity which can alter the protein.[15]

Gelatin is a denatured form of collagen obtained by acid or alkaline processing of collagen. By utilizing different denaturing techniques (alkaline or acidic treatments), gelatins with a variety of isoelectric points can be obtained. Gelatin exhibits essentially the same common properties of rigid-chain synthetic polymers, which is not the case with collagen.

Silk is extremely strong, elastic and lightweight, but is it not possible to obtain in large quantities; therefore, attention has turned to silk fibroin, a mass-producible polymer produced by silkworms (*Bombyx mori*). Silks are attractive for tissue engineering due to their biocompatibility, slow degradability, and excellent mechanical properties.

Fibrin is a protein matrix produced from fibrinogen, which can be harvested from the patient, making it immunocompatible. Polymerized fibrin is a major component of blood clots and plays a key role in wound healing. Fibrin naturally contains sites for cell binding and has been used as a substrate for cell adhesion, spreading, migration, and proliferation.

Elastin is the dominant extracellular matrix protein found in the arterial wall and possesses great elasticity. It is also a regulator of smooth muscle cell activity and is important for preventing fibrocellular pathology.[16]

In addition, cells enzymatically degrade and remodel these materials, mostly eliminating the need to tailor the scaffold degradation rate. Crosslinking of natural polymers reduces the rate of tissue ingrowth; however, crosslinking is typically necessary due to the water solubility of natural polymers.[1] A critical drawback of natural polymers is batch-to-batch variation. One strategy investigated to overcome this issue utilizes recombinant protein technologies; however, it is difficult to mimic the post-translational modifications that occur naturally to give the proteins their unique structures.

1.3. Tissue Engineering Scaffolds

1.3.1. Scaffold Design

Tissue engineering scaffolds are implanted at the site of damaged tissue to replace tissue function and support neotissue formation. To fulfill these requirements, the scaffold must possess the necessary mechanical properties to restore function. It must support cell growth instead of triggering an immune response or fibrous encapsulation such that new tissue can grow. Porosity is important for cell infiltration as well as nutrient and waste transport, but must be balanced against the decreased mechanical strength associated with higher porosities. A large surface area is necessary such that a high number of cells, sufficient to replace or restore organ function, can be cultured. The degradation rate of the scaffold needs to match the rate of neotissue formation such that there is graded load transfer to the growing cells. Graded load transfer prevents catastrophic failure due to stress shielding and promotes mechanostimulation of the

tissue into the desired native structure. An additional design consideration is the incorporation of bioactive molecules into the polymeric scaffold.[2] The fabrication technique should not degrade or denature these materials and also allow for controllable delivery.

1.3.2. Scaffold Fabrication Techniques

1.3.2.1. Porogen Leaching

A porogen, typically salt, is dispersed in a polymer solution and cast into a mold or container of the desired scaffold dimensions. The solvent is then evaporated and the porogen leached out. For example, a polymer cast with salt porogens, the scaffold is immersed in water and the salt diffuses out. This technique can result in porosities up to 93% with an interconnected pore structure. Pore sizes are controllable by controlling porogen size and pores up to 500 μm have been fabricated. However, salt pores leave sharp corners that act as stress concentrators and lower the overall mechanical properties of the scaffold.

1.3.2.2. Gas Foaming

Pores are formed in a polymer matrix by introducing gas, typically CO_2, using chemical or physical means. Overall porosity of 94% with pore sizes from 100-500 μm can be achieved in this manner. This process is advantageous because it can be performed without the use of toxic solvents; however, a non-porous skin layer typically forms on the surface of the scaffold.

1.3.2.3. Thermally Induced Phase Separation

A polymer solution is cooled in a controlled manner to induce liquid-liquid phase separation. The bicontinuous polymer and solvent phases are quenched to create a two-phase solid. Freeze-drying removes the solidified solvent, leaving a porous polymer scaffold.

1.3.2.4. Hydrogels

Hydrogels are crosslinked polymer networks that swell up to 1000X their size in water. They are fabricated in water, eliminating the need for toxic solvents. Their highly hydrated state makes them advantageous in applications where a moist environment is necessary, such as skin regeneration or wound dressings. The interconnected polymer mesh allows for nutrient and waste transport, but the hydrogel mesh size is typically on the nanometer scale, inhibiting cellular infiltration. The mechanical properties are advantageous for soft tissue regeneration, but need more mechanical support for hard tissues.

1.3.2.5. Electrospinning

Electrospinning is a technique to generate fibrous scaffolds with high porosities, large surface area-to-volume ratios, and nano- to micron-sized fiber diameters. The relative ease of modulating fiber architecture provides a means to control scaffold properties. For example, fiber alignment and fiber diameter have been shown to influence mechanical properties, degradation rate, and cell behavior. In this manner, electrospun scaffold properties can be tailored to meet the specific design criteria of a wide range of tissues. Electrospun scaffolds are typically two dimensional, limiting their

application in space-filling applications. Modifications to the setup to create tubes have been made for vascular graft or nerve conduit applications.

1.4. Electrospinning

Electrospinning is a century-old process for producing nanofiber meshes, but not until the mid-1990s has the potential for this technique in many applications been realized and explored. Electrospinning involves pumping a polymer solution at a constant rate through a needle tip that is placed a set distance away from a grounded or oppositely charged collector. When a voltage is applied at the needle tip, the droplet forms a Taylor cone from which a liquid jet originates. The electrically charged jet undergoes a bending and whipping forces as it travels to the collector. This whipping process causes stretching and thinning into micro- and nanometer diameter fibers and facilitates solvent evaporation.[17] The fiber mesh can then be removed from the collector and utilized for various tissue engineering applications.

1.4.1. Taylor Cone Formation

Before charge is applied, the polymer solution is held at the end of an orifice (typically a blunted needle) by surface tension. When charge is applied, mutual charge repulsion creates a force directly opposite the surface tension and causes the hemispherical droplet to elongate into a conical shape called the Taylor cone.[18] When the applied electric field reaches a critical value, the force of electrostatic charge

repulsion overcomes that of surface tension and a charged jet is ejected from the tip of the Taylor cone.

1.4.2. Bending/Whipping Instability

The spinning jet travels in a straight light for a short distance after which it experiences a bending instability where it begins to whip in multiple expanding loops. This bending is observed as a conical shape with its vertex at the end of the straight segment, in which the jet is contained.[19] Whipping occurs after the onset of bending instability. It is during this stage that the fiber diameter decreases into the micron to nanometer range. Rapid solvent evaporation simultaneously occurs such that the jet succumbs to one or more fluid instabilities (axisymmetric or nonaxisymmetric) which distort the jet.[20-23] The most common mode of instability is the "whipping" mode which competes with droplet break up, the other main mode of instability.

A jet that operates in the whipping mode forms electrospun fibers whereas a jet that operates in droplet breakup mode forms electrosprayed droplets. Conditions under which a fluid will electrospin (whipping) or electrospray (droplet breakup) have been modeled.[24,25] At the onset of whipping, charge repulsion dominates over surface tension. Whipping dominates at high viscosity, low field strength, and low charge density. The surface tension force must be greater than the charge repulsion force to maintain whipping. Droplet breakup will dominate at low viscosity, high field strength, and high charge density.[26] Droplet breakup occurs when the force of charge repulsion is greater than the force of surface tension. Within the whipping mode, an increasing charge

repulsion force will result in decreased fiber diameter. Parameters such as viscosity or solvent boiling point (evaporation time) arise to arrest jet narrowing. In the absence of these, the jet will eventually breakup into droplets.[24]

1.4.3. Induced Molecular Orientation

Research has shown that the large elongational forces and high draw ratio involved in electrospinning can induce molecular orientation within individual fibers. Orientation is dependent on competing extensional forces and orientation relaxation which is dependent on the polymer. Consensus states that the molecular orientation is largely determined by the events occurring in the whipping region; however, it is difficult to study this region of the jet.[27] Conventional techniques to determine molecular orientation are ineffective for electrospun meshes because they require highly aligned fibers. As a result, techniques such as wide-angle X-ray diffraction (WAXD) and polarized infrared (IR) spectroscopy produce convoluted results that are a combination of fiber alignment and molecular orientation.[28,29] However, investigation of individual fibers using atomic force microscopy (AFM) and confocal Raman spectroscopy have revealed a high level of molecular orientation within electrospun fibers.[30]

A common feature of polymers that display molecular orientation is a high crystallinity and fast crystallization kinetics. As a result, orientation is likely driven by crystallization in which nuclei form and grow at a rate comparable to the electrospinning process.[31] These crystals hinder polymer chain relaxation after the elongational force has been removed, resulting in a sustained orientation after removal from the collector. For

completely amorphous polymers, molecular orientation is dependent on T_g. A polymer with a higher T_g would better preserve molecular orientation due to decreased chain mobility. Molecular orientation has been shown to increase the modulus and tensile strength of the resultant electrospun mesh.[31,32]

1.4.4. Effects of Modulating Electrospinning Parameters

The fiber morphology and diameter are dependent on a number of processing parameters that are typically divided into the intrinsic properties of the solution (e.g. polymer, concentration, conductivity, polarity and surface tension of the solvent) and the operational conditions (e.g. strength of the applied electric field, distance to the collector, flow rate). An understanding of electrospun fiber formation and modulation of fiber morphology is necessary for precise control of scaffold properties. To this end, systematic studies have examined the roles of various processing and solution parameters on fiber morphology, **Table 1.1**.

Table 1.1. Effects of processing and solutions parameters on electrospun fiber morphology

Processing parameters	***Effect on fiber morphology***
Applied voltage	Increasing applied voltage can result in: • increased beading[33-37] • decreased fiber diameter[35,38-41]
Distance to collector	Increasing distance to collector can result in: • decreased fiber diameter[41,42] • decreased fiber wetness[39,40]
Flow rate	Increasing flow rate can result in: • increased fiber wetness[43] • increased bead formation[36,42-46]
Solution parameters	
Polymer molecular weight	Increasing molecular weight can result in decreased beading[35,47-49]
Polymer concentration	Increasing concentration can result in: • decreased beading[34-36,38-44,48-60] • increased fiber diameter[34,37,44,47,48,50-53,56,58,61,62]
Solution conductivity	Increasing conductivity through the addition of salt can result in: • defect-free fibers[33,45,55,63] • smaller diameter fibers[50,52]
Solvent dielectric constant	Increasing dielectric constant can result in decreased bead formation[46,54,64]

1.4.4.1. Processing Parameters

1.4.4.1.1. Distance

The distance from needle tip to collector will determine the flight time for the jet. A greater flight time will cause the jet to remain longer in the whipping mode and allow for more time for solvent evaporation. Increasing distance to collector can result in decreased fiber diameter and decreased wetness.

1.4.4.1.2. Voltage

The applied voltage will alter both the electrostatic charge repulsion force and the overall electric field from the needle to the collector. Increasing applied voltage can result in increased beading and decreased fiber diameter.

1.4.4.1.3. Flow Rate

Flow rate can easily be altered on the syringe pump or other pump system being used to inject the polymer solution. Flow rate can change the size of the droplet suspended at the end of the needle tip. Increasing flow rate can result in increased fiber wetness and increased bead formation.

1.4.4.2. Solution Parameters

1.4.4.2.1. Viscosity/Concentration

The electrospinning solution must be viscous enough such that the viscous force balances out the competing electrostatic repulsion force to form fibers instead of droplets.[20] Viscosity is directly related to the solution concentration. A critical entanglement concentration has been identified that defines the lowest concentration a given solution must reach to create enough chain entanglements to maintain a fiber instead of droplets. Increasing viscosity/concentration can result in decreased beading. At the point where the viscous force is much greater than the force of electrostatic charge repulsion, fiber diameter increases.

1.4.4.2.2. Polymer Molecular Weight

The critical entanglement concentration is dependent upon polymer molecular weight. As a result, increasing molecular weight independent of other variables can result in decreased beading.

1.4.4.2.3. Conductivity

The solution conductivity is mainly dictated by the choice of solvent. Additional methods to control conductivity are through the addition of salts or through utilizing a conductive polymer. Increasing solution conductivity can result in defect-free fibers and smaller diameter fibers.

1.4.4.2.4. Dielectric Constant

Dielectric constant describes the solvent properties. It is a measure of a material's ability to polarize in response to an applied electric field. Increasing dielectric constant can result in decreased bead formation.

1.4.4.3. Environmental Parameters

1.4.4.3.1. Humidity

High humidity conditions can lead to the formation of surface pores on the fibers due to thermally induced phase separation (TIPS) or vapor induced phase separation (VIPS). TIPS is generally associated with a hydrophobic polymer dissolved in a water miscible and highly volatile solvent. In this process, rapid evaporation of the solvent creates local decreases in temperature at the surface of the jet that results in water vapor condensation.[65-69] These water droplets are trapped on the skin layer and create circular

indentations. After the fiber solidifies and the water droplets evaporate, surface pores are created in the form of breath figures.[70,71] Pores formed through TIPS are typically circular since the pores are molded by solvent droplets. Typically, a hydrophobic polymer, high volatility solvent, and a water miscible solvent are necessary to facilitate VIPS. First, water vapor is absorbed into the jet due to the water miscible solvent. Phase separation occurs as the hydrophobic polymer precipitates out of the solution when water is introduced, creating polymer-rich and polymer-poor regions within the jet. Finally, rapid evaporation of the highly volatile solvent locks in the phase separated geometry, resulting in fibers with surface pores. Pores created by VIPS are typically irregularly shaped, as has been documented in the literature.

1.4.4.3.2 Temperature

It can be difficult to predict the effect of temperature on electrospun fiber morphology because it has an indirect effect. One must individually evaluate the dependence of solution density, vapor diffusivity, viscosity, relaxation time, and solvent evaporation rate on temperature. Increasing temperature causes faster solvent evaporation and decreased viscosity. For poly(vinylpyrrolidone) and cellulose acetate in ethanol solutions, increasing temperature resulted in an increased fiber diameter.[66] In the case where temperature has a greater effect on viscosity than solvent evaporation rate, a decreased fiber diameter was observed.[72]

1.4.5. Setup Modifications

1.4.5.1. Coaxial Electrospinning

Coaxial or core-shell electrospinning has been developed in the past ten years.[73,74] Two separate polymer solutions are fed into a coaxial needle or to concentrically arranged needles. A compound droplet at the end of such needle will undergo transformation into a compound Taylor cone with a compound jet electrospun from its tip. The compound jet will be stretched and whipped while concurrent solvent evaporation occurs, similarly to the traditional setup.[75] The electrospinning process is expected to be fast enough to prevent any mixing of the core and shell polymers, as well as any compounds contained in them.[73] This technique typically results in a relatively smooth core-shell interface; however, the interface was perturbed in some cases due to an onset of bending instability.[28,73,76] Coaxial electrospinning is especially beneficial for materials that will not form fibers by themselves. They can be contained in the fiber core by a polymer shell.[73] The thickness of the core and shell can be adjusted by the feed rate of the inner dope.[76] Zhang, et al. investigated methods to control the thickness of the shell by varying the concentration of the inner dope while maintaining a fixed concentration of the outer dope.[77] Increasing the inner dope concentration increased both the core size and the overall fiber diameter. Ratio of the inner diameter to outer diameter also increased.[77] Increasing inner flow rate increased fiber diameter and allowed for greater drug loading.[78] This method of drug loaded resulted in a more sustained release than a fiber blend.[78-80] Potential applications of core-shell nanofibers include preserving an unstable biological agent from an aggressive environment, preventing decomposition

of a labile compound under a certain condition, delivering a biomolecular drug in a sustained way, and functionalizing the surface of nanostructures without affecting the core material.[77] Alternately, core-shell fibers have been fabricated by electrospinning of an immiscible blend of polymers.[81] Hollow nanotubes have been fabricated through selected removal of the core.[75,77,82]

1.4.5.2. Co-electrospinning

Co-electrospinning by simultaneously spinning from multiple nozzles onto the same collector is a technique to fabricate composite scaffolds.[83,84] As many as four electrospinning jets have been performed simultaneously.[85] Electrospinning from many jets is advantageous because it is a relatively simple setup modification and allows for fiber mixtures of different materials at a desired ratio; however, interference between the electrospinning jet can be a challenge.[86] Jets must be placed far enough away to avoid interference, so translating collectors have been used to form a homogenous fiber mixture.[87] This can be utilized to create gradients from offset spinnerets.[83] Gradients can be beneficial for regeneration at the osteochondral interface where a graded transition of mechanical properties is desired. In another approach, co-electrospinning of PCL and water-soluble PEO was utilized such that the PEO could be dissolved post-fabrication to increase mesh pore size and increase cell infiltration.[84] This technique is also useful in situation where it is difficult to form a solution containing both polymers.[85] The mechanical properties of the scaffold can be controlled by modulating the weight ratio of each material in the final mesh.[85]

1.4.5.3. Patterning

Controlled deposition of electrospun fibers into patterns has been demonstrated by altering collector geometry. Aligned fibers have been achieved by electrospinning onto a rotating mandrel that pulls fibers into the direction of rotation.[29,46] An alternate method is to use two parallel grounded collectors with a gap between them and fibers will align between the two collectors due to mutual attraction to both.[88] A grid patterned collector fabricated through soft lithography has been used to align fibers along gridlines.[89]

1.5. Effects of Mesh Microarchitecture

1.5.1. Mechanical Properties

Aligned fibers increase the modulus and tensile strength compared to randomly oriented fibers, when stressed in the direction of alignment. For aligned polyurethane fibers, modulus increased from 540 to 2500 kPa and ultimate tensile strength increased from 1130 to 3520 kPa; however, ultimate elongation remained the same.[90] Larger fiber diameter increases tensile modulus of the mesh. PLGA fibers with diameters ranging from 150-6000 nm had tensile moduli ranging from 39.2-79.2 MPa, respectively. Porosity also increased from 38 to 60% due to the decreased packing efficiency of larger fibers.[91] Increasing fiber junction density within poly(ester urethane)urea scaffolds resulted in a lower bending moduli.[92] Other studies show that as the number of rigidly bonded fiber-fiber junctions increase, modulus increases.[93] Greater fiber intersection density also resulted in increased ultimate elongation in the circumferential axis, but no

change in the longitudinal axis.[94] Stella, et al. investigated the effects of strain on fiber morphology. Fibers were pulled into alignment with applied strain and at high strain levels, there was an upper bound of fiber alignment observed, corresponding to a transition from tortuous fibers to a web-like architecture with straight, interconnected fibers. When unloaded, the fibers returned to their original geometry.[95]

1.5.2. Cell Growth/Differentiation

Cell behavior can be controlled via contact guidance of the electropun fibers. This is important for mimicking the complex and hierarchical structure of many tissues. The ability to control the structure of the cells via topography can aid in the regeneration of functional tissues. Aligned fibers have been utilized to control cell growth. In neural tissue engineering, elongated cells are desired. Schwann cells cultured on aligned fiber scaffolds orient in the direction of the fibers due to contact guidance. The nucleus and focal adhesion molecule vinculin also orient with the fiber direction. Proliferation was significantly greater than on random meshes.[96,97] The advantage of these aligned Schwann cells is the enhancement in the rate and extent of neurite elongation from dorsal root ganglia cultured on these aligned cells.[97,98] Additionally, these topographic cues were shown to direct Schwann cells towards the pro-myelinating state, evidenced by the markers for myelin-specific genes MAG, P0, MBP, and PMP22.[97] Fiber alignment has also been investigated for the regeneration of the anterior cruciate ligament. The generation of extracellular matrix by human ligament fibroblasts (HLF) was investigated. Significantly more collagen was synthesized on aligned nanofiber

sheets.[90] Spindle-shaped, oriented cells with morphology similar to ligament fibroblasts *in vivo* were cultured on the aligned surfaces. Fiber diameter can affect cell growth. The effect of fiber diameter on spreading, proliferation, and differentiation of osteoblastic cells on electrospun PLA was investigated by Badami et al. A greater cell density was observed on 2.1 μm fibers compared to 0.14 μm fibers.[99]

1.5.3. Degradation Rate

Scaffold degradation rate can be tailored by altering the fiber morphology of electrospun grafts. Compared to neat films, electrospun fibers have a faster degradation rate due to the porosity and high surface area-to-volume ratio. Fiber diameter has been shown to significantly influence both in vitro and in vivo degradation (in rats).[100] Post-draw and thermal treatments on electrospun poly(glycolide-co-lactide) electrospun meshes were utilized to tailor degradation and mechanical properties. Post-drawn and annealed membranes exhibited a slower initial degradation rate but a faster rate after two weeks compared to as-spun membranes.[101] Tunable degradation in electrospun fibers is particularly important for drug delivery via surface erosion of the fibers. Larger diameter fibers have a longer period of nearly zero order release.[102]

1.6. Electrospun Tissue Engineering Scaffolds

1.6.1. Vascular Graft

Cardiovascular disease, specifically coronary artery disease resulting from arteriosclerosis, is one of the leading causes of death in the United States. A clinically

useful small diameter vascular graft must match the mechanical and structure properties of native vessels and the microenvironment must be optimized to foster cell adhesion and growth. An ideal graft matches the compliance of the native vessel while maintaining sufficiently high burst pressure. Electrospun meshes have been shown to have a lower modulus than solution cast films, which is advantageous because low modulus has been correlated to higher compliance.[103] Biodegradable electrospun vascular grafts made of poly(ester urethane) urea (PEUU) have been fabricated with 300% elongation, 7-10 MPa tensile strength, and compliance values of 2.9-4.4 x 10^{-4} $mmHg^{-1}$. These grafts remained patent for 8 weeks in vivo and formed a thin neo-intimal layer.[104] Electrospun blends of elastin and collagen have been fabricated to mimic the structure and chemistry of native vessels.[105] Stankus, et al. developed a method to simultaneously electrospin PEUU and electrospray smooth muscle cells onto a rotating mandrel to have greater cell infiltration in the vascular graft. The amount of viable cells was greater than static culture controls (2.4X more). In addition, static compliance of 1.6 x 10^{-3} $mmHg^{-1}$, dynamic compliance of 8.7 x 10^{-3} $mmHg^{-1}$, and burst pressure of 1750 mmHg were achieved.[106]

1.6.2. Nerve Guidance Channel

Large nerve gaps require a graft to bridge the proximal and distal ends of the severed nerve. Tubular constructs with uniaxially aligned topographical cues are necessary to promote axonal regrowth due to the lack of a fibrin cable. Tubular electrospun scaffolds are advantageous as nerve guidance channels to aid regeneration of

peripheral nerve over large gaps (3-10 mm). Half of rats implanted with an electrospun PLGA nerve conduit showed successful nerve regeneration after one month.[107] Plasma treatment of PCL scaffolds showed a 17% increase in Schwann cell proliferation over PCL/collagen scaffolds.[108] Successful nerve regeneration requires control over Schwann cell growth in order to form synapses and functional tissue. Aligned fibers formed via electrospinning have shown great potential for culturing nerve cells, described in section 3.2. Aligned fibers can guide neurite outgrowth from the proximal to distal end of the nerve in the absence of a fibrin cable and have been shown to significantly influence the adhesion and proliferation of Schwann cells.[96,109]

1.6.3. Skin

Wounds with excess skin loss require immediate coverage to protect the wound. An ideal dressing would protect the injury from loss of fluid and proteins, enable the removal of exudates, inhibit microorganism invasion, and reduce scar tissue formation.[110,111] Electrospun grafts can reduce post-surgical adhesion that is a major challenge in conventional bandages.[91] Electrospun collagen skin substitutes had excellent stratification with a continuous layer of basal keratinocytes *in vitro*, and 100% engraftment *in vivo*. Compared to freeze-dried scaffolds, electrospun collagen reduced wound contraction for better healing.[112] Electrospun synthetic polymers can be blended with natural polymers or hydrophilic PEO to improve surface wettability to improve cellular response at the wound site.[113]

1.6.4. Bone

Electrospun scaffolds can mimic bone extracellular matrix which is composed mainly of hydroxyapatite within a collagen type I framework. Additionally, the ease of incorporation organic and inorganic natural materials makes this technique beneficial for delivery of bioactive factors. Many researchers have investigated electrospun collagen with added hydroxyapatite to mimic the structure of bone ECM.[114-116] Alternatively, hydroxyapatite can be deposited onto the fibers after fabrication.[117] Bone morphogenetic protein 2 (BMP-2) added to silk fibroin fibers supported higher calcium deposition and enhanced transcript levels of bone-specific markers in human mesenchymal stem cells (hMSCs).[118] The effect of fiber diameter and porosity on osteogenic differentiation of MSCs has been investigated and it was found that larger fibers (which also result in higher porosity meshes) increase MSC proliferation and alkaline phosphatase (ALP) activity.[119,120]

1.7. Summary and Future Directions

A biodegradable synthetic graft that temporarily replaces the function of the damaged tissue while promoting and directing neotissue formation would combine the availability of synthetic grafts with the healing properties of autografts. To achieve functional repair, the graft needs to have appropriate mechanical properties to restore tissue function and possess the necessary bioactivity to support cell growth and direct stem cell differentiation throughout remodeling. Electrospinning, a technique to fabricate fibrous polymer meshes, has the potential to provide the required control of scaffold

properties through alteration of fiber morphology. The high tunability of electrospinning via processing, solution, or environmental parameters presents a facile method for controlling both mechanical properties and bioactivity of tissue engineering scaffolds. The relative ease of modulating fiber architecture provides a means to control scaffold properties. For example, fiber alignment and fiber diameter have been shown to influence mechanical properties, degradation rate, and cell behavior. In this manner, electrospun scaffold properties can be tailored to meet the specific design criteria of a wide range of tissues. Due in part to this tunability, electrospun scaffolds have been investigated for regeneration of vasculature, nerve, skin, and bone. An understanding of electrospun fiber formation and modulation of fiber morphology is necessary for precise control of scaffold properties. Using this knowledge of fiber formation, we can develop methods to tune scaffold mechanical properties and bioactivity through modulation of electrospun mesh microarchitecture and material chemistry.

CHAPTER II

EFFECTS OF HUMIDITY AND SOLUTION VISCOSITY ON ELECTROSPUN FIBER MORPHOLOGY*

2.1. Introduction

Tissue engineering aims to provide a temporary matrix and appropriate cues to facilitate regeneration of damaged tissue. To achieve functional repair, the biomaterial scaffold needs to have appropriate mechanical properties to restore function to the damaged tissue while supporting cell growth throughout remodeling. In addition to material chemistry, the 3D microarchitecture of the scaffold plays a large role in graft properties and cell behavior. Given that the fabrication technique dictates this microarchitecture, enormous efforts have been made to develop strategies that are both highly tunable and exhibit fine control of the resulting architecture. Electrospinning has gained popularity in recent years as a technique to generate fibrous scaffolds with high porosities, large surface area-to-volume ratios, and nano- to micron-sized fiber diameters.[17,24,121,122] The relative ease of modulating fiber architecture provides a means to control scaffold properties. For example, fiber alignment and fiber diameter have been shown to influence mechanical properties,[31,123,124] degradation rate,[100,125] and cell growth.[97,100,126-129] Thus, electrospun scaffold properties can be tailored to meet the specific design criteria of a wide range of tissues. Due in part to this tunability,

*Reprinted with permission from "Effects of Humidity and Solution Viscosity on Electrospun Fiber Morphology," by Roya M. Nezarati, Michelle B. Eifert, and Elizabeth Cosgriff-Hernandez, Tissue Engineering, Part C 2013, 19 (10), 810-819. Copyright (2013) Mary Ann Liebert, Inc.

electrospun scaffolds have been investigated for regeneration of vasculature,[104,130,131] nerve,[98,107,132] skin,[91,110,133] and bone.[118,134]

Electrospinning involves pumping a polymer solution at a constant rate through a needle tip that is placed a set distance away from a grounded or oppositely charged collector. When a voltage is applied at the needle tip, the electrostatic forces within the droplet overcome the surface tension of the droplet at the needle tip causing a liquid jet to erupt from the needle. The electrically charged jet undergoes a bending instability which causes it to rapidly whip in multiple expanding loops as it travels to the collector. This whipping process causes stretching and thinning into micro- and nanometer diameter fibers and facilitates solvent evaporation.[17] The fiber mesh can then be removed from the collector and utilized for various tissue engineering applications. The fiber morphology and diameter are dependent on a number of processing parameters that are typically divided into the intrinsic properties of the solution (e.g. polymer, concentration, conductivity, polarity and surface tension of the solvent) and the operational conditions (e.g. strength of the applied electric field, distance to the collector, flow rate). An understanding of electrospun fiber formation and modulation of fiber morphology is necessary for precise control of scaffold properties. To this end, systematic studies have examined the roles of various processing and solution parameters on fiber morphology.

Fong et al. proposed that fiber formation is dependent on the balance of forces caused by surface tension, density of net charges on the jet, and solution viscosity.[55] Surface tension drives conversion of the liquid jet into one or many spherical droplets to

reduce surface area (Rayleigh instability); whereas, the electrostatic repulsion between charges on the jet opposes this force and favors increased surface area and the formation of a thin jet. Viscoelastic forces in a polymer solution resists deformation changes in shape and also supports the formation of fibers. By shifting the balance of these forces, a range of fiber morphologies can be achieved. For example, bead formation can be eliminated by enhancing the effects of viscoelastic and charge repulsion forces over surface tension effects.[135] Although there are well-documented effects of solution concentration on fiber morphology,[33,39,49,55,136,137] it is the resultant change in solution viscosity as described above that is the root cause of these changes to the electrospun fiber morphology. Given that small variations in molecular weight and distribution are typical in different batches of polymers and can strongly influence viscosity, it is often impossible to reproduce fiber architecture by using the solution concentration reported in electrospinning literature. In addition, environmental parameters such as humidity are often not reported and have a strong impact on fiber morphology which makes reproduction of electrospun architectures from the literature even more difficult. The effects of humidity on fiber morphology are poorly understood and/or there are contradictory effects that have been observed that appear to be dependent on properties such as the type of polymer, polymer-solvent combination, molecular weight, polymer hydrophilicity, and size of the electrospun structure.[68,138-141] Both the incomplete reporting of electrospinning conditions and the limited understanding of environmental effects on fiber formation make it difficult to predict and reproduce electrospun scaffold microarchitecture.

In this study, we aim to further elucidate of the process of fiber formation under various electrospinning conditions in order to improve control of fiber morphology and scaffold reproducibility. Three commonly used polymeric biomaterials [poly(carbonate urethane), polycaprolactone, poly(ethylene glycol)] were electrospun through a range of relative humidity levels (5-75%) and the effect on fiber morphology was monitored with scanning electron microscopy. These polymers represent a broad range of hydrophobicity, and therefore, will provide predictive information of the effect of humidity on fiber formation for a wide range of polymeric biomaterials. To highlight the effect of viscosity, two batches of the commercially available poly(carbonate urethane) with different molecular weights were electrospun while maintaining either concentration or viscosity constant. The overall goal of this work is to elucidate mechanisms of electrospun fiber formation and utilize this understanding to provide a systematic method to fabricate scaffolds with tunable and reproducible properties for tissue engineering applications.

2.2. Materials and Methods

2.2.1. Materials

Polyethylene glycol (PEG, Mw = 35,000 Da, Sigma Aldrich), polycaprolactone (PCL, Mw = 70,000 Da, Scientific Polymer Products), and poly(carbonate urethane) (PCU, Carbothane® PC3575A, Mw = 217,000 Da, Lubrizol Advanced Materials) were purchased and used as received. The PCU had a polycarbonate diol soft segment and a 4,4'-methylenebis(cyclohexyl isocyanate) (H_{12}MDI) hard segment. A second batch of

PCU with Mw = 241,000 Da was purchased to study the effects of solution viscosity on fiber morphology. All other chemicals were purchased from Sigma Aldrich and used as received.

2.2.2. Water Contact Angle

Films were fabricated by spin coating (Spincoat G3P-8, Specialty Coating Systems) the electrospinning solutions onto glass slides at 750 rpm for 50 seconds and allowed to dry in a fume hood for 24 hours. Static water contact angle was determined using an optical tensiometer (CAM 200, KSV Instruments). A 5 µL droplet of deionized water was placed on the film and contact angle was measured after allowing the surface to equilibrate after 60 seconds (n=5).

2.2.3. Rheology

The zero shear viscosity was measured for the polymer solutions using a rheometer with a cone-plate configuration (Physica MCR 301, Anton Paar, n=4). Temperature of the cone and plate were kept constant at 20.5 °C. The data are displayed as mean ± standard deviation for each composition. A Student's t-test was performed to determine any statistically significant differences between compositions. All tests were carried out at a 99% confidence interval ($p<0.01$).

2.2.4. Electrospinning

PEG, PCL, and PCU were each mixed with solvent (**Table 2.1**) at ambient conditions to make the electrospinning solutions. The polymer solution was poured into a 10 mL glass syringe with a blunted 20 gauge needle tip and the solution was pumped at a constant rate of 1.0 mL/hr using a syringe pump (KDS100, KDScientific). Fibers were

collected onto a grounded 6 inch square copper plate that was covered with a PET film to facilitate removal of the fiber mesh. For PCL and PEG, the collector was positioned 12 cm away from the needle tip and a voltage of 10 kV (ES30P-5W/DDPM, Gamma Scientific) was applied at the needle tip. PCU was electrospun at a distance of 40 cm with 15 kV applied voltage. No additional methods were implemented to concentrate or direct fibers on the collector. Electrospinning was performed for 10 minutes for each run. Solution viscosity studies were all performed at ambient conditions (50% relative humidity, 20°C). PCU fibers spun for the viscosity study were electrospun onto a 5 mm diameter negatively charged (-5 kV) stainless steel rotating mandrel placed 50 cm from the needle tip.

Table 2.1. Polymer solutions and properties used for electrospinning.

Solution Properties			
Polymer	**Solvent**	**Solution Viscosity (Pa·s)***	**Concentration (wt%)**
PCU	N,N-dimethylacetamide (DMAc)	10.3 ± 0.4	25
PCL	chloroform:N,N-dimethylformamide (DMF) 80:20	9.5 ± 4.8	18
PEG	chloroform	45.3 ± 4.2	25
Solvent Properties			
Solvent	**Boiling Point (°C)**	**Water Miscibility**	**Dielectric Constant**
Water	100	-	80.0
Chloroform	61	Immiscible	4.8
DMF	153	Miscible	36.7
DMAc	166	Miscible	37.8

Electrospinning was performed in a sealed acrylic box to maintain constant humidity levels. To increase relative humidity (RH), a humidifier (ReptiFogger, Zoo Med) with a humidity controller (HygroTherm, Zoo Med) were used. To decrease relative humidity, compressed air was pumped through Drierite™ and into the sealed box until the humidity reached the desired level. Each polymer was electrospun at 5, 20, 35, 50, 60, and 75% relative humidity (± 5% RH). Relative humidity was recorded at the beginning and end of each run using a hygrometer (HI 9569, Hanna Instruments, accuracy ± 4%). Temperature of the room was controlled at 20.5 °C and was measured and recorded in the electrospinning chamber at the beginning and end of each run.

2.2.5. Electrospun Fiber Characterization

Specimens approximately 7 x 7 cm were cut from the center of each fiber mesh to avoid edge effects (3 specimens per mesh). Fiber morphology was observed using scanning electron microscopy (SEM, JEOL NeoScope JCM-5000) at 5 kV accelerating voltage. Prior to imaging, specimens were coated with 4 nm of gold using a sputter coater (Sputter Coater 108, Cressingtion Scientific Instruments). Fiber morphology was analyzed on specimens from four separate runs at each relative humidity level. Images at 2000X, 1000X and 500X magnifications of each mesh specimen were analyzed to determine representative morphologies. The percentage broken fibers was determined by counting the number of broken fibers out of the total that crossed the midline of each 1000X image. Fiber diameter was measured from the first 5 fibers to cross the midline of each 2000X micrograph. Fiber density was measured using photo editing software (GIMP) on 2000X magnification micrographs. First, a transparent layer was created on

which visible fibers were fully traced in a solid black color using a paintbrush tool. The total pixels drawn in the transparent layer (equal to the total area of deposited fibers) was determined from the histogram. Fiber density was equal to the total fiber area (pixels) divided by the total image area (pixels).

2.3. Results and Discussion

2.3.1. Effects of Solution Viscosity

First, the effect of solution viscosity on electrospun fiber morphology was investigated by mixing solutions of PCU (217 kDa) in DMAc at concentrations ranging from 15-20 wt%. As expected, increasing solution concentration resulted in increased viscosity. Representative images of fibers spun at low, intermediate, and high viscosity (**Figure 2.1**) revealed beaded fibers at low viscosity (7.2 ± 1.7 Pa•s), uniform fibers at an intermediate viscosity (10.1 ± 0.5 Pa•s), and larger fibers at high viscosity (22.5 ± 1.4 Pa•s) (fiber diameter increased from 1.2 ± 0.6 μm to 3.5 ± 0.9 μm). As expected, the lower concentration solution had insufficient viscosity to resist fiber deformation without defect at the given electric field. One scenario of bead formation in electrospun fibers occurs when the surface tension in the charged jet is sufficient to change the jet into droplets to reduce surface area.[55] This is opposed by viscoelastic forces in the jet that resist changes to the fiber shape. Therefore, it was hypothesized that the low concentrations studied here generated jets with insufficient viscoelastic forces to fully suppress droplet breakup due to the Rayleigh instability. In contrast, the increased viscosity of the higher concentration solutions created higher viscoelastic forces that

resisted the axial stretching during whipping resulting in larger fiber diameter. These observed effects of concentration/viscosity agree with literature reports.[48,51,53,55] From these results, ~10 Pa•s viscosity was selected as the viscosity where dry, uniform fibers were collected for this system.

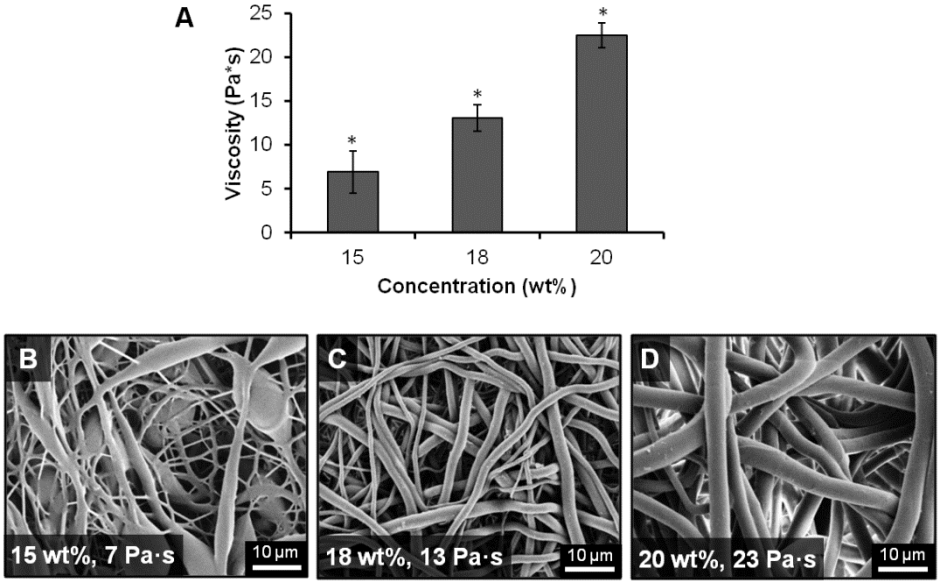

Figure 2.1. (A) Solution viscosity of PCU (217 kDa) in DMAc as a function of concentration, n=4, *p<0.01. (B-D) Scanning electron micrographs of PCU (217 kDa) electrospun at varying solution viscosities: (B) 7 Pa·s, (C) 13 Pa·s, and (D) 23 Pa·s.

The effect of solution viscosity on scaffold reproducibility was then examined by comparing two different lots of commercially available PCU. We hypothesize that a small change in molecular weight due to batch-to-batch variability causes a corollary change in viscosity that influences electrospun fiber morphology. Gel permeation chromatography analysis of 2 different batches of PCU revealed that the molecular

weights differed by ~24 kDa (Mw = 241 kDa, PDI = 2.3; Mw = 217 kDa, PDI = 2.3). This relatively small change in molecular weight was correlated with a 20% reduction in viscosity of 17 wt% polymer solutions (10 Pa•s and 8 Pa•s, respectively). The higher molecular weight PCU (241 kDa) electrospun at 17 wt% concentration and 10 Pa•s viscosity resulted in dry, uniform fibers (**Figure 2.2a**). The lower molecular weight PCU (217 kDa) solution electrospun at the same concentration (17 wt%) had a decreased viscosity (8 Pa•s) and the resulting fiber morphology under identical spinning conditions was characterized as beads-on-strings (**Figure 2.2b**). It was assumed that the reduced viscosity resulted in an imbalance in viscous solution force and electrostatic force necessary for uniform fiber formation, as described above. To obtain uniform fiber morphologies, the viscosities of the low and high molecular weight solutions were matched, rather than the concentrations. When the lower molecular weight solution concentration was increased to 18 wt%, the viscosity increased to 10 Pa•s which was comparable to the higher molecular weight solution at 17 wt%. This solution resulted in dry, uniform fibers that were similar to the higher molecular weight PCU (**Figure 2.2c**). These results highlight that solution viscosity, rather than concentration, is a better determinant of fiber morphology and is a more useful parameter to report in electrospinning methodology to enable reproduction of findings.

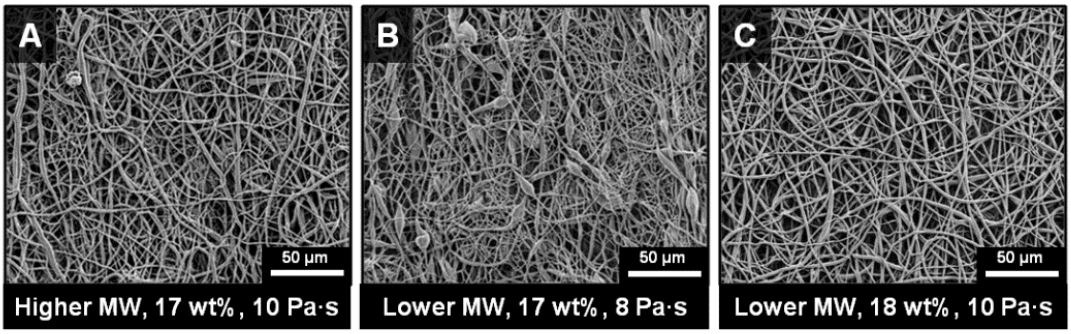

Figure 2.2. Scanning electron micrographs of PCU spun at different molecular weights, concentrations, and viscosities: (A) 241 ± 2 kDa, 17 wt%, 10 Pa·s, (B) 217 ± 2 kDa, 17 wt%, 8 Pa·s, and (C) 217 ± 2 kDa, 18 wt%, 10 Pa·s.

2.3.2. Effects of Relative Humidity

The effects of relative humidity on electrospun fiber morphology were hypothesized to be influenced by polymer hydrophobicity, solvent properties, and applied charge. The static contact angle of each polymer was used as a relative measure of hydrophobicity. The PCU was the most hydrophobic (110.6 ± 5.2°), PCL had an intermediate hydrophobicity (84.1 ± 1.6°), and PEG was hydrophilic (14.6 ± 1.6°). Solvents for each polymer were selected such that each would fully dissolve and facilitate the electrospinning process. A list of solution characteristics were identified to elucidate differences in the solutions that could potentially affect fiber formation and morphology, **Table 2.1**. Solvent boiling point was used as a relative measure of volatility and therefore fiber drying rate. The miscibility of water with the solvent was used as a relative predictor of the likelihood of water absorption at high humidity levels. Finally, solvent dielectric constant relative to water was used to provide a measure of

solution conductivity. Electrospinning parameters were first determined at 50% RH such that dry, uniform fibers were produced. PCL and PEG could be electrospun using the same processing parameters, but it was necessary to increase the distance from tip to collector and the applied voltage to fabricate dry PCU fibers due to the low volatility of DMAc. A corollary increase in the applied voltage was necessary to accelerate the jet to the collector over this larger distance. These parameters were then held constant while humidity was varied from 5-75%.

At low humidity (<50% RH), PEG meshes were characterized by broken fibers with the number of breakages increasing as the relative humidity decreased. Uniform, continuous fibers formed at 50% RH and increasing relative humidity to 60% resulted in broken fibers of distinctly larger diameter and ball-shaped fiber ends. Fibrous morphology was not evident at 75% RH and instead a polymer sheet indicative of jet beading was observed (**Figure 2.3**). Fiber breakage at low relative humidity was attributed to the increased electrostatic charge on the spinning jet due to reduced water vapor in the air. During electrospinning, a portion of charge from the electrospinning jet is discharged to the water vapor molecules in the atmosphere.[142] This is facilitated by the high dielectric constant of water (**Table 2.1**), indicating that it has a high energy storage capacity by means of polarization. Therefore, a decrease in water vapor (low humidity environment) results in a decreased amount of electrostatic discharge since fewer water molecules are available for charge transfer. As a result, the charge density on the jet is higher at low humidity causing fiber breakage. This is most likely a different mechanism than the bead or bead-on-string morphologies seen with low viscosity solutions that is

driven by surface tension, described above. We hypothesize that the fiber breakage observed at low humidity is due to increased stretching of the jet during whipping after sufficient solvent evaporation to retain fiber morphologies. At high relative humidity, the fiber breakage and loss of morphology was attributed to water absorption and polymer dissolution given the known solubility of PEG in water.

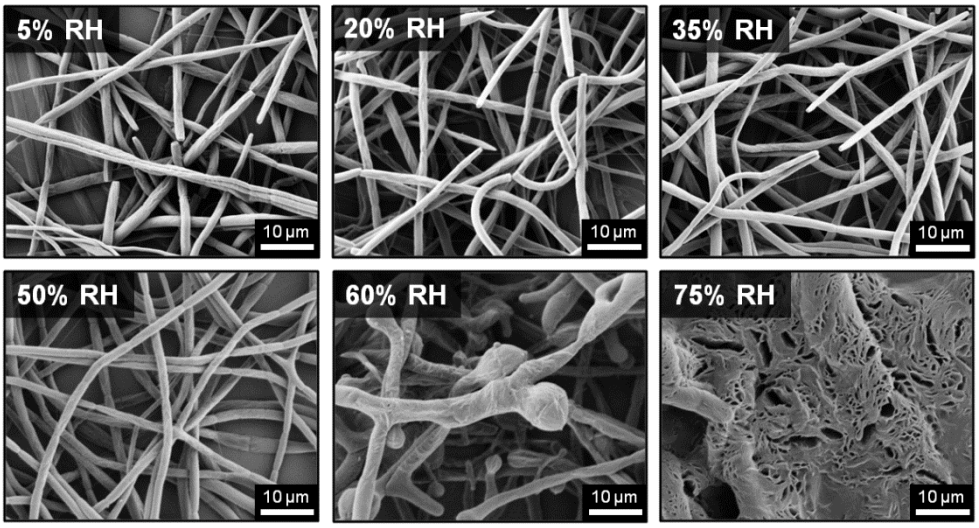

Figure 2.3. Scanning electron micrographs of poly(ethylene glycol) (PEG) electrospun at relative humidity (RH) ranging from 5-75%.

PCL fibers also exhibited a morphology characterized by broken fibers below 50% RH but formed thicker fibers with surface pores above 50% RH (**Figure 2.4**). The number and density of surface pores increased as relative humidity was increased. Broken fibers at low humidity (<50% RH) was attributed to the same decreased electrostatic charge dissipation as described for PEG. The effect of increased electrostatic force was

demonstrated by increasing the applied voltage on a run that otherwise formed continuous fibers.

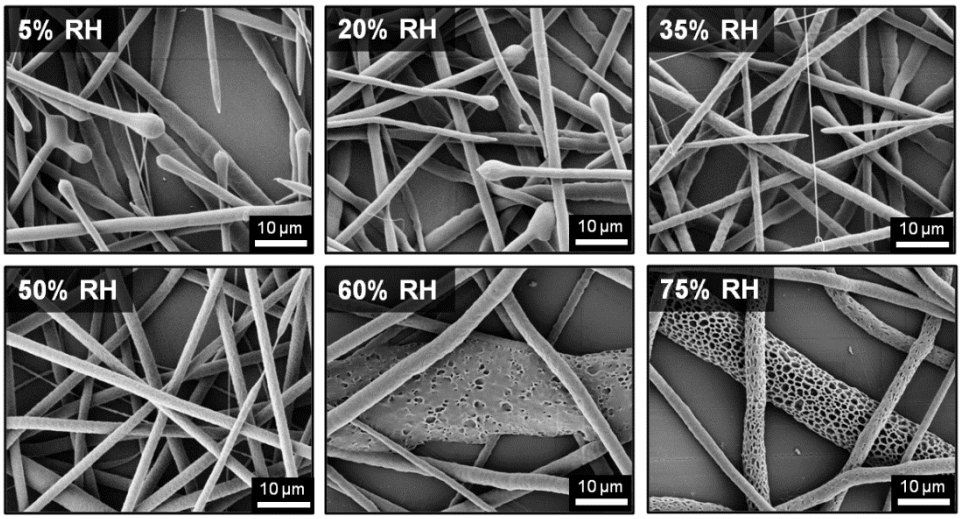

Figure 2.4. Scanning electron micrographs of poly(caprolactone) (PCL) electrospun at relative humidity (RH) ranging from 5-75%.

PCL formed continuous fibers when electrospun at 50% RH and 10 kV applied voltage, whereas broken fibers, similar in morphology to the low humidity runs, formed when the voltage was increased to 16 kV (**Figure 2.5**). The presence of surface pores at high humidity (>50% RH) was hypothesized to be caused by vapor induced phase separation (VIPS).[65,137,139,143-145] Typically, a hydrophobic polymer, high volatility solvent, and a water miscible solvent are necessary to facilitate VIPS. First, water vapor is absorbed into the jet due to the water miscible solvent. Phase separation occurs as the hydrophobic polymer precipitates out of the solution when water is introduced, creating polymer-rich and polymer-poor regions within the jet. Finally, rapid evaporation of the highly volatile

solvent locks in the phase separated geometry, resulting in fibers with surface pores. Pores created by VIPS are typically irregularly shaped, as has been documented in the literature.[65,137-139] In this study, DMF in the solvent mixture allows for water absorption, hydrophobic PCL precipitates out upon absorption of water, and the highly volatile chloroform evaporates rapidly to lock in the pore geometry.

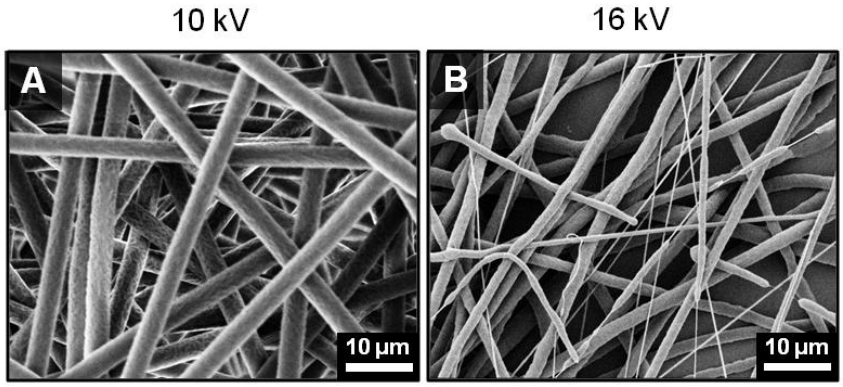

Figure 2.5. Scanning electron micrographs of PCL electrospun at 50% RH and with either (A) 10 kV or (B) 16 kV applied voltage.

PCU fibers electrospun at low humidity (5% RH) resulted in beads connected by thin fibers, but increasing the relative humidity (20-75% RH) resulted in smooth, uniform fibers (**Figure 2.6**). Additionally, fiber density decreased as relative humidity was increased from 50% to 75%. Similar to PEG and PCL, it was assumed that reduced charge dissipation at low humidities (< 50% RH) resulted in increased electrostatic forces that stretch the jet during its flight to the collector. However, both PEG and PCL solutions had a shorter distance the collector and a higher drying rate than PCU as

indicated by solvent boiling point, **Table 2.1**. This increased drying rate permitted sufficient fiber solidification prior to jet breakage to retain fiber morphologies; whereas, the slower drying PCU had fiber retraction into beads after jet breakage resulting in the observed large beads and nanofibers. Unlike PCL, the PCU did not exhibit a porous surface morphology at high relative humidity (60-75% RH) despite being a hydrophobic polymer in a water miscible solvent.

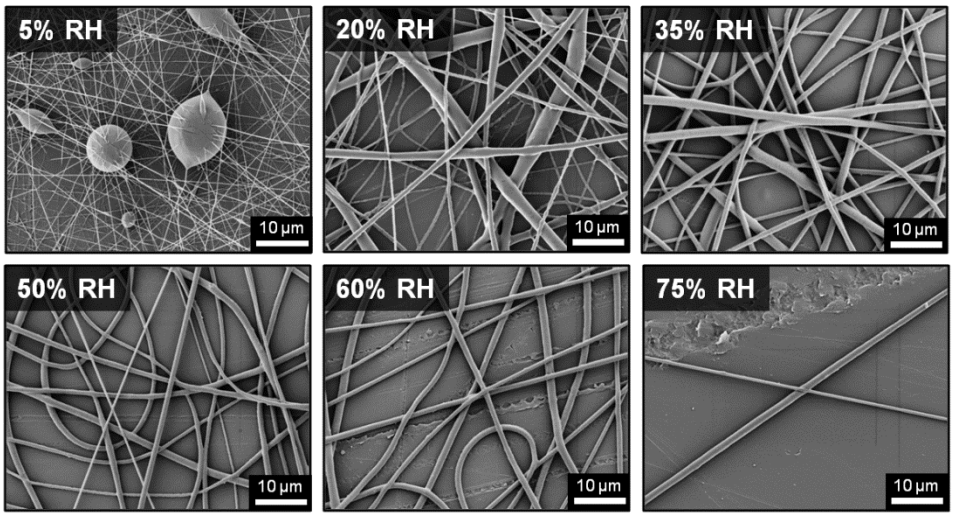

Figure 2.6. Scanning electron micrographs of poly(carbonate urethane) (PCU) electrospun at relative humidity (RH) ranging from 5-75%.

It was hypothesized that the lack of surface pores on PCU was a result of the low volatility of DMAc that does not permit rapid evaporation to lock in the phase-separated geometry. Instead, a decrease in fiber density as relative humidity increases was observed and attributed to the increased amount of water vapor that facilitates electrostatic discharge. In this scenario, the electric field is unable to selectively direct

the jet toward the collector after discharge resulting in reduced fiber collection. This effect was also observed when the distance to the collector was increased which increases jet discharge independent of humidity, **Figure 2.7**. Fibers collected over 50 cm while maintaining humidity at 50% RH resulted in a decreased fiber density (0.36 ± 0.07 and 0.05 ± 0.01 fibers/image area for 40 and 50 cm, respectively) due to greater electrostatic discharge, similar to meshes electrospun at high RH. Literature reports of electrospinning a solution with these properties (hydrophobic polymer, water miscible solvent, low volatility) have shown it is also possible to fabricate fibers with porous cores.[143,145]

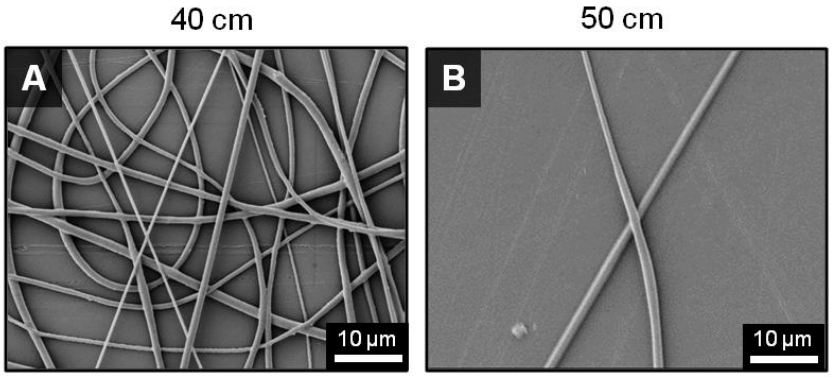

Figure 2.7. Scanning electron micrographs of PCU electrospun at 50% RH for 10 minutes and at a distance of (A) 40 cm or (B) 50 cm.

In order to provide a general overview of the role of humidity on fiber formation, the fiber morphologies for PEG, PCL, and PCU at 5-75% relative humidity are summarized in **Table 2.2**. First, the amount of fiber breakage for PEG and PCL at low relative humidity was quantified and a general trend of decreased humidity resulting in

increased fiber breakage was observed. This finding is expected give that decreased levels of electrostatic discharge are expected to result in increased fiber breakage, as described above.

Table 2.2. Description of the changes in fiber morphology in the range of 5 to 75% relative humidity

	5% RH	***20% RH***	***35% RH***	***50% RH***	***60% RH***	***75% RH***
Poly(ethylene glycol) (PEG)	21 ± 22% broken fibers	14 ± 18% broken fibers	21 ± 18% broken fibers	9 ± 10% broken fibers	Short, broken fibers with beading	Flat beads with surface morphology
Polycaprolactone (PCL)	34 ± 18% broken fibers	49 ± 17% Broken fibers	32 ± 16% broken fibers	3 ± 4% broken fibers	Porous fibers	Porous fibers
Poly(carbonate urethane) (PCU)	Beads-on-strings	Both large and small diameter fibers	Increased fiber deposition	Smooth, uniform fibers	Decreased fiber deposition	Minimal fiber deposition

The differences in fiber morphology at high relative humidity were attributed to differences in polymer hydrophobicity, water miscibility, and volatility of the solvent. In addition to the morphologies demonstrated in this study, high humidity conditions can also generate surface pores via thermally induced phase separation (TIPS) during electrospinning. Based on the current findings and review of the literature, TIPS was generally associated with a hydrophobic polymer dissolved in a water miscible and highly volatile solvent. In this process, rapid evaporation of the solvent creates local decreases in temperature at the surface of the jet that results in water vapor condensation.

These water droplets are trapped on the skin layer and create circular indentations. After the fiber solidifies and the water droplets evaporate, surface pores are created in the form of breath figures. Pores formed through TIPS are typically circular since the pores are molded by water droplets.[138,140] A summary of the theories describing formation of pores on hydrophobic polymer fibers is illustrated in **Figure 2.8**.

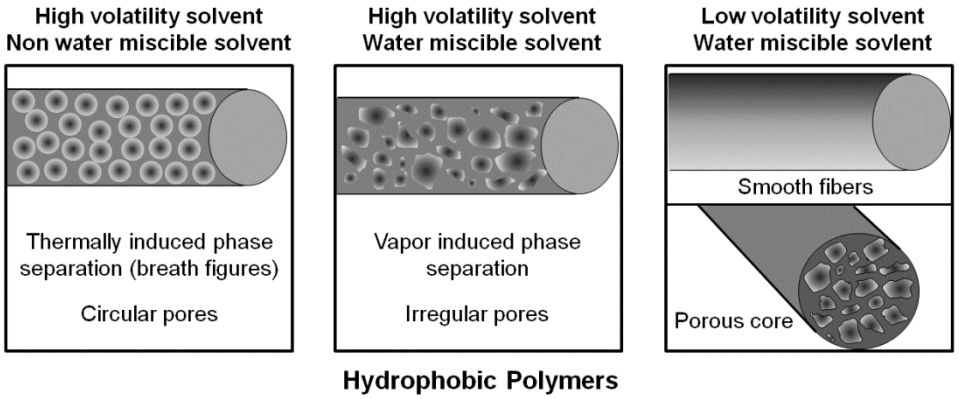

Figure 2.8. Different fiber morphologies observed for hydrophobic polymer electrospun at high percent relative humidity with different solvents

2.4. Conclusions

These studies demonstrate the effects of both solution viscosity and relative humidity on the morphology of electrospun fibers. Importantly, we have illustrated the importance of reporting and matching solution viscosity, rather than concentration, and humidity for improved reproducibility of fiber architectures between studies. Key mechanisms governing fiber formation at different humidity levels were identified for three commonly used polymeric biomaterials of different physical properties. Previously

unclear and contradictory mechanisms based on polymer and solvent properties have been elucidated to provide a system for predicting and tuning fiber morphology based on humidity and polymer hydrophobicity. Fiber breakage occurred for each of the polymers at low humidity, but the effects at high humidity were dependant on the polymer hydrophobicity as well as the solvent volatility and miscibility with water. These mechanisms are widely applicable to the design of electrospinning methodology for other synthetic polymers as well as natural polymers such as collagen, cellulose, and chitosan. Enhanced understanding of these fiber formation mechanisms provides better control of fiber morphology in order to fabricate tissue engineering scaffolds with improved properties.

CHAPTER III

ELECTROSPUN VASCULAR GRAFTS WITH IMPROVED COMPLIANCE MATCHING TO NATIVE VESSELS*

3.1. Introduction

Coronary artery bypass grafting (CABG) is one of the most commonly performed major surgeries in the United States with over 400,000 procedures performed annually at a cost of over $25 billion.[146] Autologous vessels such as the saphenous vein or mammary artery are the gold standard for treatment; however, autologous grafts are unavailable in up to 20% of patients due to disease, trauma, or anatomic abnormalities.[147-150] Synthetic vascular prostheses made of expanded poly(tetrafluoroethylene) (ePTFE) or poly(ethylene terephthalate) (PET) are a common alternative to autologous vessels. These grafts are poor options in small diameter (<4 mm) applications due to high failure rates as a result of rapid re-occlusion. Synthetic grafts have a 40-50% reduction in patency after two years and 40% of grafts completely fail within 5 years.[151,152] This re-occlusion has been attributed to the occurrence of intimal hyperplasia at the distal anastomosis.[151,153] Intimal hyperplasia is characterized by smooth muscle cell migration from the medial layer of the vessel to the intimal layer followed by proliferation, resulting in narrowed artery diameter. Current strategies are focused on inhibiting intimal hyperplasia to improve the long-term clinical success of

*Reprinted with permission from "Electrospun Vascular Grafts with Improved Compliance Matching to Native Vessels," by Roya M. Nezarati, Michelle B. Eifert, David K. Dempsey and Elizabeth Cosgriff-Hernandez, Journal of Biomedical Materials Research, Part B 2014, DOI: 10.1002/jbm.b.33201. Copyright (2014) Wiley Periodicals, Inc.

synthetic, small-diameter vascular grafts.

Recent studies have reported a strong correlation between graft mechanical properties and intimal hyperplasia onset and severity. Compliance, a measurement of graft change in diameter over a given pressure range, has been identified as a key determinant of graft success. Improved compliance between the vessel and the synthetic graft has the potential to reduce intimal hyperplasia and improve graft success. Despite having high burst pressure and suture retention strengths, PET and ePTFE compliance values are much lower than native vessel values.[151] As a result, the compliant artery will expand and contract to maintain constant wall shear stress within the vessel, whereas the stiff synthetic graft resists the corresponding change in diameter. This compliance mismatch disrupts blood flow and results in zones of recirculation, flow separation, and low wall shear stress at the endothelium.[154] Low wall shear stress initiates the release of vasoactive substances, gene activation, protein expression, and cytoskeletal rearrangement that stimulate intimal hyperplasia.[151] Therefore, a graft that more closely matches native arterial compliance can improve the long-term clinical success of synthetic vascular grafts by preventing flow disruption and the stimuli for intimal hyperplasia.

Native vessels consist of alternating layers of elastin and collagen which provide the vessel with both high burst pressure and high compliance (saphenous vein burst pressure: 1680 ± 307 mmHg[155] and compliance: 4.4 ± 0.8 %/mmHg x 10^{-4} [151]). Reproducing these features in synthetic grafts continues to be challenging given that compliance and burst pressure are often inversely related in synthetic grafts. The

hierarchical structure of alternating elastin and collagen in arteries provides tensile properties characterized by a low modulus with high elastic recovery followed by a strong strain hardening response at higher strains. A material that more closely mimics the stress response curve of native arteries has greater potential to match mechanical properties and reduce intimal hyperplasia. Segmented polyurethanes (SPUs) are a promising material due to their a high elasticity and a strong strain hardening response.[156,157] Vascular grafts fabricated from SPUs have been previously investigated, but these grafts were still unable to match the biomechanical properties of native vessels. Grafts such as the Corvita®, Thoratec®, and PulseTec® have been developed with modest improvements in compliance but were still lacking compared to autologous standards.[158] Newer commercial SPU grafts such as the UCL-Nano™ and Myolink™ grafts, now available in Europe, have exhibited improved compliance values much greater than traditional synthetic grafts; however, these grafts have no recorded burst pressure exceeding autologous vessels.[159,160] Due to the highly tunable segmented chemistry, SPUs with a range of mechanical properties and stress responses more closely matching native vessels could be achieved.[161,162] These features make SPUs a promising material for fabrication of a vascular graft with improved compliance matching.

In addition to SPU chemistry, modulation of graft microarchitecture can be utilized to provide additional control of graft mechanical properties. Electrospinning has gained popularity in recent years as a technique to generate nonwoven fibrous scaffolds with high porosities, large surface area-to-volume ratios, and nano- to micron-sized fiber diameters.[17,163,164] A polymer solution is pumped at a constant rate through a needle tip

that is placed a set distance away from a grounded or oppositely charged collector. When a voltage is applied at the needle tip, the droplet erupts into a liquid jet that narrows and solidifies during flight to be collected as a fiber.[17] Many modifications have been made to the traditional setup to improve control over mesh microarchitecture. For instance, tubular constructs have been fabricated by utilizing a rotating mandrel collector for vascular[105] or nerve[107] applications. The relative ease of modulating fiber architecture through variation of processing, solution, or environmental parameters provides a means to control scaffold properties. For example, fiber alignment and fiber diameter have been shown to influence mechanical properties.[31,123,124,165] The high tunability of electrospun scaffold microarchitecture provides an additional method for modulating vascular graft biomechanical properties.

In this study, we aim to fabricate electrospun vascular grafts with improved compliance while maintaining sufficient burst pressure by altering SPU chemistry and electrospun mesh microarchitecture. Two commercially available poly(carbonate urethanes) (Carbothane® and Chronoflex®) were first evaluated for their neat film tensile properties (elastic modulus, tensile strength, ultimate elongation) to provide a range of properties for subsequent vascular graft characterization. Electrospun graft biomechanical properties (burst pressure and compliance) were then investigated to elucidate relationships between tensile and biomechanical properties. Mesh microarchitecture was modulated to achieve biomechanical properties more closely matching that of native vessels to further improve graft performance. Mesh thickness, fiber tortuosity, and fiber fusions at junctions were varied to determine which

microarchitectures have the most profound effect on biomechanical properties and identify the combination of microarchitectures that provide both high burst pressure and compliance. These grafts are intended for use as the outer layer of a multilayer design with the inner layer composed of a thromboresistant, bioactive hydrogel.[166] In addition to fabricating an improved vascular graft, this work probes fundamental relationships between electrospun mesh microarchitecture and mechanical properties for use in various applications.

3.2. Materials and Methods

3.2.1. Materials

Two commercially available poly(carbonate urethanes) with different hard and soft segment components were investigated, **Table 3.1**. Chronoflex C® 80A (Chronoflex, AdvanSource Biomaterials, MW = 221 ± 16 kDa) and Carbothane® PC3575A (Carbothane, Lubrizol, MW = 217 ± 2 kDa), were purchased in pellet form and used as received. All other chemicals were purchased from Sigma Aldrich and used as received.

Table 3.1. Hard and soft segment components of the poly (carbonate urethanes) studied.

Polymer	Isocyanate	Polyol
Chronoflex 80A	Methylene diphenyl diisocyanate (MDI) 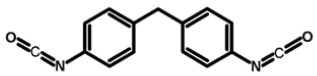	Polycarbonate diol 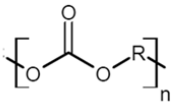
Carbothane 73A	4,4'-Methylene dicyclohexyl diisocyanate (H_{12}MDI) 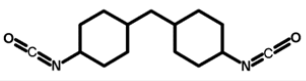	Polycarbonate diol 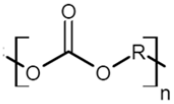

3.2.2. Material Characterization

Films 0.25 mm thick were fabricated by solvent casting 50 grams of 10 wt% in *N,N*-dimethylacetamide (DMAc) solutions in 140 mm diameter glass petri dishes under vacuum for 5 days. Heat (50 °C) was applied in addition to vacuum for the final 24 hours. Films were removed, cut into dog bones, and tested in accordance with ASTM D1708. Specimens (n=4) were strained at a rate of 100%/min based on the initial gauge length using an Instron 3345 equipped with pneumatic side action grips (Instron 2712-019, 90 psi). Elastic modulus, tensile strength, and ultimate elongation were calculated from the resultant engineering stress/strain curves. A secant modulus based on 2% strain was calculated for elastic modulus and subsequently referred to as simply "modulus".

Transmission-Fourier transform infrared spectroscopy (FTIR) specimens were prepared by dissolving specimens in dilute solutions with DMAc and solution casting onto clean KBr pellets under vacuum until all solvent was removed. Spectra were recorded with a Bruker Tensor 27 FTIR spectrometer (Billerica, MA). Hard segment

content was determined by calculating peak height ratios of the 1250 cm^{-1} (C-O bond of the soft segment carbonate) to the 1413 cm^{-1} peak (C-C bond of the hard segment ring).

3.2.3. Electrospinning

Chronoflex and Carbothane were each mixed into 18 wt% solutions in DMAc (viscosity ~10 Pa·s). To facilitate removal of the grafts, the collector (stainless steel mandrel, 5 mm diameter) was first dipped in a 5 wt% poly(ethylene glycol) (PEG, 35 kDa) in chloroform solution and allowed to dry for a minimum of 1 hour in a fume hood prior to electrospinning. The polyurethane solution was then fed at a rate of 0.5 mL/hr through a positively charged needle (20 gauge) located 50 cm from a negatively charged mandrel which was rotated at a speed of 500 rpm. The positive applied voltage (ES30P-5W/DDPM, Gamma Scientific) for each run was selected as the lowest voltage that produced a stable Taylor cone (15-20 kV) and a negative voltage of 5 kV was applied to the mandrel (ES30N-5W/DDPM, Gamma Scientific). Relative humidity was monitored at the beginning and end of each run and ranged from 45-55% which was previously determined as an acceptable range for producing uniform fibers.[167] After electrospinning, the mandrel was placed in deionized water and stirred for 12 hours to remove the sacrificial PEG layer. Meshes were then removed and cut into 40 mm long sections for biomechanical testing. To fabricate meshes of different wall thicknesses, fibers were collected for 4, 5, or 6 hours. Thickness was measured at two locations on each end of the graft using digital calipers for a total of 4 measurements. Fiber tortuosity was altered by increasing the mandrel rotation rate to 4000 rpm and placing negatively charged razor blades behind the mandrel which concentrated the electric field to

encourage fiber alignment along the blade length.[168,169] Fiber fusions were induced using either solvent vapor or heat exposure. Solvent-induced fiber fusions were generated by placing meshes in a sealed desiccator along with a petri dish containing 50 mL DMAc for 144 hours to allow the solvent vapor to swell and fuse the fibers together. Heat-induced fiber fusions were generated by placing meshes onto PTFE rods (5.0 mm diameter) and heating in an oven at 50°C for 12 or 24 hours. Meshes with altered fiber tortuosity or fusions were electrospun for 4 hours to achieve a constant thickness of 0.4 mm.

3.2.4. Electrospun Graft Conditioning

Electrospun grafts were subjected to a conditioning cycle to mimic physiological conditions. Grafts were connected via tubing to a pressure gauge and a peristaltic pump and submerged in 37 °C water. The peristaltic pump was set at either 140 or 230 rpm which resulted in a pulsatile pressure of 120 or 230 mmHg, respectively. Conditioning was performed for 24 hours. Control grafts subject to 37 °C water without conditioning.

3.2.5. Electrospun Fiber Characterization

Circumferential analysis of fiber morphology was performed using scanning electron microscopy (SEM, JEOL NeoScope JCM-5000). Specimens were prepared by cutting a 5 mm long tubular section of each graft and making a longitudinal cut to obtain a flat specimen. Prior to imaging, specimens were coated with 4 nm of gold using a sputter coater (Sputter Coater 108, Cressingtion Scientific Instruments). Fiber tortuosity was quantified by measuring the total fiber length divided by the fiber end-to-end length of the first 5 fibers that passed through the midline of each image using image editing

software (GIMP, 1000× magnification, 4 runs, 3 images per run for total n=12 images). Total fiber length was measured as the total length of a line traced over the visible fiber and fiber end-to-end length was measured as the length of a straight line connecting the two visible endpoints of the fiber. Amount of fusion was also measured in GIMP image editing software on 4000× scanning electron micrographs (4 runs, 3 images per run for total n=12 images). The line visible between two fibers when they crossed was used to rank the amount of fusion. Completely fused was defined as the absence of a visible line, partially fused was defined as when the line was visible but not discrete, and non-fused was defined as a clear, discrete line between the two fibers. For each intersection, the percentage of each that showed distinct fibers, partially fused fibers, and completely fused fibers was measured.

3.2.6. Dynamic Mechanical Analysis

Specimens for dynamic mechanical analysis (DMA) were prepared from electrospun meshes cut into 5.5 mm × 40 mm strips with the long edge aligned with the longitudinal axis of the graft. Storage and loss moduli as a function of temperature were measured using a TA RSA III dynamic mechanical analyzer in tensile mode. All specimens were subject to an oscillatory strain of 0.1% at a frequency 1 Hz and were scanned from -90 to 150 °C at 5 °C/min.

3.2.7. Differential Scanning Calorimetry

Differential scanning calorimetry (DSC) thermograms were collected on specimens of approximately 10-15 mg which were subjected to a temperature ramp of -80°C to 100°C at a rate of 5°C/min under nitrogen gas using a TA DSC Q100 (Houston,

TX). All analysis was performed on the first scan to examine processing effects from electrospinning and/or heat treatment.

3.2.8. Biomechanical Testing

Burst pressure and compliance testing was performed in accordance with ANSI/AAMI/ISO 7198 and as described previously.[166] Briefly, a nonporous latex tube lining was first inserted into 40 mm long grafts. Static compliance was determined by pumping water through a syringe pump (KDS200, KDScientific) at a rate of 4 mL/min to subject each graft to a pressure ramp (0-150 mmHg). Intraluminal pressure was monitored using an in-line digital pressure gauge (MG1-5-A-9V-R MediaGauge, SSI Technologies, Inc) and graft outer diameter was measured with a He-Ne laser micrometer (Lasermike). Compliance (C) was calculated from the recorded pressure, P, and inner diameter, D, according to the following equation:

$$C = \Delta D/(D_0 \bullet \Delta P) = (D_{120} - D_{80})/(D_{80} \bullet 40)$$

Inner diameter was calculated by subtracting the two times the wall thickness from the measured external diameter, assuming incompressibility of the graft wall. Burst pressure was determined by pumping deionized water into each latex lined graft at 100 mL/min using a syringe pump (KDS200, KDScientific). The ends of each graft were firmly secured and sealed to prevent leakage. Pressure was measured using a high pressure gauge (0 to 60 psi pressure range, NoShok) connected downstream of the graft. Burst pressure was recorded as the maximum pressure prior to construct failure.

3.2.9. Statistical Analysis

The data are displayed as mean ± standard deviation for each composition. A Student's t-test was performed to determine any statistically significant differences between compositions. All tests were carried out at a 99% confidence interval ($p<0.01$).

3.3. Results and Discussion

3.3.1. Tensile Testing

Altering material chemistry provides a method for tuning polyurethane tensile properties which we hypothesize can be correlated to vascular graft biomechanical properties. It has previously been demonstrated that hard segment content and chemistry strongly influence resultant mechanical properties.[161,162,170] The polymers investigated in this study allow us to compare the effects of hard segment chemistry on tensile as well as biomechanical properties. Chronoflex and Carbothane are both poly(carbonate urethanes); however, Chronoflex contains an aromatic hard segment (MDI) whereas Carbothane contains an aliphatic hard segment (H_{12}MDI), **Table 3.1**. Peak height analysis (1250 cm^{-1}/1413 cm^{-1}) of FTIR spectra revealed that both polymers had similar hard segment content (Carbothane = 4.35 ± 0.63 and Chronoflex = 4.78 ± 0.25). A comparison of the stress-strain behavior of polyurethane films is displayed in **Figure 3.1** with average moduli and tensile strengths provided in **Table 3.2**. Both polyurethanes exhibited low initial modulus followed by a plateau of almost constant stress and strain hardening at higher strains. Previous microstructural analysis of segmented polyurethanes provides insight into the observed stress response. The initial elastomeric

stretching of the soft segment is followed by rotational movement of the rigid hard segments in the direction of strain and yielding associated with hard domain break up. The observed strain hardening is commonly attributed to strain-induced crystallization of the soft segment.[157] Compared to Carbothane, the Chronoflex curve was characterized by a higher initial modulus, an earlier onset of strain hardening, and greater tensile strength. These differences were consistent with literature reports on the effects of hard segment chemistry and content on mechanical properties; specifically that polyurethanes with aromatic hard segments have a higher initial modulus and tensile strength than aliphatic counterparts.[162,171,172] The effect of hard segment chemistry on electrospun graft biomechanical properties and the correlation with the observed tensile properties was then investigated.

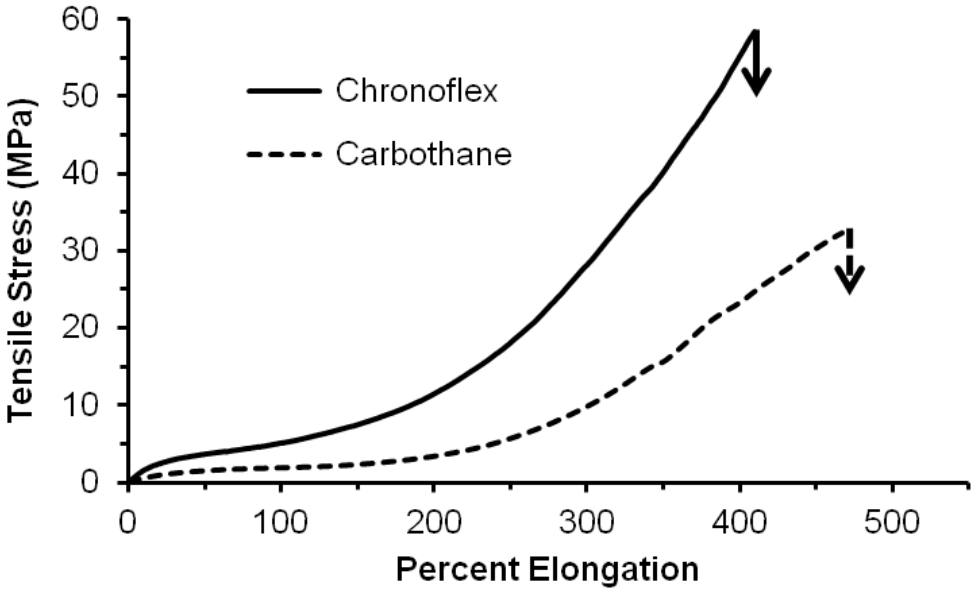

Figure 3.1. Stress vs. strain curves for neat polyurethane films.

Table 3.2. Tensile and biomechanical properties of the different poly (carbonate urethanes). Electrospun mesh thickness = 0.4 mm; n=4; mean ± standard deviation displayed.

Tensile Properties		
Polymer	**Initial Modulus (MPa)**	**Tensile Strength (MPa)**
Carbothane	7.1 ± 0.4	33.9 ± 4.7
Chronoflex	19.8 ± 0.9	58.8 ± 5.8
Electrospun Graft Properties		
Polymer	**Compliance (%/mmHg x 10^{-4})**	**Burst Pressure (mmHg)**
Carbothane	4.6 ± 0.9	900 ± 414
Chronoflex	2.0 ± 0.3	1700 ± 210

3.3.2. Effects of Material Chemistry on Biomechanical Properties

Electrospun graft biomechanical properties (burst pressure and compliance) were investigated to elucidate relationships between tensile and biomechanical properties. The tensile and biomechanical properties of the two polymers are summarized in **Table 3.2**. As often observed in the literature, grafts with higher compliance values also possessed lower burst pressures.[130,173,174] Compliance was correlated to polyurethane initial modulus with lower initial modulus resulting in increased compliance. Similarly, burst pressure was correlated to tensile strength with higher tensile strength resulting in higher burst pressure (**Figure 3.2**). These findings suggest that polyurethanes with low initial modulus and high tensile strength have greater potential to be fabricated into an electrospun vascular graft with improved compliance while maintaining burst pressure. By this measure, Carbothane was selected for subsequent studies on modulating graft microarchitecture.

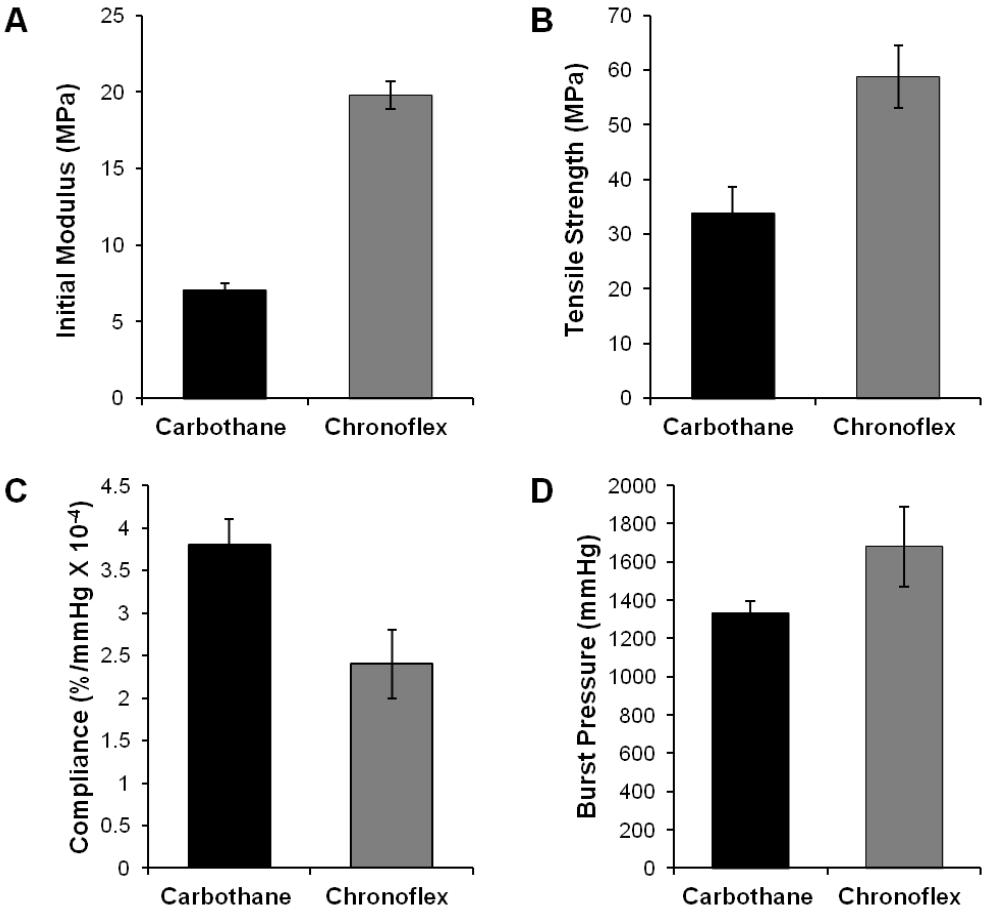

Figure 3.2. Tensile properties of poly (carbonate urethanes): (A) initial modulus and (B) tensile strength. Biomechanical properties of electrospun meshes (0.4 mm thickness) fabricated from different polyurethanes: (C) compliance and (D) burst pressure.

3.3.3. Electrospun Graft Microarchitecture

Scanning electron micrographs of the electrospun grafts display the characteristic fibrous microstructure with uniform fiber diameter (1.3 ± 0.1 μm) (**Figure 3.3**). Altered collection time was used to modulate graft wall thickness with collection times of 4, 5, and 6 hours corresponding to graft thicknesses of 0.4, 0.5, and 0.6 mm, respectively (**Figure 3.4**).

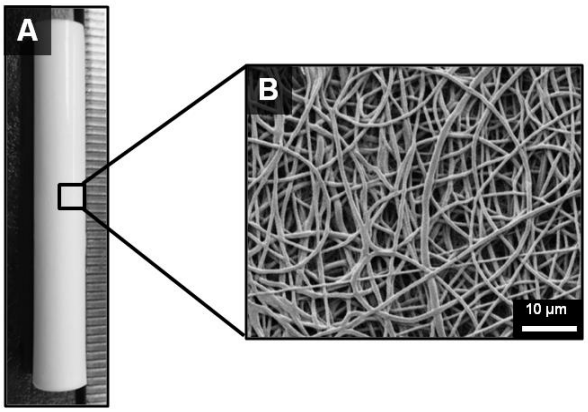

Figure 3.3. (A) Tubular electrospun mesh fabricated by electrospinning onto a rotating mandrel and (B) representative scanning electron micrograph of the fiber morphology.

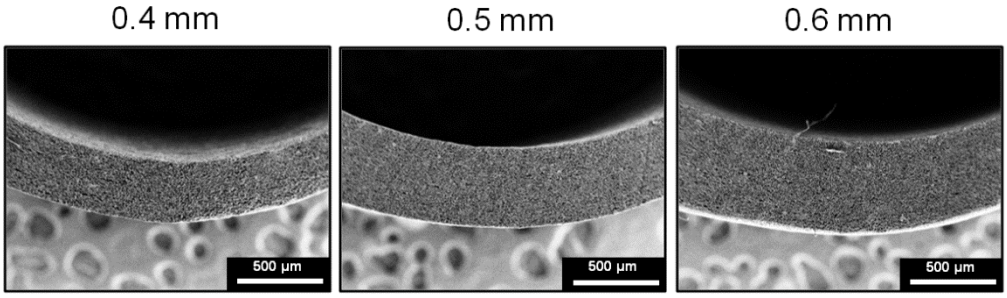

Figure 3.4. Scanning electron micrographs of electrospun mesh tubes with varying thicknesses. Cross-sectional views of (A) low thickness tube (wall thickness = 0.4 mm), (B) medium thickness tube (wall thickness = 0.5 mm), and (C) high thickness tube (wall thickness = 0.6 mm).

Grafts with low fiber tortuosity (1.2 ± 0.4) compared to as-spun fiber tortuosity (1.7 ± 0.8) were achieved by increasing the mandrel rotation rate to 4000 rpm and placing a row of vertically aligned and negatively charged razor blades behind the rotating mandrel (**Figure 3.5**). Fiber alignment using a similar rotating mandrel setup has been reported previously.[96,129,175] The addition of aligned razor blades was used to enhance

fiber alignment and was determined necessary to reduce fiber tortuosity in this electrospinning setup.[168,169] Fiber fusions at intersections were induced by placing as-spun grafts in the presence of solvent vapor that induced swelling of the polyurethane and enhanced fusion at junctions without loss of fibrous architecture (**Figure 3.6**).

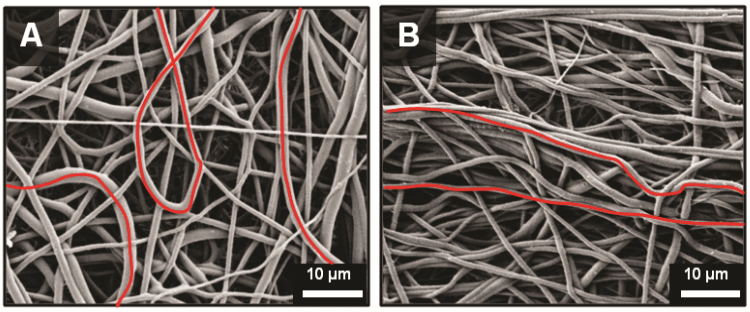

Figure 3.5. Scanning electron micrographs of electrospun meshes with different degrees of tortuosity: (A) high tortuosity and (B) low tortuosity.

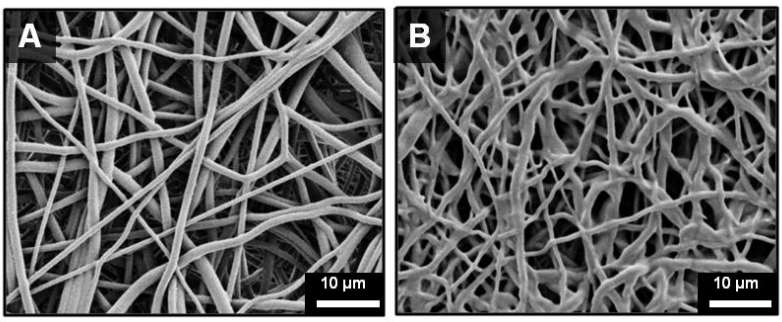

Figure 3.6. Scanning electron micrographs of electrospun meshes with different amounts of fiber fusion at junctions: (A) low fustion at junctions and (B) high fusion at junctions.

A method was utilized to quantify the level of fusion using SEM analysis of fiber junctions. After incubation in DMAc vapor, meshes were generated with increased fusion at junctions, roughly 50% completely fused, 30% partially fused, and 20% non-fused fibers. Grafts after heat treatment were also characterized by increased fiber fusion to a lower extent with the amount of fusion increasing with length of heat treatment (**Figure 3.7**). Meshes undergoing heat treatment for 24 hours had roughly 2% completely fused, 32% partially fused, and 66% non-fused fibers. The individual and synergistic effects of these variations in microarchitecture on biomechanical properties were then investigated.

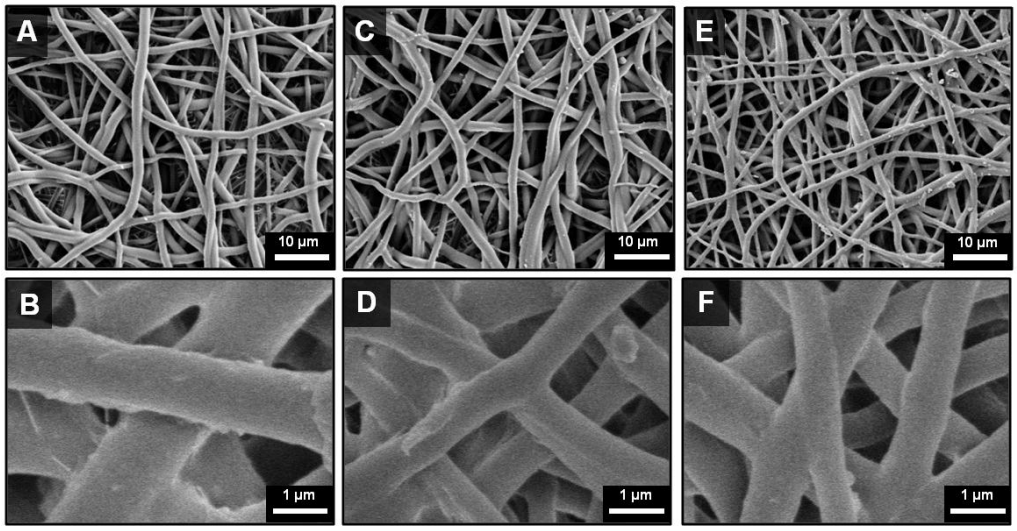

Figure 3.7. Scanning electron micrographs heat-treated Carbothane grafts: (A-B) Before heat treatment (C-D) After 12 hr heat treatment (E-F) After 24 hr heat treatment.

3.3.4. Effects of Graft Microarchitecture on Biomechanical Properties

3.3.4.1. Effects of Mesh Thickness

Biomechanical properties for Carbothane meshes with decreasing wall thickness from 0.6 to 0.4 mm are summarized in **Figure 3.8**. Compliance values for meshes 0.6, 0.5, and 0.4 mm thick were 1.3 ± 0.6, 2.1 ± 0.4, and 3.8 ± 0.3 %/mmHg x 10^{-4}, respectively (1 mmHg = 0.133 kPa). The corresponding burst pressures for meshes 0.6, 0.5, and 0.4 mm thick were 1560 ± 170, 1470 ± 40, 1330 ± 70 mmHg, respectively. It was hypothesized that decreased mesh thickness resulted in a decreased circumferential stress that resulted in the observed increases in compliance and decreases in burst pressure. Importantly, large increases in compliance were achieved with only small sacrifices in burst pressure, suggesting the potential to improve compliance while maintaining a sufficient burst pressure. For example, when mesh thickness was decreased from 0.6 mm to 0.5 mm, a 63% increase in compliance was achieved with only a 6% loss in burst pressure. Further reduction of mesh thickness to 0.4 mm resulted in an 83% increase in compliance and a 9% loss in burst pressure. By altering mesh thickness alone, a compliance that approaches the saphenous vein was achieved with burst pressure only 21% lower than the saphenous vein (saphenous vein burst pressure: 1680 ± 310 mmHg[155] and compliance: 4.4 ± 0.8 %/mmHg x 10^{-4} [151]). These results suggest the potential for improved arterial matching through modulation of graft fabrication parameters.

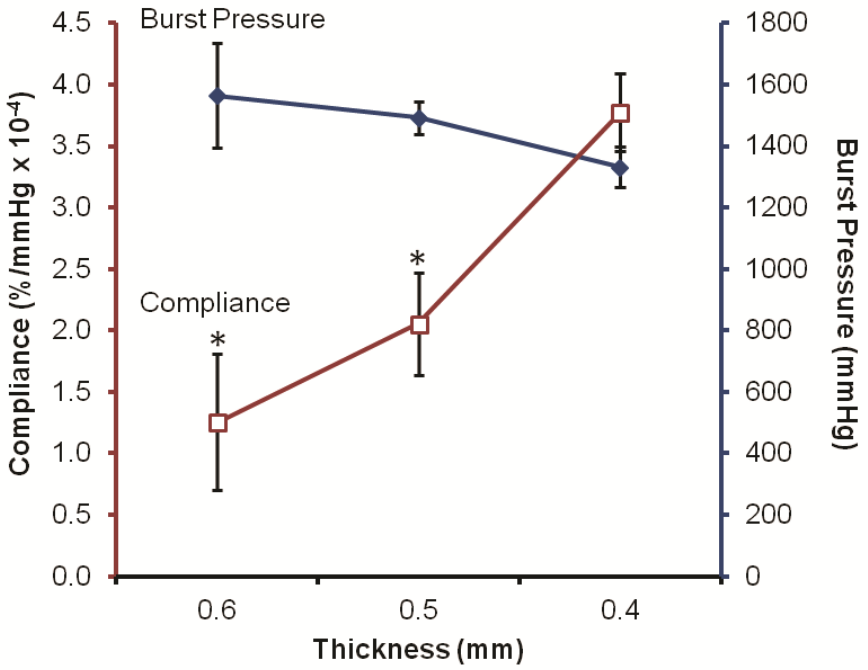

Figure 3.8. Biomechanical properties of Carbothane meshes with varying thicknesses (□ compliance and ♦ burst pressure). Note: decreasing thickness from left to right. *statistically different from 0.4 mm ($p<0.01$)

3.3.4.2. Effects of Fiber Tortuosity

The biomechanical properties of grafts with decreased tortuosity and fusions compared to control electrospun meshes are summarized in **Figure 3.9**. An increase in burst pressure and corresponding decrease in compliance were observed in the grafts with decreased tortuosity. Burst pressure was improved to 2190 ± 110 mmHg compared to 1330 ± 70 mmHg for the control, which also exceeded the saphenous vein autograft. Compliance decreased from the as-spun control values of 3.8 ± 0.3 %/mmHg x 10^{-4} to 2.6 ± 1.3 %/mmHg x 10^{-4}. Electrospun fiber meshes have been described as tortuous networks which transform into interconnected web-like architectures when strained.[176]

These tortuous fibers were observed to change their direction of orientation under an applied load. Therefore, we hypothesized that tortuous fibers have the ability to elongate under small applied loads before being constrained by fiber junctions, resulting in increased compliance. In this case, the increased burst pressure and decreased compliance observed with decreased tortuosity was attributed to the increased alignment of the fibers. These findings are supported by literature reports that aligned fibers have increased modulus and tensile strength (properties correlating to decreased compliance and increased burst pressure) compared to randomly oriented fibers when stressed in the direction of alignment.[90]

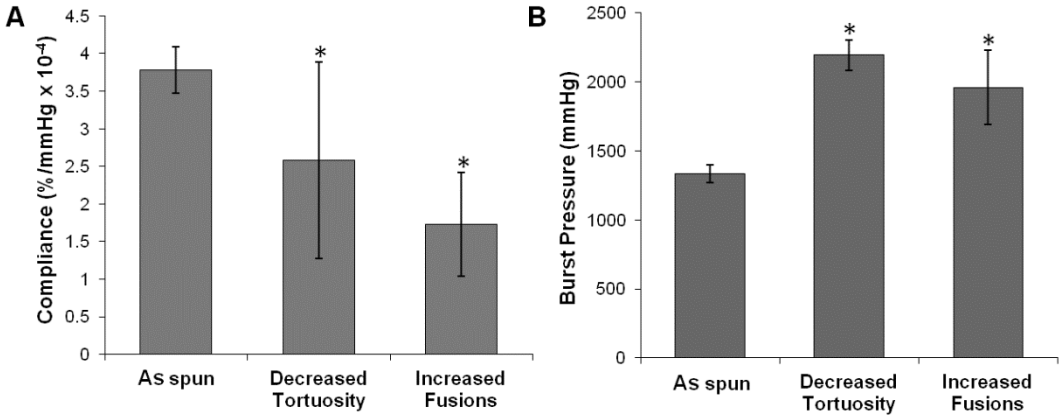

Figure 3.9. (A) Compliance and (B) burst pressure of Carbothane grafts with decreased tortuosity and fusions compared to control grafts. Electrospun meshes are all 0.4 mm thick. *statistically different from controls ($p<0.01$)

3.3.4.3 Effects of Fiber Fusion

Biomechanical testing of grafts with solvent-induced fusions created via incubation in DMAc vapor resulted in increased burst pressure and decreased

compliance. Burst pressure greater than the saphenous vein autograft and the as-spun control was achieved in the meshes with increased fiber fusion (1960 ± 270 mmHg). As expected, there was a decrease in compliance from the as-spun control value of 3.8 ± 0.3 %/mmHg x 10^{-4} to 1.7 ± 0.7 %/mmHg x 10^{-4}. Literature has shown that increased amount of fiber intersections results in increased modulus and ultimate elongation in the circumferential axis of a tubular graft.[92-94] The induction of fiber fusions introduces a physical connection between fibers with chain entanglements that restricts dilation and results in increased burst pressure.

The biomechanical properties of the heat-treated electrospun grafts are summarized in **Figure 3.10**. Heat treatment resulted in an increase in compliance to 6.0 ± 0.6 %/mmHg x 10^{-4} and an increase in burst pressure to 2260 ± 160 mmHg.

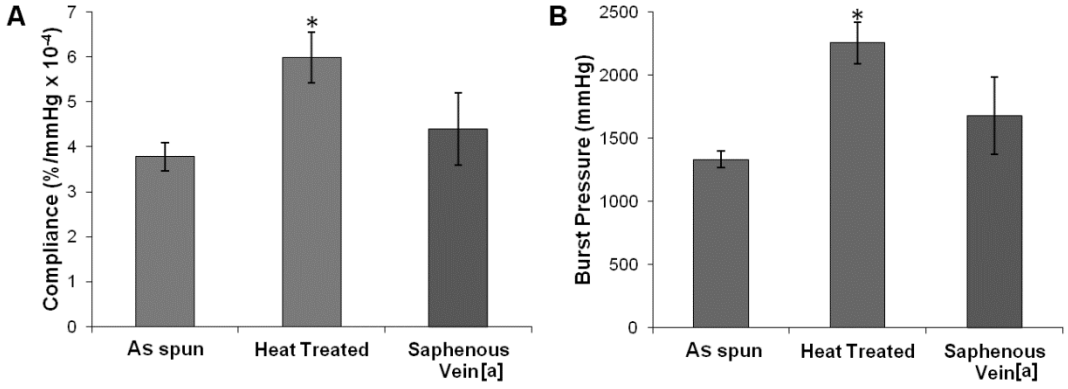

Figure 3.10. (A) Compliance and (B) burst pressure of Carbothane grafts with and without heat treatment compared to the saphenous vein. *statistically different from control ($p<0.01$). [a] values from Salacinski, et al. "The mechanical behavior of vascular grafts: a review." *Journal of Biomaterials Applications* 2001;15:241.

By fabricating heat-induced fusions into electrospun meshes, a vascular graft with both compliance and burst pressure that exceeded the saphenous vein autograft was achieved. Burst pressure increases similarly to the grafts with fusions via solvent vapor; however, the increase in compliance observed was attributed to changes in the polyurethane morphology. It is well established that thermal annealing provides energy to alter polyurethane microphase morphology.[170,177] Dynamic mechanical analysis (DMA) was used in this study to examine the effect of heat treatment on polyurethane phase morphology. Storage moduli of as-spun grafts, heated for 12 hours, heated for 24 hours, and with solvent-induced fusions are summarized in **Figure 3.11**. Both the as-spun and solvent induced fusions storage moduli were characterized by a lower plateau modulus, broad T_g transition, and melting transition (T_m) from 30-40 °C attributed to melting of crystalline soft domains.[178] In contrast, the heat-treated meshes exhibited a higher plateau modulus, sharper T_g transition, and reduced (12 hr) or eliminated (24 hr) melting transition. These data indicate a reduction in soft segment crystallinity and an increase in phase separation in the electrospun meshes after heat treatment which was not observed for meshes with solvent-induced fiber fusions. This reduction in soft segment crystallinity was confirmed using DSC. Minimal change in crystallinity was observed after 12 hr heat treatment whereas a reduction in crystallinity and formation of higher order crystals occurs after 24 hr heat treatment, **Figure 3.12**. Formation of higher order crystals after heat treatment is consistent with annealing studies of semi-crystalline polymers.[179,180] Annealing of semi-crystalline polymers results in a modification of crystal segments through lamellae thickening and partial melting/recrystallization.[181] As

heat treatment for 12 hours was insufficient to result in these morphological changes in the soft segment crystal structure, heating for 24 hours was employed to improve crystal structure and resultant graft biomechanical properties.

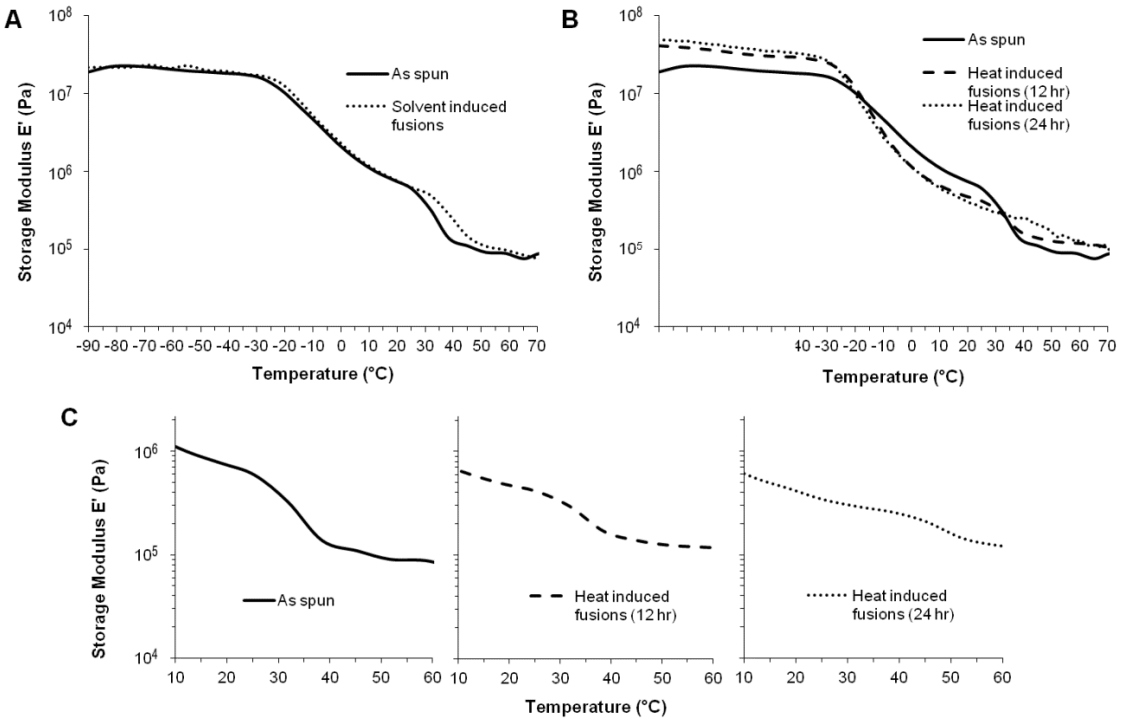

Figure 3.11. Storage moduli of electrospun Carbothane grafts (A) with solvent-induced fusions and (B) heat-induced fusions. (C) Change in melting transition with heat treatment.

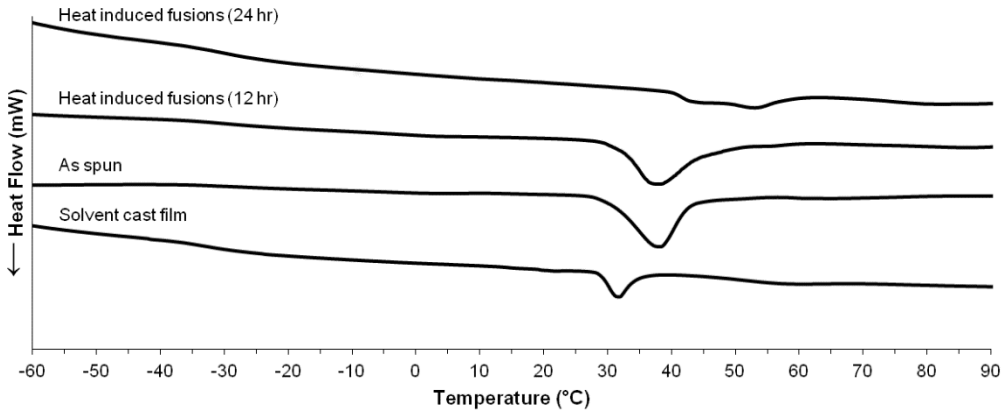

Figure 3.12. Differential scanning calorimetry thermograms of heat treated Carbothane electrospun meshes compared to as spun and neat film controls.

Previous studies have reported soft segment crystallization of electrospun polycaprolactone polyurethanes due to alignment of polymer chains during the electrospinning process.[182,183] We hypothesize that similar soft segment crystallization of the electrospun polyurethane grafts in these studies could introduce rigid physical crosslinks that are lost upon heat treatment, resulting in a more compliant graft. This is supported by the loss of the melting transition after heat treatment and was confirmed using DSC. Compared to a solvent cast film, as spun electrospun meshes have greater soft segment crystallinity and higher order crystals, **Figure 3.12**. In addition, electrospinning results in poor phase separation of polyurethanes due to rapid drying of the fibers which does not provide sufficient time for well-ordered hard domains to form.[182,183] The increased phase separation indicated by the reduction in Tg breadth after annealing was hypothesized to result in decreased modulus which we previously correlated to an increase in compliance. The effects of heat treatment can also be

contributed to a loss of molecular orientation within individual fibers. Literature reports that molecular orientation in the fiber direction occurs due to the high elongational forces and high draw ratio during electrospinning. In crystalline polymers, this orientation facilitates crystallization in the fiber directions, which opposes relaxation upon fiber deposition and locks in the molecular orientation. Therefore, heat treatment not only partially melts electrospun strain-induced crystals, but relaxes polymers chains, allowing new crystals to form and/or rotating existing crystals into an unoriented state. The 24-hour heat treated grafts show decreased crystallinity from the as spun grafts and are hypothesized to have reduced molecular orientation. This correlates to the observed increased in compliance. Thus, compliance increases with a loss of crystal orientation, decreased crystallinity, and increased phase separation.

Due to the fact that the melting transition in the DMA thermograms of these electrospun grafts occurs near physiological temperature, additional tests to assess biomechanical properties in a warm room at 37 °C and 100 % were performed. This test would elucidate any potential changes in properties that would occur when implanted. Both as spun grafts and grafts with heat induced fusions (24 hr) were tested. As spun control compliance increased from the room temperature controls to 6.7 ± 1.5 %/mmHg x 10^{-4} and burst pressure decreased to 1220 ± 460 mmHg. Grafts with heat induced fusions had a compliance of 7.2 ± 1.4 %/mmHg x 10^{-4} and a burst pressure of 1530 ± 140 mmHg when tested in physiological conditions (**Figure 3.13**).

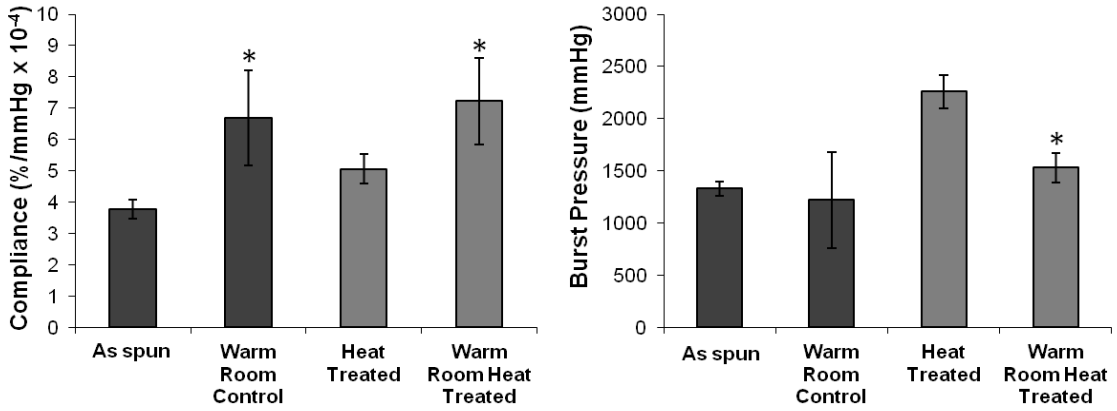

Figure 3.13. Compliance and burst pressure of Carbothane grafts tested in a warm room (37 °C, 100% humidity) compared to their respective controls. *statistically different from control ($p<0.01$).

Increased compliance is attributed to loss of molecular orientation and a lower modulus at elevated temperature. The control grafts maintained burst pressure when tested in the warm room. It would be expected that the lower modulus at elevated temperature would result in a lower burst pressure; however, this is counteracted by the increase in fiber fusions which contributes to an increase in burst pressure. Under the given conditions, these two opposing actions resulted in burst pressure comparable to room temperature-tested controls. Due to the fact that the heat treated grafts tested in the warm room already had induced fusions at 50 °C, testing in the warm room likely has minimal effect on increasing fiber fusion. As a result, the lower modulus at elevated temperatures would have a greater contribution to the burst pressure, as evidenced by the DMA curves (**Figure 3.14**). This is observed as a decreased burst pressure compared to the room temperature-tested, heat treated controls.

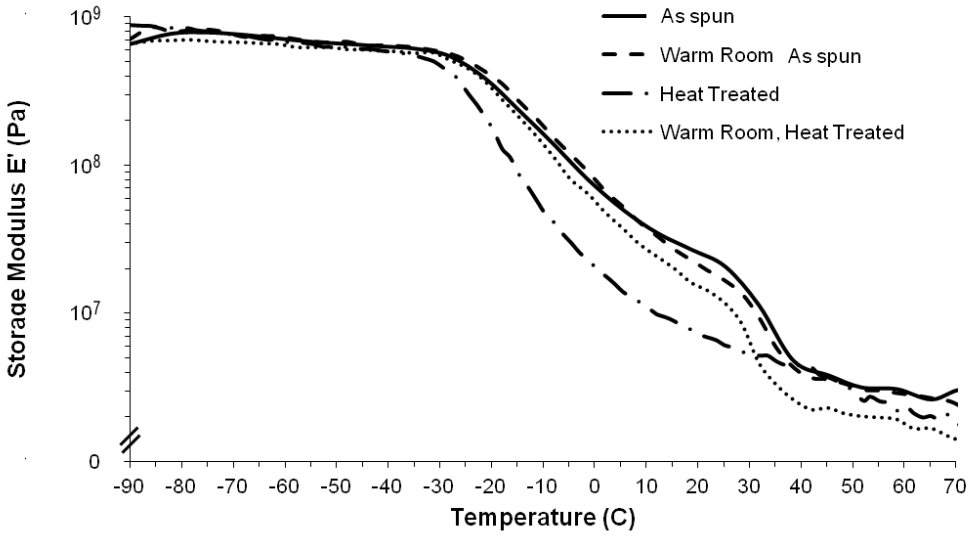

Figure 3.14. Storage moduli of as-spun and heat treated electrospun Carbothane grafts tested at room temperature or in a warm room (37 °C, 100% humidity)

Overall, the observed increase in compliance was attributed to a morphological change (increased phase separation, reduced soft segment crystallinity, loss of molecular orientation) and the increase in burst pressure was attributed to a change in mesh microarchitecture (increased fiber fusions via heating). To the best of our knowledge, this is the first record of a small diameter vascular graft with both compliance and burst pressure exceeding the saphenous vein autograft.

3.3.4.4. Effects of Conditioning

Grafts conditioned at 120 and 230 mmHg pulsatile pressure both exhibited an increase in both compliance and burst pressure compared to the control. Conditioning at 120 mmHg resulted in a compliance of 6.7 ± 0.8 %/mmHg x 10^{-4} and a burst pressure of

1570 ± 100 mmHg. Conditioning at 230 mmHg resulted in a compliance of 7.5 ± 0.6 %/mmHg x 10^{-4} and a burst pressure of 1670 ± 250 mmHg (**Figure 3.15**).

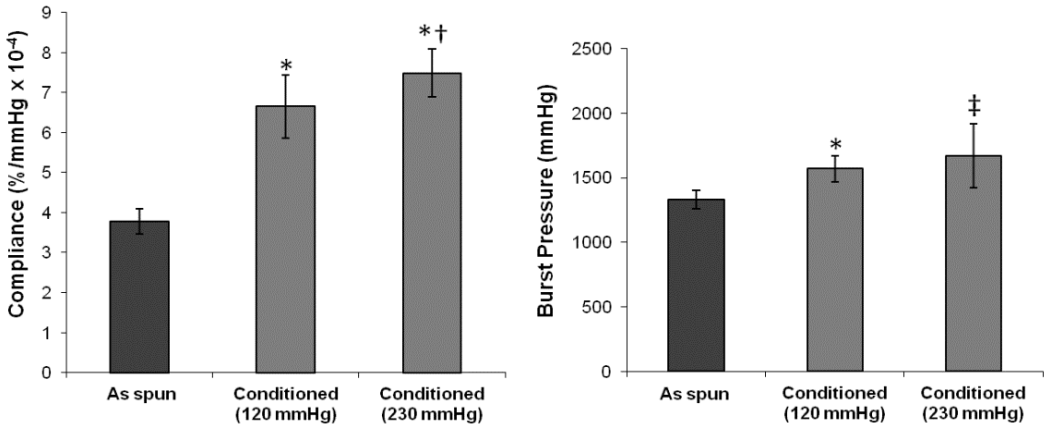

Figure 3.15. Compliance and burst pressure of Carbothane grafts with conditioning at 120 or 230 mmHg compared to as-spun controls. *statistically different from control ($p<0.01$), †statistically different from 120 mmHg conditioned ($p<0.01$), ‡statistically different from control ($p<0.07$).

The increase in compliance after both conditioning treatments can be attributed to a loss in molecular orientation due to the immersion in 37 °C water during the conditioning as well as prevention of higher order crystal formation. DSC thermograms of grafts subjected to 37 °C without conditioning show that higher order crystals are formed when subject to this heat treatment. When compared to the DSC thermograms of conditioned meshes, this higher order crystal peak is either reduced (120 mmHg) or eliminated (230 mmHg), **Figure 3.16**. This suggests that the conditioning pressure prevents formation of the higher order crystal population, and that as pressure increases, fewer higher order crystals are able to form. A summary of DSC enthalpies and transition temperatures is

displayed in **Table 3.3**. The slight increase in burst pressure is attributed to increased fiber fusions that occur when subject to 37 °C during the conditioning cycles (**Figure 3.17**).

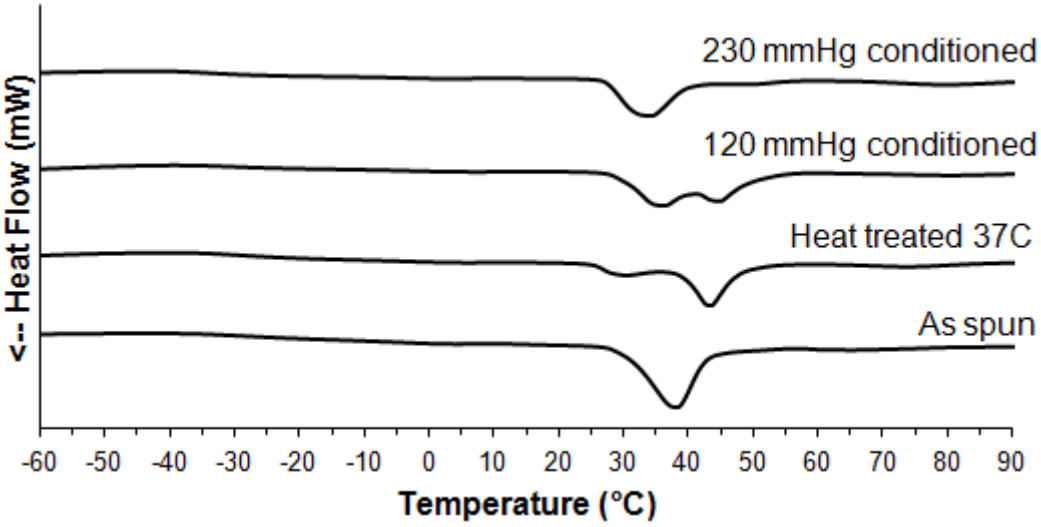

Figure 3.16. DSC thermograms of Carbothane grafts subject to different treatments.

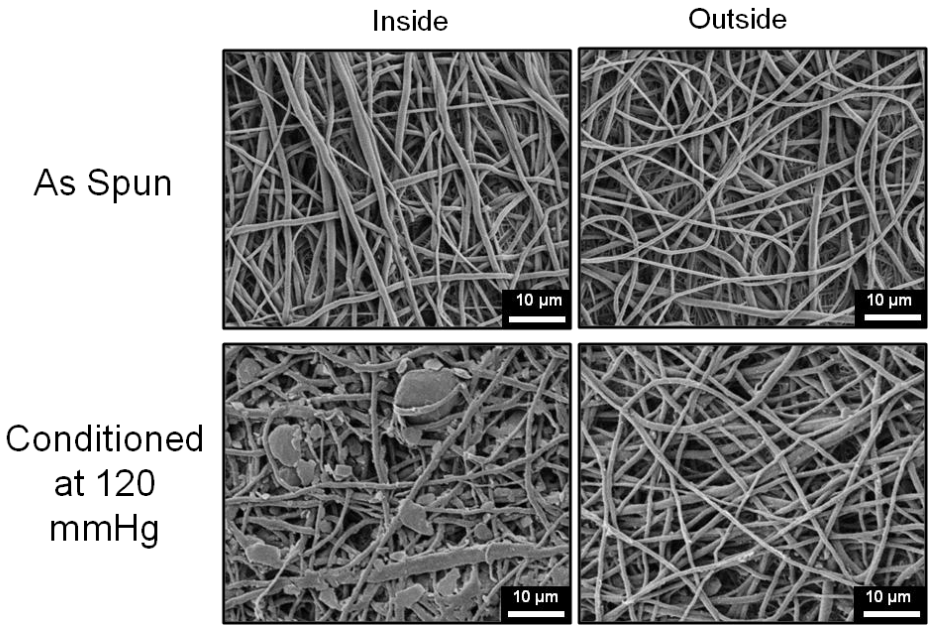

Figure 3.17. Scanning electron micrographs of as-spun and conditioned (120 mmHg) Carbothane grafts

A final vascular graft composition was conditioned at 120 mmHg while immersed in 37 °C water and evaluated for biomechanical properties at 37 °C and 100 % humidity. This treatment was selected as it most closely resembles the conditions upon implantation. These grafts had a compliance of 6.8 ± 0.7 %/mmHg x 10^{-4} and a burst pressure of 1170 ± 120 mmHg (**Figure 3.18**). Decreased burst pressure in the warm room has been attributed to a lower modulus of the grafts at higher temperatures.

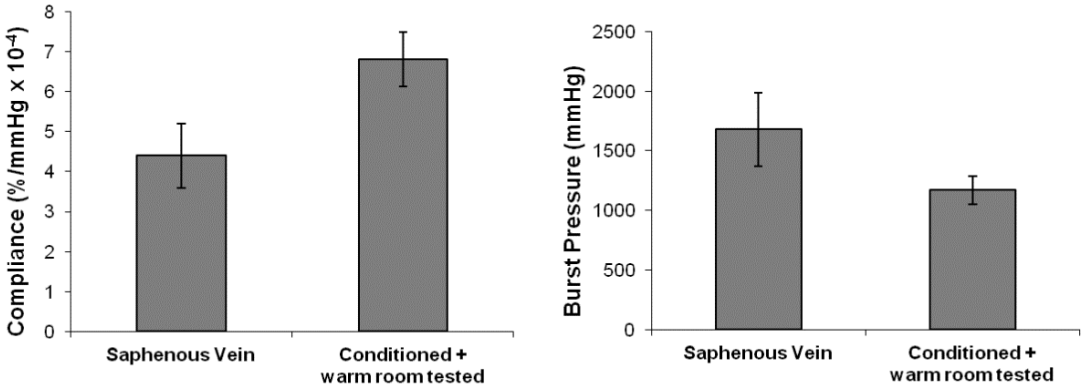

Figure 3.18. Compliance and burst pressure of Carbothane grafts with conditioning (120 mmHg) and tested in a warm room (37 °C, 100% humidity).

Table 3.3. Enthalpies and melting temperatures calculated from DSC thermograms.

Mesh	***ΔH (J/g)***	***Tm (°C)***	***Tm 2 (°C)***
Solvent cast film	3.949	31.68	-
As spun	17.81	38.13	-
Heat treated (12 hrs)	15.05	37.75	-
Heat treated (24 hrs)	4.669	42.81	52.71
Heat treated (37 °C)	14.10	30.04	43.53
Warm room, as spun	19.65	37.09	-
Warm room, heat treated	24.74	37.49	
120 mmHg conditioned	14.81	36.07	44.90
230 mmHg conditioned	13.44	33.97	-

3.4. Conclusions

These studies illustrate methods to fabricate electrospun vascular grafts with improved compliance while maintaining sufficient burst pressure by altering segmented polyurethane chemistry and electrospun mesh microarchitecture. Tensile testing and electrospun graft biomechanical testing elucidated relationships for rational selection of polymers based on commonly reported tensile properties. A polymer with low modulus

and high tensile strength correlated to a vascular graft with high compliance and burst pressure. The effects of mesh thickness, fiber tortuosity, and fiber fusions at junctions on biomechanical properties were investigated to identify microarchitecture variables that have the most profound effect on biomechanical properties. Heat treatment was identified as the most promising method to enhance both compliance and burst pressure by enhancing microphase separation and inducing fiber fusions. In this way, an electrospun small diameter synthetic vascular graft with compliance and burst pressure exceeding the saphenous vein autograft was fabricated for the first time. This graft has the potential to reduce intimal hyperplasia associated with low compliance in synthetic grafts and improve long term clinical success. Additionally, the fundamental relationships between electrospun mesh microarchitecture and mechanical properties identified in this work can be utilized in various tissue engineering applications.

CHAPTER IV

CO-ELECTROSPUN SCAFFOLDS CONSISTING OF *IN SITU* CROSSLINKED GELATIN AND A BIODEGRADABLE POLYURETHANE UREA

4.1. Introduction

Electrospinning has gained popularity in recent years as a technique to fabricate nonwoven fibrous scaffolds with high porosities, large surface area-to-volume ratios, and nano- to micron-sized fiber diameters.[17,163,164] To generate these scaffolds, a polymer solution is pumped at a constant rate through a needle tip that is placed a set distance away from a grounded or oppositely charged collector. When a voltage is applied at the needle tip, the droplet erupts into a liquid jet that narrows and solidifies during flight to be collected as a fiber.[17] The relative ease of modulating fiber architecture through variation of processing, solution, or environmental parameters provides a means to tune cell growth, degradation rate, and mechanical properties. For example, fiber alignment and fiber diameter have been shown to influence mechanical properties.[31,123,124,165] As a result, control over electrospun fiber morphology is an important factor in scaffold design. By utilizing the high tunability of electrospun scaffolds, properties can be tailored to meet specific design criteria of a variety of clinical applications from the high tensile strength to the flexibility of skin grafts. To improve the regeneration potential of these grafts, the research has focused on the development of methods to incorporate bioactive molecules that promote and guide cell growth and differentiation.

Bioactive materials have a positive effect on living cells and include minerals, growth factors, and proteins/peptides. Gelatin, a natural polymer derived from collagen, has been utilized for tissue engineering and has been shown to enhance cell adhesion and proliferation[184,185] Crosslinking of gelatin is necessary for implementation as a tissue engineering scaffold to prevent dissolution and retain the 3-dimensional structure. The most commonly implemented technique for crosslinking gelatin is via exposure to glutaraldehyde vapor. Glutaraldehyde is an undesirable crosslinker due to the risk of toxic residues[186-188] and because it has been associated with calcification *in vivo*.[189-191] Glutaraldehyde crosslinking of gelatin fibers and subsequent immersion in water typically causes the mesh to swell and gel unless high concentrations are used, which can contribute to an increased risk of toxicity due to residual crosslinker.[186,192] To overcome these limitations, 1-ethyl-3-(3-dimethylaminopropyl)carbodiimide hydrochloride (EDC) has been investigated and is advantageous as a zero-length cross-linking agent.[193,194] Genipen, a molecule isolated from gardenia fruits, has also been utilized for crosslinking of natural polymers and has displayed a greater biocompatibility than glutaraldehyde.[195,196] Significant work has been devoted to improving biocompatibility of crosslinked gelatin; however, there has been minimal emphasis on retaining the original fiber morphology of electrospun gelatin scaffolds post-crosslinking. Numerous researchers report enlarged, swollen, and/or fused fibers after their chosen crosslinking procedure.[197-199] As it is well established that the fiber morphology has a large influence over scaffold mechanical properties, degradation rate,

and cell behavior, maintaining fiber morphology post-implantation is necessary for design of scaffolds with and predictable properties.

In addition, gelatin scaffolds have relatively weak mechanical properties that necessitate additional modification to make them suitable for implantation in many applications. Strong and tunable mechanical properties are necessary for ligament/tendon grafts which require a strong material with good fatigue life to withstand daily motion or a wound dressing needs a material that is strong, elastic, and flexible to conform to skin.[200] Synthetic polymers have good mechanical properties but have poor cell affinity due to a lack of cell recognition sites. A scaffold that combines the mechanical properties of synthetic polymers with the bioactivity of gelatin offers distinct advantage as improved tissue engineering scaffolds. Biazar et al. reported that poly(3-hydroxybutyrate-co-3-hydroxyvalerate) (PHBV) fiber meshes coated with gelatin showed improved wound closure *in vivo*.[201] Methods utilized to confer bioactivity to synthetic electrospun scaffolds include fiber blending,[98,185,200,202-206] fiber coating,[201] co-axial electrospinning,[77,207] and addition of small peptides.[208-210] Blending small molecules or natural polymers into synthetic fibers often results in reduced mechanical properties.[200,203] Fibers coated with natural polymers are typically uncrosslinked and the coating quickly dissolves, resulting in a rapid loss of bioactivity. The high cost of small peptides and their lack of 3-dimensional structure make addition of small peptides unsuitable for large-scale fabrication. Co-electrospinning from two offset spinnerets has been demonstrated as a facile technique to confer bioactivity without sacrificing mechanical properties.[211]

This work describes a method for *in situ* crosslinking of gelatin to fabricate electrospun meshes with controlled bioactivity to direct tissue regeneration and improved fiber morphology retention upon implantation. A double barrel syringe with an attached mixing head and a diisocyanate crosslinker were utilized to generate these scaffolds. The effects of increasing crosslinker ratio on tensile properties and fiber morphology after immersion in water were investigated. To fabricate a scaffold with strong, highly tunable mechanical properties as well as the desired cellular viability and adhesion, these bioactive gelatin fibers were co-electrospun with a biodegradable synthetic polyurethane urea (B-PUR). Segmented polyurethanes have tunable properties via material chemistry and phase morphology[161,162,170] that provide a highly elastic, strong material to replace tissue properties and prevent catastrophic failure. Confocal fluorescence microscopy was utilized to confirm the presence of two fiber populations and scanning electron microscopy was used to characterize overall fiber morphology. Finally, hydrated tensile properties as well as human mesenchymal stem cell viability and adhesion were quantified on co-electrospun meshes to evaluate their potential as tissue engineering scaffolds.

4.2. Materials and Methods

4.2.1. Materials

All chemicals were purchased from Sigma-Aldrich and used as received unless otherwise stated.

4.2.2. Biodegradable Poly(ether ester urethane)urea (B-PUR) Synthesis

Poly(ethylene glycol) (PEG, MW 400 Da) was azeotropically dried at 90 °C with toluene under vacuum to remove residual water before use. Poly(ε-caprolactone) (PCL, MW 530 Da) was dried under vacuum for 48 hours to remove residual water before use. N,N-dimethylforamide (DMF) was dried over molecular sieves.

Poly(ethylene glycol) diisocyanate (PEG-DI) was synthesized in bulk by adding PEG (0.02 mol) diol dropwise (1 drop per 10 seconds) via addition funnel into a three-neck round bottom flask charged with hexamethylene diisocyanate (0.06 mol) under a nitrogen atmosphere at 75 °C for 5 hours. The completion of the reaction was confirmed using Fourier transform infrared spectroscopy (FTIR) by the disappearance of the hydroxyl peak at 3515 cm^{-1}. The PEG-DI was then washed three times with hexane (30 mL per 10 g of product) to remove any unreacted HDI. The final product was placed under high vacuum overnight before use.

A poly(ether ester) triblock (PCL–PEG–PCL) was synthesized by reacting PEG-DI (0.027 mol) with PCL (0.055 mol) in 10 wt% DMF with 0.2 wt% stannous octoate. The triblock was prepared by adding PCL with stannous octoate dropwise to the solution of PEG-DI under a nitrogen atmosphere and continuous stirring. Polymerization was carried out at 80 °C for 15 hours. The solution was then transferred into an addition funnel via cannula to minimize exposure to air for the poly(ether ester urethane) urea synthesis.

The biodegradable poly(ether ester urethane)urea (B-PUR) was synthesized under a dry nitrogen atmosphere in a 2000 mL three-necked round bottom flask using a

two-step solution. The reactant stoichiometry was 4.4:1:4.4 of HDI:triblock:diamine chain extender. A 10 wt% solution of HDI in DMF was continuously stirred via overhead stirrer while a 10 wt% solution of triblock diol in DMF was added dropwise with 0.2% stannous octoate in the first polymerization step. The mixture was allowed to react at 80 °C until no change in the hydroxyl stretch was observed via FTIR (5 hours). The prepolymer solution was cooled to room temperature and isopropyl alcohol (50% v/v) was added to flask. The addition of IPA was used to prevent gelation upon the reaction with the diamines by disrupting hydrogen bonding sites.[212] A solution of 50/50 (mol/mol) of 1,3-diaminopropane and 1,2-diaminopropane in 10 wt% DMF was then added dropwise while stirring for chain extension. The reaction was continued at room temperature for 1 hour resulting in a poly(ether ester urethane)urea with a ~30% hard segment. The polymer solution was precipitated in distilled water. Finally, the polymer was dried under vacuum under ambient conditions for 48 hours.

B-PUR films were prepared from an 18 wt% solution in 2,2,2-triflouroethanol (TFE) and cast onto a glass dish. The solvent was evaporated under vacuum at room temperature for 2 days. The resulting 0.25 mm thick films obtained were sectioned for subsequent characterization.

4.2.3. Fourier Transform Infrared (FTIR) Spectroscopy

B-PUR solutions in TFE (5 wt%) were cast onto KBr pellets and placed under vacuum for 1 hour under ambient conditions to remove all solvent. B-PUR chemical structure was confirmed using Fourier transform infrared (FTIR) spectroscopy. Spectra

were recorded using a Bruker ALPHA FTIR spectrometer with 2 cm^{-1} resolution and 64 scans.

4.2.4. Gel Permeation Chromatography (GPC)

B-PUR specimens were dissolved in 0.1 M LiBr DMF/IPA 50/50 (v/v) at 5 mg/mL and incubated at 70°C for 6 hours with mild agitation then filtered using a 0.22 µm filter. B-PUR molecular weights were determined by gel permeation chromatography (GPC Max, Viscotek, Malvern, PA) equipped with two columns (Phenomenex) with 10^3 and 10^5 Å diameter pores using monodisperse polystyrene standards. Measurements were made with 0.05 M LiBr DMF as the eluent at 80 °C and a flow rate of 1 mL/min and refractive index response.

4.2.5. Dynamic Mechanical Thermal Analysis (DMTA)

Specimens (n=3) for dynamic mechanical thermal analysis (DMTA) were prepared from electrospun meshes cut into 5.5 mm × 40 mm strips with the long edge aligned with the longitudinal axis of the graft. Storage and loss moduli as a function of temperature were measured using a TA RSA III dynamic mechanical analyzer in tensile mode. All specimens were subject to an oscillatory strain of 0.1% at a frequency 1 Hz and were scanned from -90 to 150 °C at 5 °C/min.

4.2.6. Differential Scanning Calorimetry (DSC)

Differential scanning calorimetry (DSC) thermograms (n=2) were collected on specimens of approximately 10-15 mg which were subjected to a temperature ramp of -80 °C to 100 °C at a rate of 5 °C/min under nitrogen gas using a TA DSC Q100 (Houston, TX).

4.2.7. Electrospinning

In situ crosslinking of electrospun gelatin was performed using double barrel syringes (1:1 barrel ratio) (Nordson EFD) with attachable mixing heads (3.1 mm ID x 53.5 mm length). One barrel was loaded with a 10 wt% solution of bovine-derived gelatin in 2,2,2-trifluoroethanol (TFE). A catalyst, 1,4-diazabicyclo[2,2,2]octane (DABCO), was added at 5 wt% of solids was added to the gelatin solution prior to loading the syringe. The second barrel was loaded with a solution of hexamethylene diisocyanate (HDI) in TFE. The concentration of HDI was varied such that the crosslinker density would equal a 1X, 5X, or 10X ratio of isocyanate/amine. For crosslinker ratio calculations, 11 lysines per gelatin molecule were assumed. A blunted 18 gauge needle was attached via a Luer-Slip fitting to the mixing head and the syringe was placed in a syringe pump (KDS100, KDScientific) set to a constant flow rate of 1.0 mL/hr. A high voltage of 10 kV (ES30P-5W/DDPM, Gamma Scientific) was applied at the needle tip and fibers were collected on a 6 cm square copper plate set 12 cm away from the needle tip. The front of the flat plate collector was covered with a thin latex film which facilitated removal of the mesh after deposition. Each mesh had a total collection time of 3 hours. Halfway through each run, the mixing head was replaced to avoid clogging due to crosslinking within the mixing head.

Co-electrospun meshes were fabricated by electrospinning the *in situ* crosslinked gelatin and B-PUR onto a negatively charged (-5 kV) rotating mandrel. The two spinnerets were placed perpendicular to the mandrel to minimize interaction of the electric fields. The B-PUR spinneret consisted of a glass syringe filled with an 18 wt%

solution of B-PUR in TFE/toluene 75/25 that was pumped in a syringe pump at a constant rate of 0.5 mL/hr. All electrospinning runs were performed at ambient conditions (20 °C, 45-55% relative humidity). Meshes were vacuum dried for a minimum of 12 hours prior to characterization.

4.2.8. Electrospun Fiber Characterization

Specimens (n=4) approximately 7 cm square were cut from the center of each fiber mesh to avoid edge effects. Fiber morphology was observed using scanning electron microscopy (SEM, Phenom Pro, NanoScience Instruments) at 10 kV accelerating voltage. Prior to imaging, specimens were coated with 4 nm of gold using a sputter coater (Sputter Coater 108, Cressingtion Scientific Instruments). Fiber characterization after immersion in water was performed by cutting circular punches (10 mm diameter) and placing each on a glass coverslip in a well plate. Punches were weighted to ensure immersion and the wells were filled with reverse osmosis water. Specimens were removed at 24 h, 48 h, 72 h, and 1 week timepoints, frozen at -80 °C overnight, and lyophilized prior to imaging with SEM.

Fluorescence microscopy of co-electrospun meshes (n=3) was performed using an inverted microscope (Nikon Eclipse TE2000-E) with a confocal fluorescence imaging system (Nikon D-Eclipse C1). The B-PUR solution was mixed with 2 wt% fluorescein and the gelatin solution was mixed with 0.1 wt% rhodamine B and co-electrospun onto a glass slide.

4.2.9. Tensile Testing

Dogbone specimens (n=4) were cut in accordance with ASTM D1708 and strained to failure at a rate of 100 %/min based on the initial gauge length using an Instron 3345 uniaxial tensile tester equipped with a 100 N load cell and pneumatic side action grips (Instron 2712-019). An environmental control chamber was attached such that simulated physiological conditions (37 °C and 100% humidity) were maintained throughout testing. Elastic modulus, tensile strength, and ultimate elongation were calculated from the resultant engineering stress/strain curves. A secant modulus based on 2% strain was calculated for elastic modulus and subsequently referred to as simply "modulus."

4.2.10. Cell Adhesion

Bone marrow-derived human mesenchymal stem cells (hMSCs) were obtained as Passage 1 in a cryovial from the Center for the Preparation and Distribution of Adult Stem Cells. Cells were cultured in growth media containing 16.5% fetal bovine serum (FBS, Atlanta Biologicals), 1% L-glutamine (Life Technologies) and Minimum Essential Media α (MEM α, Life Technologies) to 80% confluency and utilized at Passages 5. Adhesion analysis of hMSCs on electrospun *in situ* crosslinked gelatin (5X), electrospun B-PUR, and co-electrospun B-PUR/gelatin was conducted using the Live/Dead® Assay (Molecular Probes) to determine material cytocompatibility in comparison to glutaraldehyde crosslinked gelatin fibers. Specimens were sterilized for 3 hours in 70% ethanol, subjected to a wetting ladder to increase wettability, washed 4 times with PBS, and incubated overnight in MEM α at 5% CO_2, 37°C. The overnight

incubation was performed without serum to isolate the effect of the material alone on cell adhesion and viability; however, FBS was included in the culture media to simulate physiological conditions. Cells were seeded at 10,000 cells/cm^2 in growth media supplemented with 1 vol% penicillin-streptomycin and Live/Dead staining was performed at 24 and 72 hours. Cell adhesion was calculated from manual cell counts of images obtained through raster patterning of 4 specimens (n = 20) with a fluorescence microscope (Nikon Eclipse TE2000-S).

4.2.11. Statistical Analysis

The data are displayed as mean ± standard deviation for each composition. A Student's t-test was performed to determine any statistically significant differences between compositions. All tests were carried out at a confidence interval ($p<0.01$).

4.3. Results and Discussion

4.3.1. In Situ *Crosslinked Gelatin*

In situ crosslinking of electrospun gelatin was achieved using a double barrel syringe which enabled isolation of the gelatin and hexamethylene diisocyanate (HDI) individual solutions until mixing through a mixing head, **Figure 4.1**. Gelatin contains many primary amines on the lysine amino acids that react readily with isocyanates to form a disubstitued urea without heat. Previous methods for *in situ* crosslinking of gelatin relied on UV light near the electrospinning jet.[213] To the best of our knowledge, this is the first report of a double barrel syringe used to fabricate crosslinked electrospun fibers.

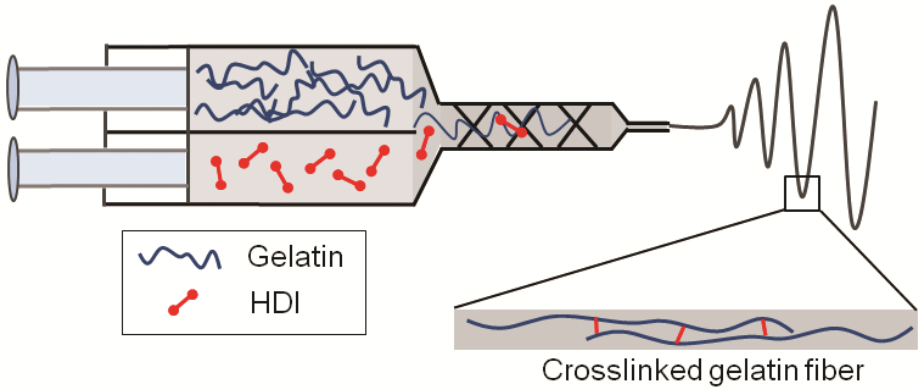

Figure 4.1. Schematic of double-barrel syringe setup for *in situ* crosslinking of gelatin during electrospinning

The crosslinker ratio (isocyanate/amine) was varied to evaluate the effect on fiber morphology retention and mechanical properties. At each crosslinker ratio tested, smooth, uniform fibers with similar fiber diameters were electrospun. The 1X mesh average fiber diameter was 0.74 ± 0.32 µm, 5X was 0.77 ± 0.17 µm, and 10X was 0.72 ± 0.29 µm. The fiber morphology after immersion in water for 1 week was characterized using SEM of lyophilized meshes, **Figure 4.2**. Large, flattened fibers, indicative of partial dissolution were observed for the 1X gelatin fibers. 5X and 10X meshes retained similar fiber diameters to their as spun counterparts with an increase in fiber fusion. Uncrosslinked gelatin fibers immersed in water exhibit a morphology characteristic of freeze dried scaffolds and glutaraldehyde crosslinked fibers show flattened and fused fibers indicative of dissolution. Compared to these controls, the 5X and 10X *in situ* crosslinked gelatin demonstrated an improved retention of fiber morphology. An excess of HDI likely improves crosslinking because coupling of HDI molecules would allow

longer crosslinks to form, whereas only one functional group may have reacted with gelatin in the 1X composition, leaving a free end. It is hypothesized that *in situ* crosslinking overcomes limitations of vapor crosslinking by initiating the crosslinking prior to leaving the needle tip rather than relying on diffusion through the polymer mesh. Various degrees of fiber morphology retention are reported in the literature using vapor crosslinking, likely due to the fact that it is difficult to control the amount and homogeneity of crosslinking. This is influenced by crosslinker transport which is dependent on mesh thickness. Diffusivity through the mesh is also decreased as the permeant interacts with functional groups on the polymer (crosslinks)[214] and as crosslink density increases throughout the process.[215] *In situ* crosslinking provides a more effective crosslinking strategy due to homogenous mixing at the needle tip prior to electrospinning.

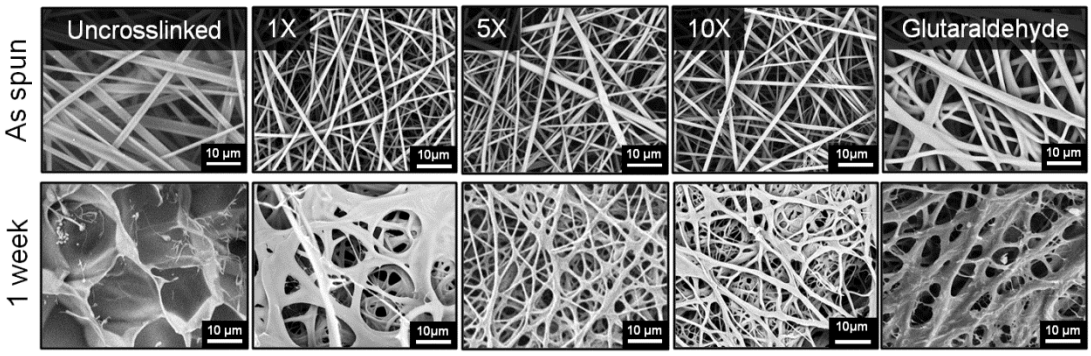

Figure 4.2. Scanning electron micrographs of *in situ* crosslinked gelatin with different crosslinker ratios (1X, 5X or 10X isocyanate to amine) compared to uncrosslinked and traditional glutaraldehyde crosslinked meshes, as-spun and after a 1 week incubation in water.

Tensile mechanical properties of *in situ* crosslinked meshes were tested in an environmental testing chamber that maintained temperature at 37 °C and humidity at 100% throughout testing in order to simulate physiological mechanical properties. Literature has reported that hydrated gelatin meshes have significantly different properties than dry.[216] Here, only hydrated properties were tested because these properties are clinically relevant for tissue engineering applications. The mechanical properties of 1X, 5X, and 10X crosslinked gelatin are summarized in **Figure 4.3** and **Table 4.1**. As crosslinker ratio increases, initial modulus and tensile strength increased while ultimate elongation decreased. A greater effect of crosslinker ratio was observed for 1X to 5X, compared to 5X to 10X. This suggests that the amount of available crosslinking sites is reduced and which limits the effect of increasing crosslinker.

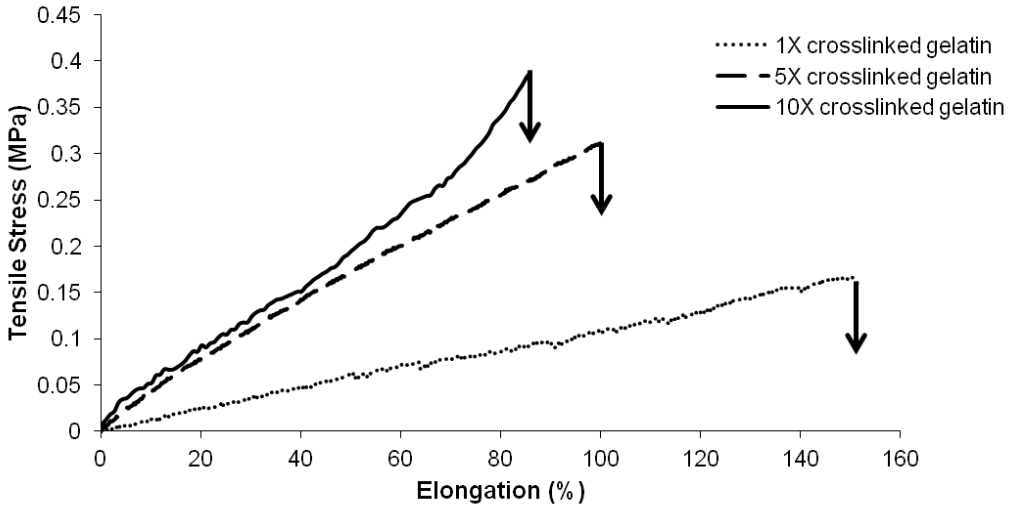

Figure 4.3. Tensile properties of *in situ* crosslinked gelatin with 1X, 5X, or 10X crosslinker ratio (isocyanate to amine).

Table 4.1. Tensile properties of *in situ* crosslinked gelatin with 1X, 5X, or 10X crosslinker ratio (isocyanate to amine).

Crosslinker Ratio	***2% Secant Modulus (MPa)***	***Ultimate Tensile Strength (MPa)***	***Elongation (%)***
1X	0.4 ± 0.2	0.2 ± 0.1	150 ± 10
5X	0.7 ± 0.3	0.3 ± 0.1	100 ± 30
10X	0.8 ± 0.3	0.5 ± 0.5	90 ± 40

4.3.2. Biodegradable Poly(ether ester urethane)urea (B-PUR) Synthesis

As *in situ* crosslinked gelatin meshes are fairly weak on their own, a biodegradable polyurethane was synthesized and co-electrospun with the 5X gelatin to confer improved mechanical properties. Traditionally, commercially available biodegradable polyurethanes and polyurethane ureas incorporate long polyester blocks which form crystalline domains. Soft segment crystalline domains contribute to the high modulus and strength observed for these polymers because they act as rigid physical crosslinks. A major limitation of crystalline polyurethanes is the large amount of permanent set due to deformation of the soft segment crystalline domains. Additionally, soft segment relaxation over time due to crystal melting results in a reduction in mechanical properties which can be detrimental in long term applications. Finally, degradation of polyurethanes can be hindered due to the soft segment crystals protecting hydrolytically labile chains within the crystal structure and reducing water penetration into the bulk.[217-221] As both degradation rate and mechanical properties are dictated by crystallinity, these properties are linked and cannot be independently tuned.

To circumvent these drawbacks, we synthesized a biodegradable polyurethane urea with a non-crystalline soft segment that retained the modulus and tensile strength typically observed with crystalline soft segments. The soft segment contained a triblock structure of PEG was encapped with PCL using a urethane linkage which was unable to crystallize due to the low number of PCL repeat units. This synthesis scheme detailed in **Figure 4.4** had a yield after purification above 93%.

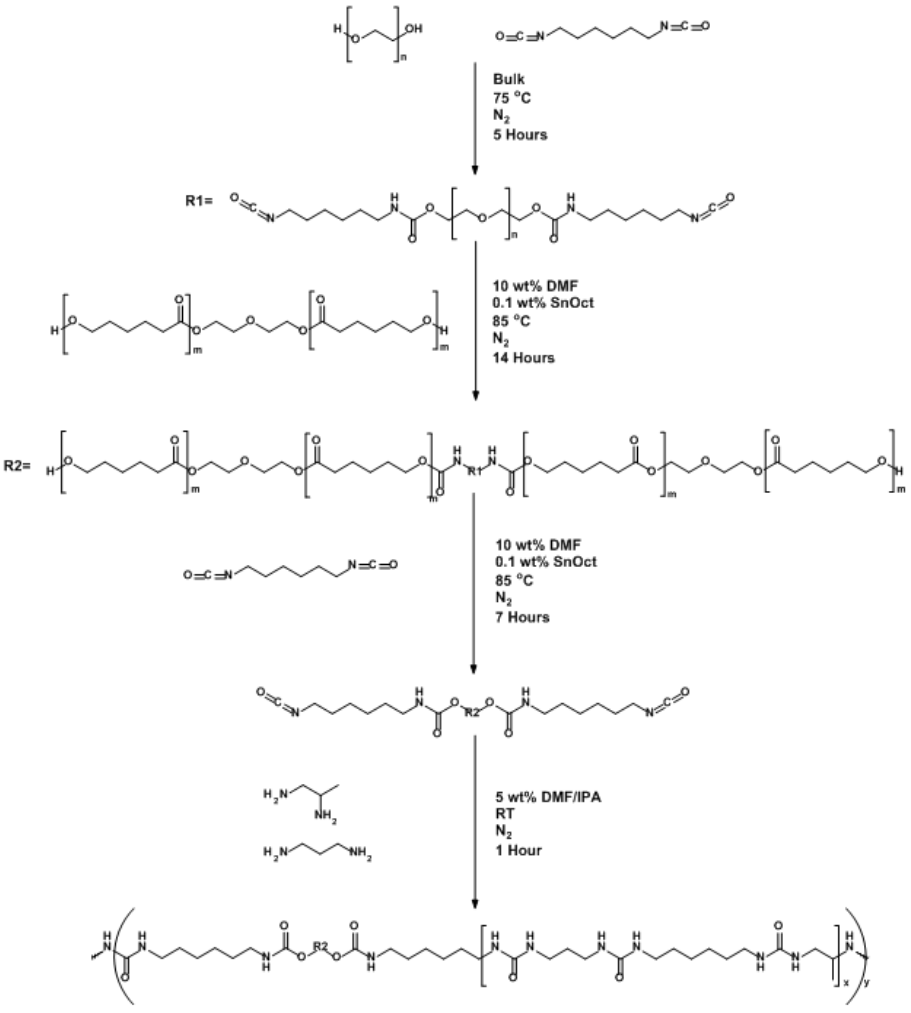

Figure 4.4. Biodegradable polyurethane (B-PUR) reaction scheme.

FTIR spectrum confirmed the structure of the B-PUR by the presence of the carbonyl or the ester/urethane peak at 1730 cm^{-1} and hydrogen bonded urea peaks at 1640 cm^{-1} (**Figure 4.5**). The soft segment structure was confirmed by the ether peak of the PEG at 1105 cm^{-1}. No unreacted isocyanates were detected by the absence of the isocyanate peak at 2267 cm^{-1}. GPC confirmed a weight average molecular weight of 143 kDa and PDI of 2.02 relative to polystyrene standards.

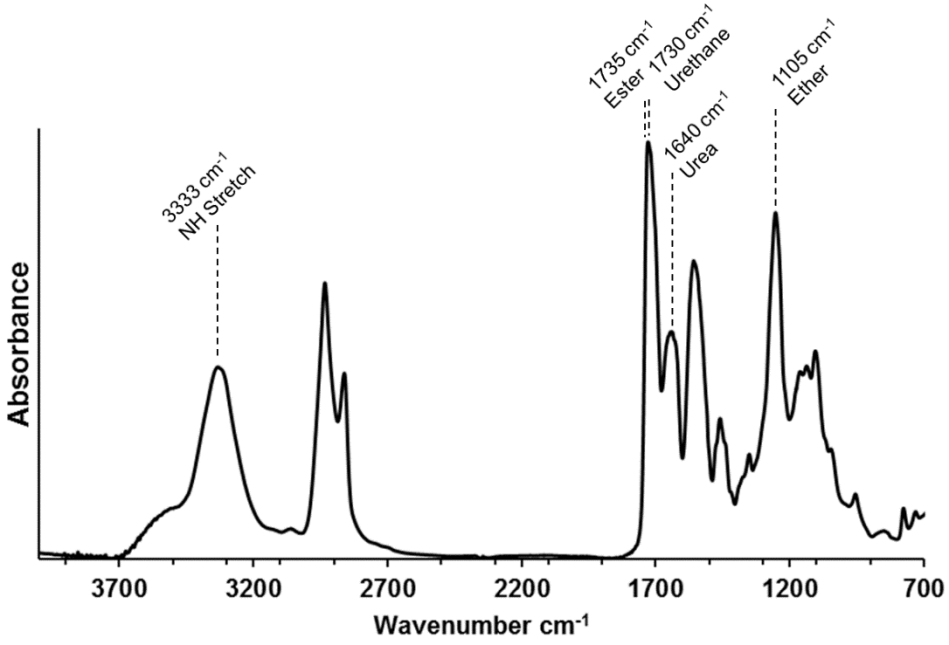

Figure 4.5. FTIR spectrum of the biodegradable polyurethane (B-PUR).

Mechanical and thermal analysis of B-PUR electrospun meshes is illustrated in **Figure 4.6**. Uniaxial tensile testing of the B-PUR films resulted in an initial modulus of 75 ± 7 MPa, tensile stress of 22 ± 2 MPa, and an elongation of 620 ± 44%. Strain hardening in the stress-strain plot was minimal due to the reduced ability of the soft segment to

crystallize under strain. DMTA of electrospun fibers displayed a two-phase polymer system with an α transition representing the glass transition temperature of the soft segment blocks. DSC confirmed the glass transition temperature at -39 °C and a lack of crystalline endotherms due to the triblock soft segment. High modulus and tensile strength similar to crystalline soft segment polyurethanes was achieved by chain extending with mixed diamines. This strategy creates a mixed registry that disrupts some hydrogen bonding sites in the hard segment but still allows for bi-dentate hydrogen bonding. Due to the strong bi-dentate hydrogen bonding, we were able to achieve high modulus and tensile strength without crystalline soft segments. Overall, we have synthesized a biodegradable polyurethane urea with high strength and elasticity that has the potential to temporarily replace tissue function.

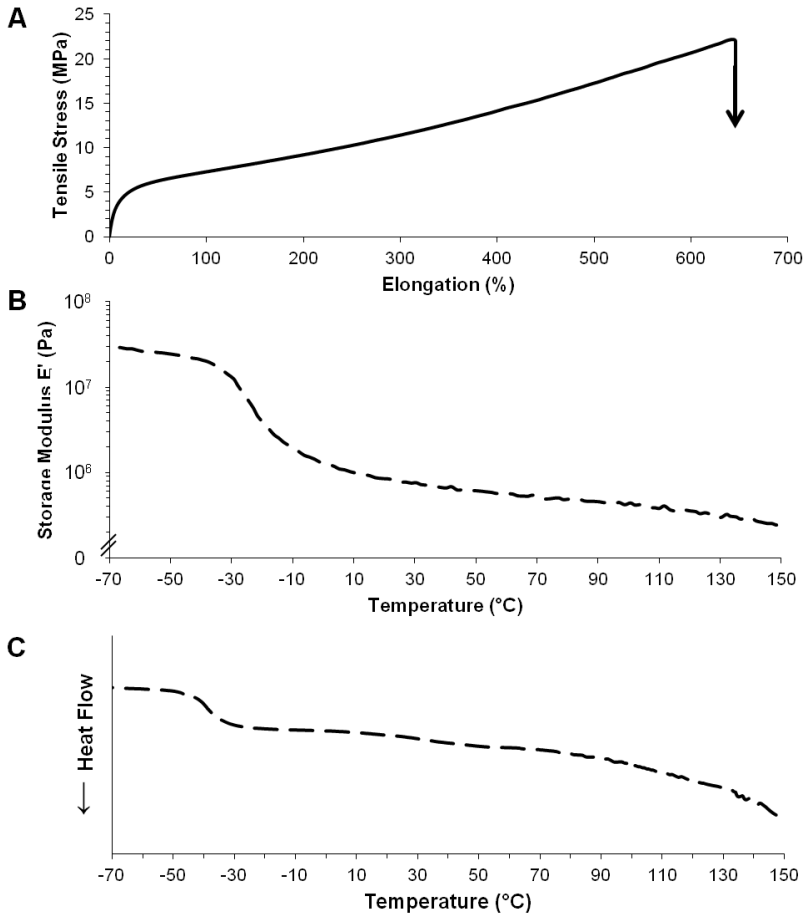

Figure 4.6. A) Tensile stress-strain plot of biodegradable polyurethane (B-PUR) film. B) Storage moduli of B-PUR electrospun fiber mesh. C) DSC thermogram of B-PUR fiber mesh.

4.3.3. Co-electrospun B-PUR/gelatin

Although the synthetic B-PUR has the strength to replace tissue function, it lacks cell recognition sites to support cell attachment and proliferation. Therefore, a composite scaffold that combines the strength of synthetic polymers with the bioactivity of gelatin would provide an improved scaffold for implantation. The most commonly reported composite fiber scaffold is fabricated by blend electrospinning of gelatin with

PCL;[98,185,206,222] however, few other synthetic polymers have been investigated with gelatin. These studies have reported a maximum tensile strength less than 1 MPa (~30% of pure PCL) and elongation under 200%.[98,206] Additionally, to heterogeneity within individual fibers due to phase separation between dissimilar polymers has been reported for blends of PCL with gelatin to collagen when the PCL content was increased above 30%, thus limiting the range of properties achievable with this system.[223-225] This issue has lead investigations to create a homogenous blend of gelatin and PCL through the addition of acetic acid; however, the blended gelatin hinders crystallization of the PCL which improves tensile strength to ~3 MPa while maintaining an elongation of ~200%.[226] This co-electrospinning technique is able to overcome this limitation by creating a mesh of individual gelatin and polyurethane fibers that retain their mechanical properties.

Successful co-electrospinning of B-PUR and 5X crosslinked gelatin was confirmed via fluorescence imaging. The 5X crosslinker ratio was chosen because it was the lowest ratio that demonstrated the best fiber morphology retention. As a result, this composition would have the greatest potential for good cytocompatibility *in vivo*. Representative images of co-electrospun meshes clearly identified two distinct and homogenously mixed fiber populations (**Figure 4.7**).

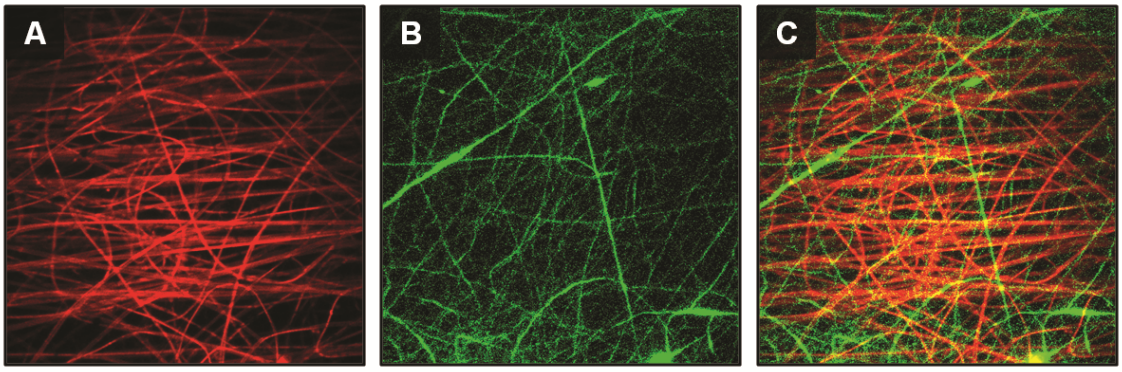

Figure 4.7. Confocal fluorescent images of co-electrospun mesh A) B-PUR only B) in situ crosslinked gelatin only and C) the combined co-electrospun mesh.

Tensile properties of co-electrospun meshes compared to B-PUR fiber meshes and 5X gelatin meshes are displayed in **Figure 4.8** and **Table 4.2**. B-PUR modulus, tensile strength, and elongation were reduced compared to the neat film, as expected based on literature reports for electrospun meshes;[103] however, the electrospun B-PUR mechanical properties were greater than those for the *in situ* crosslinked gelatin. Electrospun B-PUR had a modulus of 6.6 ± 1.9 MPa, tensile strength of 5.3 ± 0.1 MPa, and elongation of 140 ± 20%. Co-electrospun meshes had small increase in modulus and elongation compared to gelatin meshes, but with improved tensile strength to 0.8 ± 0.4 MPa. These properties are intermediate between the B-PUR and gelatin individual components as expected for a composite blend of fibers.[206] Gelatin/polyurethane blended fibers also displayed a slight increase in modulus and elongation with a greater increase in tensile strength compared to pure gelatin meshes.[200] Compared to these reports of gelatin/polyurethane blends, the co-electrospun meshes reported here had a slightly lower modulus, tensile strength, and elongation; however, we hypothesize that these

lower mechanical properties are a result of a low ratio of B-PUR/gelatin. Studies on gelatin/PCL fiber blends illustrate that mechanical response can be altered by varying compositional ratio.[227] As such, it is hypothesized that co-electrospun mesh tensile properties can be modified by altering the compositional ratio of the B-PUR and gelatin to tune the mechanical properties for different applications.

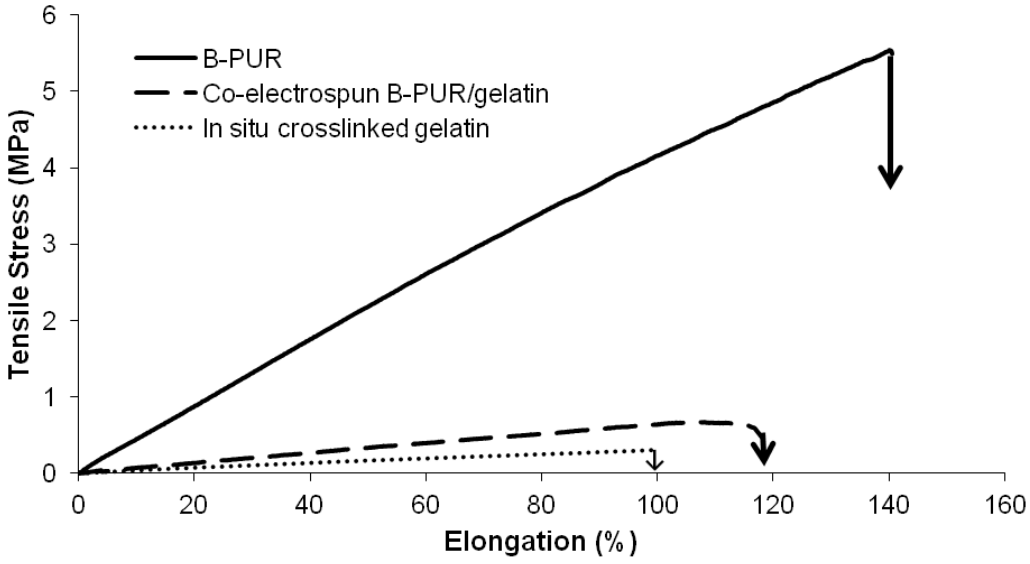

Figure 4.8. Tensile properties of biodegradable polyurethane (B-PUR), *in situ* crosslinked gelatin (5X), and the co-electrospun mesh.

Table 4.2. Tensile properties of biodegradable polyurethane (B-PUR), *in situ* crosslinked gelatin (5X), and the co-electrospun mesh.

Electrospun Mesh	***2% Secant Modulus (MPa)***	***Ultimate Tensile Strength (MPa)***	***Elongation (%)***
B-PUR	6.6 ± 1.9	5.3 ± 0.1	140 ± 20
In situ crosslinked gelatin	0.7 ± 0.3	0.3 ± 0.1	100 ± 30
Co-electrospun B-PUR/gelatin	1.2 ± 0.5	0.8 ± 0.4	110 ± 20

4.3.4. Cell Adhesion

Natural polymers are innately biocompatible, whereas synthetic polymers promote cell attachment via cell interactions with adsorbed protein. As a result, it was hypothesized that the addition of gelatin to the synthetic polymer mesh by co-electrospinning would improve the biocompatibility compared to the B-PUR alone. **Figure 4.9** portrays hMSC adhesion and representative fluorescent images on electrospun meshes. Stained cells appear adhered and spread on glutaraldehyde crosslinked meshes, *in situ* crosslinked meshes, and co-electrospun meshes. Very few cells were apparent on the B-PUR meshes and those that were had a balled morphology which justifies the low adhesion. Adhesion to the B-PUR meshes was low (12 ± 16 cells/mm^2, 72 h) but was improved with the addition of gelatin in the co-electrospun mesh to 38 ± 33 cells/mm^2. Low adhesion on synthetic polyurethanes which was improved with the attachment of an adhesion peptide has been reported in the literature.[228,229] The *in situ* crosslinked meshes exhibited similar cell behavior to the glutaraldehyde meshes with adhesion of 78 ± 44 and 71 ± 38 cells/mm^2, respectively.

These findings coincide with improved cell viability, adhesion, and proliferation observed in gelatin/PCL blended fibers compared to PCL fibers alone.[98,222] Blended fiber meshes are typically uncrosslinked and it therefore assumed the gelatin component rapidly dissolves from the fibers. *In situ* crosslinking of gelatin in the co-electrospun mesh is advantageous because crosslinking is expected to reduce the degradation rate, therefore the meshes would maintain bioactivity over a longer time period.

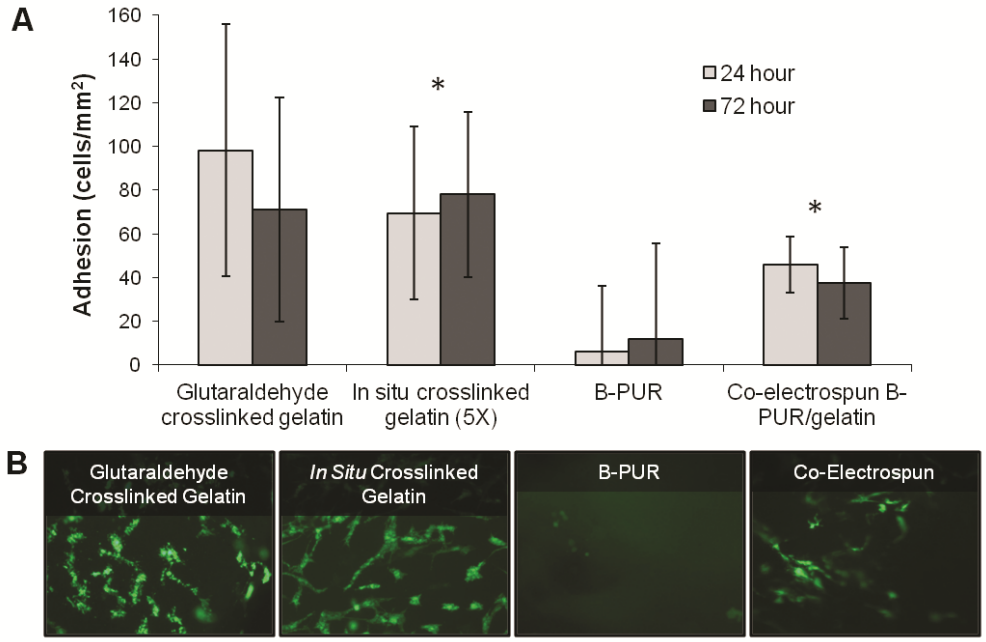

Figure 4.9. A) Adhesion of hMSCs to glutaraldehyde crosslinked gelatin, *in situ* crosslinked gelatin (5X), biodegradable polyurethane (B-PUR), and co-electrospun B-PUR/gelatin. B) Representative fluorescent images of hMSCs cultured on B-PUR and co-electrospun meshes (72 h). *$p<0.01$ compared to B-PUR.

4.4. Conclusions

This work describes a method for *in situ* crosslinking of gelatin to produce electrospun fibers with improved fiber morphology retention in water. Relationships between crosslinker ratio and tensile mechanical properties at simulated physiological conditions were identified. Initial modulus, tensile strength, and ultimate elongation increased as crosslinker ratio increased. Mechanical properties were further improved by co-electrospinning *in situ* crosslinked gelatin with a biodegradable polyurethane urea (B-PUR). Adhesion of hMSCs was improved on the co-electrospun mesh compared to the B-PUR demonstrating that the gelatin bioactivity is conferred to the composite scaffold. Co-electrospun scaffolds of gelatin and biodegradable polyurethane retain the desirable bioactivity and mechanical properties of each component which provides the potential for use as an improved scaffold for diverse tissue engineering applications.

CHAPTER V

CONCLUSIONS

5.1. Summary

In this work, a variety of electrospun fiber scaffolds were developed having tunable properties for various tissue engineering applications. The electrospinning process is simple, inexpensive, and highly tunable via solution, processing, and environmental parameters, making these meshes advantageous as tissue engineering scaffolds as fiber morphology can be altered to affect mechanical properties, degradation rate, and cell behavior. Although the effects of solution and processing parameters have been extensively studied for a number of systems, the effects of environmental parameters remain relatively unknown. Fundamental knowledge of electrospun fiber formation was first expanded in these studies with the investigation of the effects of solution viscosity and humidity on fiber morphology. This knowledge facilitates rational design of future electrospun scaffolds with controllable and predictable properties.

Control of electrospun fiber morphology was utilized to fabricate a small diameter (<4 mm) vascular graft for coronary artery bypass surgeries with biomechanical properties similar to native vessels. Compliance matching is necessary for reducing intimal hyperplasia which causes narrowed artery diameter and ultimately resulting in revision surgery. By utilizing segmented polyurethanes, compliance and burst pressure were first modulated through material chemistry. The exceptional tunability of segmented polyurethanes provides an additional method to fine-tune graft properties. We investigated structure-property relationships of SPUs in order to

rationally select polymers with desirable mechanical properties for vascular grafts. Further tuning of biomechanical properties was achieved by altering the fiber tortuosity, fiber junctions, and mesh thickness. Finally, heat treatment and conditioning of the grafts was utilized to achieve a graft with improved compliance greater than the saphenous vein control while maintaining burst pressure.

The principles learned about fiber morphology were utilized to fabricate a bioactive and biodegradable scaffold for tissue engineering. A method for *in situ* crosslinking of electrospun gelatin was developed to improve fiber morphology retention in water such that scaffold properties, determined by fiber microarchitecture, can be readily controlled. Electrospinning of natural polymers such as gelatin also improves bioactivity of the scaffold as these natural polymers have cell binding sites for controlled cell adhesion and spreading. *In situ* crosslinked gelatin was co-electrospun with a biodegradable synthetic polyurethane (B-PUR) that provides strong and highly tunable mechanical properties for various tissue engineering applications such as ligament or skin. Co-electrospun scaffolds had improved cell adhesion over B-PUR alone and improved mechanical properties compared to gelatin alone.

In summary, this body of work provides new approaches for developing electrospun tissue engineering scaffolds with tailored bioactivity and mechanical properties. We have also elucidated a fundamental understanding of electrospun fiber formation which will facilitate future development of electrospun meshes with fine-tuned architecture and mechanical properties for various applications.

5.2. Significance of Work

In Chapter 2, we elucidated poorly understood mechanisms of electrospun fiber formation. Controlling electrospun fiber morphology is necessary to control and predict the resultant mesh properties. The effects of processing and solution parameters on electrospun fiber morphology have been widely studied and are generally understood; however, the effects environmental parameters such as temperature and humidity on fiber morphology are poorly understood and/or contradictory effects have been observed. Additionally, given that small variations in molecular weight and distribution are typical in different batches of polymers and can strongly influence viscosity, it is often impossible to reproduce fiber architecture by using the solution concentration reported in electrospinning literature. Fiber tortuosity and fiber fusion have been observed in the literature but systematic studies investigating modulation of these properties and their effects on mechanical properties are lacking. This work provides a fundamental understanding of fiber formation that can be utilized for rational design and improved reproducibility of electrospun scaffolds.

In Chapter 3, vascular grafter with improved mechanical properties were developed and fabricated. The current gold standards in coronary artery bypass graft procedure, autologous saphenous veins and mammary arteries, are not available for up to 20% of patients due to disease, trauma, or anatomic abnormalities. In cases where autografts are unavailable, synthetic grafts made of polyethylene terephthalate (PET) and expanded polytetrafluoroethylene (ePTFE) are used. These synthetic grafts are viable options for large diameter applications (>4 mm); however, these grafts occlude over time

via intimal hyperplasia due to mechanical property mismatch between the graft and artery. Despite having high burst pressures, synthetic grafts have low compliance values which have been correlated to the development of intimal hyperplasia. Segmented polyurethanes have stress responses characterized by an area of high elastic recovery followed by strain hardening which is similar to that of arteries. This response can be further tuned by altering material chemistry. Combining the tunability of segmented polyurethanes with electrospun mesh microarchitecture provides fine control over vascular graft biomechanical properties that allowed high burst pressure and compliance simultaneously. This synthetic vascular graft has the potential for improved long-term clinical success by reducing intimal hyperplasia.

In Chapter 4, we developed a methodology for *in situ* crosslinking of gelatin fibers. Current commonly used strategies for crosslinking gelatin scaffolds have cytotoxicity concerns and/or have ineffective retention of fiber morphology after exposure to water. Isocyanate crosslinkers have been shown to have lower toxicity levels than glutaraldehyde. The rapid reaction of isocyanates with the amine residues on gelatin allows for crosslinking of fibers during electrospinning rather than in a post-processing technique. This procedure eliminates the swelling or partial dissolution of fibers due to immersion crosslinking and therefore results in improved fiber morphology retention. This strategy for crosslinking electrospun scaffolds provides greater control of fiber morphology. Co-electrospinning was utilized to improve the mechanical properties of electrospun gelatin and provides a method for fabricating scaffolds with independently tunable mechanical properties and bioactivity.

Overall, we have developed tunable scaffolds for tissue engineering applications. A tissue engineering scaffold must possess the requisite mechanical properties to temporarily restore function to damaged tissue. A tunable system allows for utility for regeneration of soft or hard tissues which require different mechanical properties. Elucidating the relationships between fiber morphology and mechanical properties provides a method to design scaffolds with the appropriate mechanical properties for the tissue of interest. In addition to these relationships highlighted in the vascular graft case study, further modulation of scaffold bioactivity is advantageous for the enhanced control of cell behavior. The control of both mechanical properties and bioactivity allows for fabrication of scaffolds with greater healing potential. This work provides a methodology for fabricating and rationally designing electrospun scaffolds for various tissue engineering applications.

5.3. Challenges and Future Directions

Although this work illustrates the potential of electrospun scaffolds for improved tissue regeneration, extensive investigation remains prior to clinical usage. The vascular grafts improve upon current synthetic options by exceeding the compliance of the saphenous vein autograft; however, further improvements can be implemented with the goal of achieving values comparable to arterial grafts. The internal mammary artery, also a current clinical standard, has a compliance of 11.5 ± 3.9 %/mmHg x 10^{-4}.[230] The structure-property relationships elucidated in this work provide the tools necessary to design a second generation of grafts with arterial compliance values. Polyurethane

choice can be altered such that a material without a crystalline transition near body temperature is utilized. This would facilitate prediction of *in vivo* properties without the use of a warm room. A longer conditioning study is necessary to ensure that no further changes in material properties occur after 24 hours, as these grafts are intended for long-term usage. As with most synthetic materials, these grafts are inherently thrombogenic and when implanted alone would require medical intervention. To overcome this limitation, the ultimate graft design incorporates an inner layer composed of a bioactive, thromboresistant hydrogel.[166] As these grafts are intended for long term implantation, the effects of sterilization and storage as well as biostability warrant evaluation. Although the weaker hydrogel layer is not expected to influence the overall biomechanical properties of the graft, evaluation of the burst pressure and compliance of composite grafts may be performed. Future *in vivo* studies in a porcine animal model will be performed to assess the ability to resist intimal hyperplasia and resultant long term patency of these vascular grafts.

In situ crosslinking of gelatin fibers is a promising strategy for improving fiber morphology retention in electrospun scaffolds while conferring bioactivity. More extensive studies are needed to evaluate cytocompatibility of these scaffolds, specifically for the presence of toxic hexamethylene diisocyanate leachables. As crosslinker ratio is expected to affect degradation rate, a study to evaluate the range of degradation times achievable in this system is necessary. Crosslinker ratios are calculated based on theoretical amount of primary amines available, but evaluating the actual amount may improve crosslinking. Additionally, quantifying the percent of available amines after

crosslinking will provide information on the efficiency of this crosslinking method. Hexamethylene diisocyanate (HDI) was chosen as a model crosslinker and establishes proof-of-concept for this crosslinking strategy; however, an array of diisocyanate crosslinkers may be used to improve crosslinking or confer additional advantages to the scaffold. An excess of HDI was used to achieve good fiber morphology retention and it was hypothesized that coupling of the HDI molecules enabled longer-range crosslinks. Using an excess of crosslinker raises toxicity concerns, so a higher molecular weight crosslinker could reduce the excess while still providing good crosslinking.

Co-electrospinning of gelatin with a synthetic biodegradable polyurethane (B-PUR) provides a means to tune the mechanical properties of the scaffold while retaining mesh bioactivity. In the co-electrospun scaffolds presented here, only a minimal increase in mechanical properties was observed due to the addition of B-PUR. From previous work with a non-biodegradable polyurethane, we expect mechanical properties intermediate of the gelatin and B-PUR in the co-electrospun scaffold. Investigation into why low properties are observed is necessary. We hypothesize that poor collection of the B-PUR during electrospinning may cause the B-PUR to comprise a lower portion of the composite scaffold, thus limiting its effect on mechanical properties. A study quantifying the relative ratio of gelatin to B-PUR is necessary to test this hypothesis. Interaction between the two electrospinning jets may be causing the B-PUR jet to deflect and reduce collection. Additional shields may be implemented to minimize this interaction. Finally, Low viability is observed on B-PUR scaffolds which is attributed to low adhesion;

however, further studies to evaluate indirect cytocompatibility due to potential leachables from the polymer need to be conducted.

While many studies are necessary before these grafts/scaffolds have reached the stage in which they can be used clinically, the work described here lays the foundation for future development of scaffolds with more advanced properties by elucidating key and structure-property relationships. The vascular graft already demonstrates an improved potential to serve as an off-the-shelf solution for coronary artery bypass grafting procedures. Forthcoming investigations into improved synthetic and bioactive scaffolds will expand on the structure-property relationships of polyurethane and electrospun fiber morphology detailed in this work to achieve a library of tunable parameters for design of tissue engineering scaffolds with precise mechanical properties and bioactivity.

REFERENCES

1 Widmer, M. & Mikos, A. Fabrication of biodegradable polymer scaffolds for tissue engineering in *Frontiers in Tissue Engineering* (eds CW Patrick, AG Mikos, & VL McIntire) (Elsevier, New York, NY, 1998).

2 Thomson, R., Shung, A., Yaszemski, M. & Mikos, A. Polymer scaffold processing in *Principles of Tissue Engineering* (eds R Lanza, R Langer, & JP Vacanti) (Academic Press, Burlington, MA, 2000).

3 Gunatillake, P. & Adhikari, R. Biodegradable synthetic polymers for tissue engineering. *European Cells and Materials* **5**, 1-16, (2003).

4 Gunatillake, P., Mayadunne, R. & Adhikari, R. Recent developments in biodegradable synthetic polymers. *Biotechnology Annual Review* **12**, 301-347, (2006).

5 Gogolewski, S. & Pennings, A. J. Biodegradable materials of polylactides, 4. Porous biomedical materials based on mixtures of polylactides and polyurethanes. *Die Makromolekulare Chemie, Rapid Communications* **3**, 839-845, (1982).

6 Gogolewski, S. & Galletti, G. Degradable, microporous vascular prosthesis from segmented polyurethane. *Colloid & Polymer Sci* **264**, 854-858, (1986).

7 Gogolewski, S. & Pennings, A. J. An artificial skin based on biodegradable mixtures of polylactides and polyurethanes for full-thickness skin wound covering. *Die Makromolekulare Chemie, Rapid Communications* **4**, 675-680, (1983).

8 Stokes, K. & McVenes, R. Polyurethane elastomer biostability. *Journal of Biomaterials Applications* **9**, 321-354, (1995).

9 Lamba, N. M. K., Woodhouse, K. A. & Cooper, S. L. *Polyurethanes in Biomedical Applications*. (CRC Press LLC, Boca Raton, FL, 1998).

10 Szycher, M. & Reed, A. Biostable polyurethane elastomers. *Medical Device Technology* **3**, 42–51, (1992).

11 Lelah, M. D. & Cooper, S. L. *Polyurethanes in Medicine*. (CRC Press, Inc., Boca Raton, FL, 1986).

12 Oertel, G. *Polyurethane Handbook.* (Hanser Gardner Publications, Inc., Berlin, 1994).

13 Szycher, M. *Szycher's Handbook of Polyurethanes*. (CRC Press, Inc., Boca Raton, 1999).

14 AbiSaleh, T., Anderson, M., Barker, M., Biesmans, G., Bosman, J. *et al. The Polyurethanes Book.* (John Wiley & Sons, Ltd., New York, NY, 2002).

15 Sell, S. A., Wolfe, P. S., Garg, K., McCool, J. M., Rodriguez, I. A. *et al.* The use of natural polymers in tissue engineering: a focus on electrospun extracellular matrix analogues. *Polymers* **2**, 522-553, (2010).

16 Malafaya, P. B., Silva, G. A. & Reis, R. L. Natural–origin polymers as carriers and scaffolds for biomolecules and cell delivery in tissue engineering applications. *Advanced Drug Delivery Reviews* **59**, 207-233, (2007).

17 Doshi, J. & Reneker, D. H. Electrospinning process and applications of electrospun fibers. *Journal of Electrostatics* **35**, 151-160, (1995).

18 Taylor, G. Disintegration of water drops in an electric field. *Proceedings of the Royal Society of London. Series A, Mathematical and Physical Sciences* **280**, 383-397, (1964).

19 Reneker, D., Yarin, A., Fong, H. & Koombhongse, S. Bending instability of electrically charged liquid jets of polymer solutions in electrospinning. *Journal of Applied Physics* **87**, 4531-4547, (2000).

20 Rutledge, G. & Fridrikh, S. Formation of fibers by electrospinning. *Advanced Drug Delivery Reviews* **59**, 1384-1391, (2007).

21 Han, T., Reneker, D. & Yarin, A. Buckling of jets in electrospinning. *Polymer* **48**, 6064-6076, (2007).

22 Yarin, A., Koombhongse, S. & Reneker, D. Bending instability in electrospinning of nanofibers. *Journal of Applied Physics* **89**, 3018-3026, (2001).

23 Carroll, C. & Joo, Y. Axisymmetric instabilities in electrospinning of highly conducting, viscoelastic polymer solutions. *Physics of Fluids* **21**, 103101-103110, (2009).

24 Hohman, M., Shin, M., Rutledge, G. & Brenner, M. Electrospinning and electrically forced jets. I. Stability theory. *Physics of Fluids* **13**, 2201-2220, (2001).

25 Carroll, C. P. & Yong Lak, J. Discretized modeling of electrically driven viscoelastic jets in the initial stage of electrospinning. *Journal of Applied Physics* **109**, 094315-094319, (2011).

26 Fang, J., Wang, H., Niu, H., Lin, T. & Wang, X. Evolution of fiber morphologies during poly(acrylonitrile) electrospinning. *Macromolecular Symposia* **287**, 155-161, (2010).

27 Richard-Lacroix, M. & Pellerin, C. Molecular orientation in electrospun fibers: from mats to single fibers. *Macromolecules* **46**, 9473-9493, (2013).

28 Wang, M., Yu, J. H., Kaplan, D. L. & Rutledge, G. C. Production of submicron diameter silk fibers under benign processing conditions by two-fluid electrospinning. *Macromolecules* **39**, 1102-1107, (2006).

29 Kim, K., Lee, K., Khil, M., Ho, Y. & Kim, H. The effect of molecular weight and the linear velocity of drum surface on the properties of electrospun poly(ethylene terephthalate) nonwovens. *Fibers and Polymers* **5**, 122-127, (2004).

30 Tan, E. P. S., Goh, C. N., Sow, C. H. & Lim, C. T. Tensile test of a single nanofiber using an atomic force microscope tip. *Applied Physics Letters* **86**, 073115-073118, (2005).

31 Wong, S.-C., Baji, A. & Leng, S. Effect of fiber diameter on tensile properties of electrospun poly(ε-caprolactone). *Polymer* **49**, 4713-4722, (2008).

32 Pedicini, A. & Farris, R. J. Mechanical behavior of electrospun polyurethane. *Polymer* **44**, 6857-6862, (2003).

33 Jarusuwannapoom, T., Hongrojjanawiwat, W., Jitjaicham, S., Wannatong, L., Nithitanakul, M. *et al.* Effect of solvents on electro-spinnability of polystyrene solutions and morphological appearance of resulting electrospun polystyrene fibers. *European Polymer Journal* **41**, 409-421, (2005).

34 Ki, C. S., Baek, D. H., Gang, K. D., Lee, K. H., Um, I. C. *et al.* Characterization of gelatin nanofiber prepared from gelatin–formic acid solution. *Polymer* **46**, 5094-5102, (2005).

35 Geng, X., Kwon, O. & Jang, J. Electrospinning of chitosan dissolved in concentrated acetic acid solution. *Biomaterials* **26**, 5427-5432, (2005).

36 Zong, X., Kim, K., Fang, D., Ran, S., Hsiao, B. *et al.* Structure and process relationship of electrospun bioabsorbable nanofiber membranes. *Polymer* **43**, 4403-4412, (2002).

37 Deitzel, J., Kleinmeyer, J., Harris, D. & Tan, N. The effect of processing variables on the morphology of electrospun nanofibers and textiles. *Polymer* **42**, 261-272, (2001).

38 Katti, D. S., Robinson, K. W., Ko, F. K. & Laurencin, C. T. Bioresorbable nanofiber-based systems for wound healing and drug delivery: Optimization of fabrication parameters. *Journal of Biomedical Materials Research Part B: Applied Biomaterials* **70B**, 286-296, (2004).

39 Lee, J. S., Choi, K. H., Ghim, H. D., Kim, S. S., Chun, D. H. *et al.* Role of molecular weight of atactic poly(vinyl alcohol) (PVA) in the structure and properties of PVA nanofabric prepared by electrospinning. *Journal of Applied Polymer Science* **93**, 1638-1646, (2004).

40 Buchko, C. J., Chen, L. C., Shen, Y. & Martin, D. C. Processing and microstructural characterization of porous biocompatible protein polymer thin films. *Polymer* **40**, 7397-7407, (1999).

41 Lee, K., Kim, H., La, Y., Lee, D. & Sung, N. Influence of a mixing solvent with tetrahydrofuran and N,N-dimethylformamide on electrospun poly(vinyl chloride) nonwoven mats. *Journal of Polymer Science Part B: Polymer Physics* **40**, 2259-2268, (2002).

42 Yuan, X., Zhang, Y., Dong, C. & Sheng, J. Morphology of ultrafine polysulfone fibers prepared by electrospinning. *Polymer International* **53**, 1704-1710, (2004).

43 Jeun, J., Lim, Y. & Nho, Y. Study on morphology of electrospun poly(caprolactone) nanofiber. *Journal of Industrial and Engineering Chemistry* **11**, 573-578, (2005).

44 Zhang, C., Yuan, X., Wu, L., Han, Y. & Sheng, J. Study on morphology of electrospun poly(vinyl alcohol) mats. *European Polymer Journal* **41**, 423-432, (2005).

45 Zuo, W., Zhu, M., Yang, W., Yu, H., Chen, Y. *et al.* Experimental study on relationship between jet instability and formation of beaded fibers during electrospinning. *Polymer Engineering & Science* **45**, 704-709, (2005).

46 Wannatong, L., Sirivat, A. & Supaphol, P. Effects of solvents on electrospun polymeric fibers: preliminary study on polystyrene. *Polymer International* **53**, 1851-1859, (2004).

47 Koski, A., Yim, K. & Shivkumar, S. Effect of molecular weight on fibrous PVA produced by electrospinning. *Materials Letters* **58**, 493-497, (2004).

48 Tao, J. & Shivkumar, S. Molecular weight dependent structural regimes during the electrospinning of PVA. *Materials Letters* **61**, 2325-2328, (2007).

49 Duan, B., Dong, C., Yuan, X. & Yao, K. Electrospinning of chitosan solutions in acetic acid with poly(ethylene oxide). *Journal of Biomaterials Science, Polymer Edition* **15**, 797-811, (2004).

50 Zhao, Z., Li, J., Yuan, X., Li, X., Zhang, Y. *et al.* Preparation and properties of electrospun poly(vinylidene fluoride) membranes. *Journal of Applied Polymer Science* **97**, 466-474, (2005).

51 Gupta, P., Elkins, C., Long, T. E. & Wilkes, G. L. Electrospinning of linear homopolymers of poly(methyl methacrylate): exploring relationships between fiber formation, viscosity, molecular weight and concentration in a good solvent. *Polymer* **46**, 4799-4810, (2005).

52 Mit-uppatham, C., Nithitanakul, M. & Supaphol, P. Ultrafine electrospun polyamide-6 fibers: effect of solution conditions on morphology and average fiber diameter. *Macromolecular Chemistry and Physics* **205**, 2327-2338, (2004).

53 Jiang, H., Fang, D., Hsiao, B. S., Chu, B. & Chen, W. Optimization and characterization of dextran membranes prepared by electrospinning. *Biomacromolecules* **5**, 326-333, (2004).

54 Son, W., Youk, J., Lee, T. & Park, W. The effects of solution properties and polyelectrolyte on electrospinning of ultrafine poly(ethylene oxide) fibers. *Polymer* **45**, 2959-2966, (2004).

55 Fong, H., Chun, I. & Reneker, D. Beaded nanofibers formed during electrospinning. *Polymer* **40**, 4585-4592, (1999).

56 Kenawy, E. R., Layman, J. M., Watkins, J. R., Bowlin, G. L., J.A., M. *et al.* Electrospinning of poly(ethylene-co-vinyl alcohol) fibers. *Biomaterials* **24**, 907-913, (2003).

57 McKee, M., Wilkes, G., Colby, R. & Long, T. Correlations of solution rheology with electrospun fiber formation of linear and branched polyesters. *Macromolecules* **37**, 1760-1767, (2004).

58 Ryu, Y., Kim, H., Lee, K., Park, H. & Lee, D. Transport properties of electrospun nylon 6 nonwoven mats. *European Polymer Journal* **39**, 1883-1889, (2003).

59 Cha, D., Kim, H., Lee, K., Jung, Y., Cho, J. *et al.* Electrospun nonwovens of shape-memory polyurethane block copolymers. *Journal of Applied Polymer Science* **96**, 460-465, (2005).

60 Kim, H., Kim, K., Jin, H. & Chin, I. Morphological characterization of electrospun nano-fibrous membranes of biodegradable poly(L-lactide) and poly(lactide-co-glycolide). *Macromolecular Symposia* **224**, 145-154, (2005).

61 Tong, H. & Wang, M. Electrospinning of fibrous polymer scaffolds using positive voltage or negative voltage: a comparative study. *Biomedical Materials* **5**, 1-15, (2010).

62 Ding, B., Kim, H.-Y., Lee, S.-C., Shao, C.-L., Lee, D.-R. *et al.* Preparation and characterization of a nanoscale poly(vinyl alcohol) fiber aggregate produced by an electrospinning method. *Journal of Polymer Science Part B: Polymer Physics* **40**, 1261-1268, (2002).

63 Huang, L., Nagapudi, K., P.Apkarian, R. & Chaikof, E. L. Engineered collagen-PEO nanofibers and fabrics. *Journal of Biomaterials Science, Polymer Edition* **12**, 979-993, (2001).

64 Guarino, V., Cirillo, V., Taddei, P., Alvarez-Perez, M. A. & Ambrosio, L. Tuning size scale and crystallinity of PCL electrospun fibres via solvent permittivity to address hMSC response. *Macromolecular Bioscience* **11**, 1694-1705, (2011).

65 Casper, C. L., Stephens, J. S., Tassi, N. G., Chase, D. B. & Rabolt, J. F. Controlling surface morphology of electrospun polystyrene fibers: effect of humidity and molecular weight in the electrospinning process. *Macromolecules* **37**, 573-578, (2004).

66 De Vrieze, S., Van Camp, T., Nelvig, A., Hagström, B., Westbroek, P. *et al.* The effect of temperature and humidity on electrospinning. *Journal of Materials Science* **44**, 1357-1362, (2009).

67 Kim, G. T., Lee, J. S., Shin, J. H., Ahn, Y. C., Jeong, K. H. *et al.* Effect of humidity on the microstructures of electrospun polystyrene nanofibers. *Microscopy and Microanalysis* **10**, 554-555, (2004).

68 Hardick, O., Stevens, B. & Bracewell, D. Nanofibre fabrication in a temperature and humidity controlled environment for improved fibre consistency. *Journal of Materials Science* **46**, 3890-3898, (2011).

69 Park, J.-Y. & Lee, I.-H. Relative humidity effect on the preparation of porous electrospun polystyrene fibers. *Journal of Nanoscience and Nanotechnology* **10**, 3473-3477, (2010).

70 Zhao, B., Li, C., Lu, Y., Wang, X., Liu, Z. *et al.* Formation of ordered macroporous membranes from random copolymers by the breath figure method. *Polymer* **46**, 9508-9513, (2005).

71 Park, M. S. & Kim, J. K. Breath figure patterns prepared by spin coating in a dry environment. *Langmuir* **20**, 5347-5352, (2004).

72 Thompson, C., Chase, G., Yarin, A. & Reneker, D. Effects of parameters on nanofiber diameter determined from electrospinning model. *Polymer* **48**, 6913-6922, (2007).

73 Sun, Z., Zussman, E., Yarin, A. L., Wendorff, J. H. & Greiner, A. Compound core–shell polymer nanofibers by co-electrospinning. *Advanced Materials* **15**, 1929-1932, (2003).

74 Li, D., Babel, A., Jenekhe, S. A. & Xia, Y. Nanofibers of conjugated polymers prepared by electrospinning with a two-capillary spinneret. *Advanced Materials* **16**, 2062-2066, (2004).

75 Loscertales, I. G., Barrero, A., Márquez, M., Spretz, R., Velarde-Ortiz, R. *et al.* Electrically forced coaxial nanojets for one-step hollow nanofiber design. *Journal of the American Chemical Society* **126**, 5376-5377, (2004).

76 Jiang, H., Hu, Y., Li, Y., Zhao, P., Zhu, K. *et al.* A facile technique to prepare biodegradable coaxial electrospun nanofibers for controlled release of bioactive agents. *Journal of Controlled Release* **108**, 237-243, (2005).

77 Zhang, Y., Huang, Z., Xu, X., Lim, C. & Ramakrishna, S. Preparation of core-shell structured PCL-r-gelatin bi-component nanofibers by coaxial electrospinning. *Chemistry of Materials* **16**, 3406-3409, (2004).

78 Zhang, Y., Wang, X., Feng, Y., Li, J., Lim, C. *et al.* Coaxial electrospinning of (fluorescencein isothiocyanate-conjugated bovine serum albumin)-encapsulated poly(e-caprolactone) nanofibers for sustained release. *Biomacromolecules* **7**, 1049-1057, (2006).

79 Jiang, H., Hu, Y., Zhao, P., Li, Y. & Zhu, K. Modulation of protein release from biodegradable core–shell structured fibers prepared by coaxial electrospinning. *Journal of Biomedical Materials Research Part B: Applied Biomaterials* **79B**, 50-57, (2006).

80 He, C. L., Huang, Z. M., Han, X. J., Liu, L., Zhang, H. S. *et al.* Coaxial electrospun poly(L-lactic acid) ultrafine fibers for sustained drug delivery. *Journal of Macromolecular Science, Part B* **45**, 515-524, (2006).

81 Bazilevsky, A. V., Yarin, A. L. & Megaridis, C. M. Co-electrospinning of core−shell fibers using a single-nozzle technique. *Langmuir* **23**, 2311-2314, (2007).

82 Wang, M., Jing, N., Su, C., Kameoka, J., Chou, C.-K. *et al.* Electrospinning of silica nanochannels for single molecule detection. *Applied Physics Letters* **88**, 033106-033109, (2006).

83 Samavedi, S., Olsen Horton, C., Guelcher, S. A., Goldstein, A. S. & Whittington, A. R. Fabrication of a model continuously graded co-electrospun mesh for regeneration of the ligament–bone interface. *Acta Biomaterialia* **7**, 4131-4138, (2011).

84 Baker, B. M., Shah, R. P., Silverstein, A. M., Esterhai, J. L., Burdick, J. A. *et al.* Sacrificial nanofibrous composites provide instruction without impediment and enable functional tissue formation. *Proceedings of the National Academy of Sciences* **109**, 14176–14181, (2012).

85 Ding, B., Kimura, E., Sato, T., Fujita, S. & Shiratori, S. Fabrication of blend biodegradable nanofibrous nonwoven mats via multi-jet electrospinning. *Polymer* **45**, 1895-1902, (2004).

86 Theron, S. A., Yarin, A. L., Zussman, E. & Kroll, E. Multiple jets in electrospinning: experiment and modeling. *Polymer* **46**, 2889-2899, (2005).

87 Kidoaki, S., Kwon, I. & Matsuda, T. Mesoscopic spatial designs of nano- and microfiber meshes for tissue-engineered matrix and scaffold based on newly devised multilayeing and mixing electrospinning techniques. *Biomaterials* **26**, 37-46, (2005).

88 Li, D., Wang, Y. & Xia, Y. Electrospinning of polymeric and ceramic nanofibers as uniaxially aligned arrays. *Nano Letters* **3**, 1167-1171, (2003).

89 Dempsey, D. K., Schwartz, C. J., Ward, R. S., Iyer, A. V., Parakka, J. P. *et al.* Micropatterning of electrospun polyurethane fibers through control of surface topography. *Macromolecular Materials and Engineering* **295**, 990-994, (2010).

90 Lee, C., Shin, H., Cho, I., Kang, Y., Kim, I. *et al.* Nanofiber alignment and direction of mechanical strain affect the ECM production of human ACL fibroblast. *Biomaterials* **26**, 1261-1270, (2005).

91 Kumbar, S. G., Nukavarapu, S. P., James, R., Nair, L. S. & Laurencin, C. T. Electrospun poly(lactic acid-co-glycolic acid) scaffolds for skin tissue engineering. *Biomaterials* **29**, 4100-4107, (2008).

92 Amoroso, N. J., D'Amore, A., Hong, Y., Rivera, C. P., Sacks, M. S. *et al.* Microstructural manipulation of electrospun scaffolds for specific bending stiffness for heart valve tissue engineering. *Acta Biomaterialia* **8**, 4268-4277, (2012).

93 Engelmayr, J. G. C. & Sacks, M. S. A structural model for the flexural mechanics of nonwoven tissue engineering scaffolds. *Journal of Biomechanical Engineering* **128**, 610-622, (2006).

94 Amoroso, N. J., D'Amore, A., Hong, Y., Wagner, W. R. & Sacks, M. S. Elastomeric electrospun polyurethane scaffolds: the interrelationship between fabrication conditions, fiber topology, and mechanical properties. *Advanced Materials* **23**, 106-111, (2011).

95 Stella, J., Liao, J., Hong, Y., Merryman, W., Wagner, W. *et al.* Tissue-to-cellular level deformation coupling in cell micro-integrated elastomeric scaffolds. *Biomaterials* **29**, 3228-3236, (2008).

96 Subramanian, A., Krishnan, U. & Sethuraman, S. Fabrication, characterization and in vitro evaluation of aligned PLGA–PCL nanofibers for neural regeneration. *Annals of Biomedical Engineering* **40**, 2098-2110, (2012).

97 Chew, S., Mi, R., Hoke, A. & Leong, K. The effect of the alignment of electrospun fibrous scaffolds on Schwann cell maturation. *Biomaterials* **29**, 653-661, (2008).

98 Ghasemi-Mobarakeh, L., Prabhakaran, M., Morshed, M., Nasr-Esfahani, M. & Ramakrishna, S. Electrospun poly(e-caprolactone)/gelatin nanofibrous scaffolds for nerve tissue enginering. *Biomaterials* **29**, 4532-4539, (2008).

99 Badami, A. S., Kreke, M. R., Thompson, M. S., Riffle, J. S. & Goldstein, A. S. Effect of fiber diameter on spreading, proliferation, and differentiation of osteoblastic cells on electrospun poly(lactic acid) substrates. *Biomaterials* **27**, 596-606, (2006).

100 Bolgen, N., Menceloglu, Y., Acatay, K., Vargel, I. & Piskin, E. *In vitro* and *in vivo* degradation of non-woven materials made of poly(ε-caprolactone) nanofibers prepared by electrospinning under different conditions. *Journal of Biomaterials Science Polymer Edition* **16**, 1537-1555, (2005).

101 Zong, X., Ran, S., Fang, D., Hsiao, B. & Chu, B. Control of structure, morphology and property in electrospun poly(glycolide-co-lactide) non-woven membranes via post-draw treatments. *Polymer* **44**, 4959-4967, (2003).

102 Cui, W., Li, X., Zhu, X., Yu, G., Zhou, S. *et al.* Investigation of drug release and matrix degradation of electrospun poly(dl-lactide) fibers with paracetanol inoculation. *Biomacromolecules* **7**, 1623-1629, (2006).

103 McKee, M., Park, T., Unal, S., Yilgor, I. & Long, T. Electrospinning of linear and highly branched segmented poly(urethane urea)s. *Polymer* **46**, 2011-2015, (2005).

104 Hong, Y., Ye, S., Nienponice, A., Soletti, L., Vorp, D. *et al.* A small diameter, fibrous vascular conduit generated from a poly(ester urethane)urea and a phospholipid pollymer blend. *Biomaterials* **30**, 2457-2467, (2009).

105 Lee, S. J., Yoo, J. J., Lim, G. J., Atala, A. & Stitzel, J. In vitro evaluation of electrospun nanofiber scaffolds for vascular graft application. *Journal of Biomedical Materials Research, Part A* **83A**, 999-1008, (2007).

106 Stankus, J., Soletti, L., Fujimoto, K., Hong, Y., Vorp, D. *et al.* Fabrication of cell microintegrated blood vessel constructs through electrohydrodynamic atomization. *Biomaterials* **28**, 2738-2746, (2007).

107 Bini, T., Gao, S., Tan, T., Wang, S., Lim, A. *et al.* Electrospun poly(L-lactide-*co*-glycolide) biodegradable polymer nanofibre tubes for peripheral nerve regeneration. *Nanotechnology* **15**, 1459-1464, (2004).

108 Prabhakaran, M., Venugopal, J., Chan, C. & Ramakrishna, S. Surface modified electrospun nanofibrous scaffolds for nerve tissue engineering. *Nanotechnology* **19**, 1-8, (2008).

109 Timnak, A., Yousefi Gharebaghi, F., Pajoum Shariati, R., Bahrami, S., Javadian, S. *et al.* Fabrication of nano-strctured electrospun scaffold intended for nerve tissue engineering. *Journal of Materials Science: Materials in Medicine* **22**, 1555-1567, (2011).

110 Zhu, X., Cui, W., Li, X. & Jin, Y. Electrospun fibrous mats with high porosity as potential scaffolds for skin tissue engineering. *Biomacromolecules* **9**, 1795-1801, (2008).

111 Zhou, Y., Yang, D., Chen, X., Xu, Q., Lu, F. *et al.* Electrospun water-soluble carboxyethyl chitosan/poly(vinyl alcohol) nanofibrous membrane as potential wound dressing for skin regeneration. *Biomacromolecules* **9**, 349-354, (2008).

112 Powell, H., Supp, D. & Boyce, S. Influence of electrospun collagen on wound contraction of engineered skin substitutes. *Biomaterials* **29**, 834-843, (2008).

113 Cui, W., Zhu, X., Yang, Y., Li, X. & Jin, Y. Evaluation of electrospun fibrous scaffolds of poly(DL-lactide) and poly(ethylene glycol) for skin tissue engineering. *Materials Science and Engineering C* **29**, 1869-1876, (2009).

114 Zhang, Y., Venugopal, J., El-Turki, A., Ramakrishna, S., Su, B. *et al.* Electrospun biomimetic nanocomposite nanofibers of hydroxyapatite/chitosan for bone tissue engineering. *Biomaterials* **29**, 4314-4322, (2008).

115 Venugopal, J., Vadgama, P., Kumar, T. & Ramakrishna, S. Biocomposite nanofibres and osteoblasts for bone tissue engineering. *Nanotechnology* **18**, 1-8, (2007).

116 Thomas, V., Zhang, X., Catledge, S. & Vohra, Y. Functionally graded electrospun scaffolds with tunable mechanical properties for vascular tissue regeneration. *Biomedical Materials* **2**, 224-232, (2007).

117 Ngiam, M., Liao, S., Patil, A., Cheng, Z., Yang, F. *et al.* Fabrication of mineralized polymeric nanofibrous composites for bone graft materials. *Tissue Engineering: Part A* **15**, 535-546, (2009).

118 Li, C., Vepari, C., Jin, H.-J., Kim, H. J. & Kaplan, D. L. Electrospun silk-BMP-2 scaffolds for bone tissue engineering. *Biomaterials* **27**, 3115-3124, (2006).

119 Takahashi, Y. & Tabata, Y. Effect of the fiber diameter and porosity of non-woven PET fabrics on the osteogenic differentiation of mesenchymal stem cells. *Journal of Biomaterials Science, Polymer Edition* **15**, 41-57, (2004).

120 Sisson, K., Zhang, C., Farach-Carson, M. C., Chase, D. B. & Rabolt, J. F. Fiber diameters control osteoblastic cell migration and differentiation in electrospun gelatin. *Journal of Biomedical Materials Research, Part A* **94A**, 1312-1320, (2010).

121 Reneker, D. & Chun, I. Nanometre diameter fibres of polymer, produced by electrospinning. *Nanotechnology* **7**, 216-223, (1996).

122 Shin, Y. M., Hohman, M. M., Brenner, M. P. & Rutledge, G. C. Electrospinning: a whipping fluid jet generates submicron polymer fibers. *Applied Physics Letters* **78**, 1149-1151, (2001).

123 Stylianopoulos, T., Bashur, C., Goldstein, A., Guelcher, S. A. & Barocas, V. Computational predictions of the tensile properties of electrospun fibre meshes:

Effect of fibre diameter and fibre orientation. *Journal of the Mechanical Behavior of Biomedical Materials* **1**, 326-335, (2008).

124 Tan, E. P. S., Ng, S. Y. & Lim, C. T. Tensile testing of a single ultrafine polymeric fiber. *Biomaterials* **26**, 1453-1456, (2005).

125 Kim, K., Yu, M., Zong, X., Chiu, J., Fang, D. *et al.* Control of degradation rate and hydrophilicity in electrospun non-woven poly(d,l-lactide) nanofiber scaffolds for biomedical applications. *Biomaterials* **24**, 4977-4985, (2003).

126 Baiguera, S., del Gaudio, C., Fioravanzo, L., Bianco, A., Grigioni, M. *et al.* In vitro astrocyte and cerebral endothelial cell response to electrospun poly(e-caprolactone) mats of different architecture. *Journal of Materials Science: Materials in Medicine* **21**, 1353-1362, (2010).

127 Gupta, D., Venugopal, J., Prabhakaran, M., Dev, V., Low, S. *et al.* Aligned and random nanofibrous substrate for the in vitro culture of Schwann cells for neural tissue engineering. *Acta Biomaterialia* **5**, 2560-2569, (2009).

128 Keun Kwon, I., Kidoaki, S. & Matsuda, T. Electrospun nano- to microfiber fabrics made of biodegradable copolyesters: structural characteristics, mechanical properties and cell adhesion potential. *Biomaterials* **26**, 3929-3939, (2005).

129 Yang, F., Murugan, R., Wang, S. & Ramakrishna, S. Electrospinning of nano/micro scale poly(L-lactic acid) aligned fibers and their potential in neural tissue engineering. *Biomaterials* **26**, 2603-2610, (2005).

130 Soletti, L., Hong, Y., Guan, J., Stankus, J. J., El-Kurdi, M. S. *et al.* A bilayered elastomeric scaffold for tissue engineering of small diameter vascular grafts. *Acta Biomaterialia* **6**, 110-122, (2010).

131 Xu, C., Inai, R., Kotaki, M. & Ramakrishna, S. Electrospun nanofiber fabrication as synthetic extracellular matrix and its potential for vascular tissue engineering. *Tissue Engineering* **10**, 1160-1168, (2004).

132 Prabhakaran, M., Venugopal, J., Chyan, T., Hai, L., Chan, C. *et al.* Electrospun biocomposite nanofibrous scaffolds for neural tissue engineering. *Tissue Engineering, Part A* **14**, 1787-1797, (2008).

133 Khil, M., Cha, D., Kim, H., Kim, I. & Bhattarai, N. Electrospun nanofibrous polyurethane membrane as wound dressing. *Journal of Biomedical Materials Research, Part B* **67B**, 675-679, (2003).

134 Yoshimoto, H., Shin, Y., Terai, H. & Vacanti, J. A biodegradable nanofiber scaffold by electrospinning and its potential for bone tissue engineering. *Biomaterials* **24**, 2077-2082, (2003).

135 Li, D. & Xia, Y. Electrospinning of nanofibers: reinventing the wheel? *Advanced Materials* **16**, 1151-1170, (2004).

136 Demir, M., Yilgor, I., Yilgor, E. & Erman, B. Electrospinning of polyurethane fibers. *Polymer* **43**, 3303-3309, (2002).

137 Megelski, S., Stephens, J. S., Chase, D. B. & Rabolt, J. F. Micro- and nanostructured surface morphology on electrospun polymer fibers. *Macromolecules* **35**, 8456-8466, (2002).

138 Medeiros, E. S., Mattoso, L. H. C., Offeman, R. D., Wood, D. F. & Orts, W. J. Effect of relative humidity on the morphology of electrospun polymer fibers. *Canadian Journal of Chemistry* **86**, 590-599, (2008).

139 Huang, L., Bui, N.-N., Manickam, S. S. & McCutcheon, J. R. Controlling electrospun nanofiber morphology and mechanical properties using humidity. *Journal of Polymer Science, Part B: Polymer Physics* **49**, 1734-1744, (2011).

140 Kim, G. T., Lee, J. S., Shin, J. H., Ahn, Y. C., Hwang, Y. J. *et al.* Investigation of pore formation for polystyrene electrospun fiber: effect of relative humidity. *Korean J. Chem. Eng.* **22**, 783-788, (2005).

141 Peresin, M. S., Habibi, Y., Vesterinen, A.-H., Rojas, O. J., Pawlak, J. J. *et al.* Effect of moisture on electrospun nanofiber composites of poly(vinyl alcohol) and cellulose nanocrystals. *Biomacromolecules* **11**, 2471-2477, (2010).

142 Kalayci, V., Patra, P., Kim, Y., Ugbolue, S. & Warner, S. Charge consequences in electrospun polyacrylonitrile (PAN) nanofibers. *Polymer* **46**, 7191-7200, (2005).

143 Lin, J., Ding, B., Yu, J. & Hsieh, Y. Direct fabrication of highly nanoporous polystyrene fibers via electrospinning. *ACS Applied Materials and Interfaces* **2**, 521-528, (2010).

144 Pai, C.-L., Boyce, M. C. & Rutledge, G. C. Morphology of porous and wrinkled fibers of polystyrene electrospun from dimethylformamide. *Macromolecules* **42**, 2102-2114, (2009).

145 Zheng, J., Zhang, H., Zhao, Z. & Han, C. C. Construction of hierarchical structures by electrospinning or electrospraying. *Polymer* **53**, 546-554, (2012).

146 Roger, V. L., Go, A. S., Lloyd-Jones, D. M., Adams, R. J., Berry, J. D. *et al.* Heart disease and stroke statistics--2011 update: a report from the American Heart Association. *Circulation* **123**, e18-e209, (2011).

147 Goldman, S., Sethi, G. K., Holman, W., Thai, H., McFalls, E. *et al.* Radial artery grafts vs saphenous vein grafts in coronary artery bypass surgery a randomized trial. *JAMA, Journal of the American Medical Association* **305**, 167-174, (2011).

148 Darling, R. C. & Linton, R. R. Durability of femoropopliteal reconstructions: Endarterectomy versus vein bypass grafts. *The American Journal of Surgery* **123**, 472-479, (1972).

149 McKee, J. A., Banik, S. S. R., Boyer, M. J., Hamad, N. M., Lawson, J. H. *et al.* Human arteries engineered in vitro. *European Molecular Biology Organization Reports* **4**, 633-638, (2003).

150 Williams, S. Tissue engineered vascular grafts: from bench to clinical use. *The FASEB Journal* **14**, 305, (2000).

151 Salacinski, H., Goldner, S., Giudiceandrea, A., Hamilton, G. & Seifalian, A. The mechanical behavior of vascular grafts: a review. *Journal of Biomaterials Applications* **15**, 241-278, (2001).

152 Green, R. M., Abbott, W. M., Matsumoto, T., Wheeler, J. R., Miller, N. *et al.* Prosthetic above-knee femoropopliteal bypass grafting: Five-year results of a randomized trial. *Journal of Vascular Surgery* **31**, 417-425, (2000).

153 Clowes, A., Gown, A., Hanson, S. & Reidy, M. Mechanisms of arterial graft failure 1. Role of cellular proliferation in early healing of PTFE prostheses. *American Journal of Pathology* **118**, 43-54, (1985).

154 Greenwald, S. E. & Berry, C. L. Improving vascular grafts: the importance of mechanical and haemodynamic properties. *Journal of Pathology* **190**, 292-299, (2000).

155 L'Heureux, N., Stoclet, J.-C., Auger, F. A., Lagaud, G. J.-L., Germain, L. *et al.* A human tissue-engineered vascular media: a new model for pharmacological studies of contractile responses. *The FASEB Journal* **15**, 515-524, (2001).

156 Silver, F. H., Snowhill, P. B. & Foran, D. J. Mechanical behavior of vessel wall: a comparative study of aorta, vena cava, and carotid artery. *Annals of Biomedical Engineering* **31**, 793-803, (2003).

157 Christenson, E. M., Anderson, J. M., Baer, E. & Hiltner, A. Relationship between nanoscale deformation process and elastic behavior of polyurethane elastomers. *Polymer* **46**, 11744-11754, (2005).

158 Eberhart, A., Zhang, Z., Guidoin, R., Laroche, G., Guay, L. *et al.* A new generation of polyurethane vascular prostheses: rara avis or ignis fatuus? *Journal of Biomedical Materials Research* **48**, 546-558, (1999).

159 Tiwari, A., Salacinski, H., Seifalian, A. M. & Hamilton, G. New prostheses for use in bypass grafts with special emphasis on polyurethanes. *Cardiovascular Surgery* **10**, 191-197, (2002).

160 Sarkar, S., Burriesci, G., Wojcik, A., Aresti, N., Hamilton, G. *et al.* Manufacture of small calibre quadruple lamina vascular bypass grafts using a novel automated extrusion-phase-inverison method and nanocomposite polymer. *Journal of Biomechanics* **42**, 722-730, (2009).

161 Madhavan, K. & Reddy, B. S. R. Synthesis and characterization of poly(dimethylsiloxane-urethane) elastomers: Effect of hard segments of polyurethane on morphological and mechanical properties. *Journal of Polymer Science, Part A: Polymer Chemistry* **44**, 2980-2989, (2006).

162 Miller, J., Lin, S., Hwang, K., Wu, K., Gibson, P. *et al.* Properties of polyether-polyurethane block copolymers: effects of hard segment length distribution. *Macromolecules* **18**, 32-44, (1985).

163 Pham, Q. P., Sharma, U. & Mikos, A. G. Electrospinning of polymeric nanofibers for tissue engineering applications: a review. *Tissue Engineering* **12**, 1197-1211, (2006).

164 Ramakrishna, S., Fujihara, K., Teo, W., Lim, T. & Ma, Z. *An Introduction to Electrospinning and Nanofibers*. (World Scientific Publishing Co. Pte. Ltd., Singapore, 2005).

165 Lee, K., Kim, H., Ryu, Y., Kim, K. & Choi, S. Mechanical behavior of electrospun fiber mats of poly(vinyl chloride)/polyurethane polyblends. *Journal of Polymer Science Part B: Polymer Physics* **41**, 1256-1262, (2003).

166 Browning, M. B., Dempsey, D., Guiza, V., Becerra, S., Rivera, J. *et al.* Multilayer vascular grafts based on collagen-mimetic proteins. *Acta Biomaterialia* **8**, 1010-1021, (2012).

167 Nezarati, R., Eifert, M. & Cosgriff-Hernandez, E. Effects of humidity and solution viscosity on electrospun fiber morphology. *Tissue Engineering, Part C* **19**, 810-819, (2013).

168 Teo, W., Kotaki, M., Mo, X. & Ramakrishna, S. Porous tubular structures with controlled fibre orientation using a modified electrospinning method. *Nanotechnology* **16**, 918-924, (2005).

169 Teo, W. & Ramakrishna, S. Electrospun fibre bundle made of aligned nanofibres over two fixed points. *Nanotechnology* **16**, 1878-1884, (2005).

170 Li, Y., Ren, Z., Zhao, M., Yang, H. & Chu, B. Multiphase structure of segmented polyurethanes: effects of hard-segment flexibility. *Macromolecules* **26**, 612-622, (1993).

171 Ng, H. N., Allegrezza, A. E., Seymour, R. W. & Cooper, S. L. Effect of segment size and polydispersity on the properties of polyurethane block polymers. *Polymer* **14**, 255-261, (1973).

172 Lee, D.-K. & Tsai, H.-B. Properties of segmented polyurethanes derived from different diisocyanates. *Journal of Applied Polymer Science* **75**, 167-174, (2000).

173 Rodriguez, M., Juran, C., McClendon, M., Eyadiel, C. & McFetridge, P. S. Development of a mechanically tuneable 3D scaffold for vascular reconstruction. *Journal of Biomedical Materials Research, Part A* **100A**, 3480-3489, (2012).

174 Doi, K., Nakayama, Y. & Matsuda, T. Novel compliant and tissue-permeable microporous polyurethane vascular prosthesis fabricated using an excimer laser ablation technique. *Journal of Biomedical Materials Research* **31**, 27-33, (1996).

175 Xu, C., Inai, R., Kotaki, M. & Ramakrishna, S. Aligned biodegradable nanofibrous structure: a potential scaffold for blood vessel engineering. *Biomaterials* **25**, 877-886, (2004).

176 Stella, J., Wagner, W. & Sacks, M. Scale-dependent fiber kinematics of elastomeric electrospun scaffolds for soft tissue engineering. *Journal of Biomedical Materials Research, Part A* **93A**, 1032-1042, (2009).

177 Leung, L. M. & Koberstein, J. T. DSC annealing study of microphase separation and multiple endothermic behavior in polyether-based polyurethane block copolymers. *Macromolecules* **19**, 706-713, (1986).

178 Eceiza, A., Larranaga, M., de la Caba, K., Kortaberria, G., Marieta, C. *et al.* Structure–Property Relationships of Thermoplastic Polyurethane Elastomers Based on Polycarbonate Diols. *Journal of Applied Polymer Science* **1087**, 3092-3103, (2007).

179 Lin, Y. G. & Winter, H. H. Formation of high melting crystal in a thermotropic aromatic copolyester. *Macromolecules* **21**, 2439-2443, (1988).

180 Bajsic, E. G., Rek, V., Sendijarevic, A., Sendijarevic, V. & Frisch, K. C. DSC Study of morphological changes in segmented polyurethane elastomers. *Journal of Elastomers and Plastics* **32**, 162-182, (2000).

181 Wang, L., Zhang, Q.-P., Wang, J.-H., Yang, B., Yang, M.-B. *et al.* Effects of annealing on the hierarchical crystalline structures and mechanical properties of injection-molded bars of high-density polyethylene. *Polymer International* **63**, 296-306, (2014).

182 Zhuo, H., Hu, J. & Chen, S. Electrospun polyurethane nanofibres having shape memory effect. *Materials Letters* **62**, 2074-2076, (2008).

183 Zhuo, H., Hu, J., Chen, S. & Yeung, L. Preparation of polyurethane nanofibers by electrospinning. *Journal of Applied Polymer Science* **109**, 406-411, (2008).

184 Wu, S.-C., Chang, W.-H., Dong, G.-C., Chen, K.-Y., Chen, Y.-S. *et al.* Cell adhesion and proliferation enhancement by gelatin nanofiber scaffolds. *Journal of Bioactive and Compatible Polymers* **26**, 565-577, (2011).

185 Guarino, V., Alvarez-Perez, M., Cirillo, V. & Ambrosio, L. hMSC interaction with PCL and PCL/gelatin platforms: A comparative study on films and electrospun membranes. *Journal of Bioactive and Compatible Polymers* **26**, 144-160, (2011).

186 Farina, A., Fievet, M. H., Plassart, F., Menet, M. C. & Thuillier, A. Residual glutaraldehyde levels in fiberoptic endoscopes: measurement and implications for patient toxicity. *Journal of Hospital Infection* **43**, 293-297, (1999).

187 van Luyn, M. J. A., van Wachem, P. B., Olde Damink, L., Dijkstra, P. J., Feijen, J. *et al.* Relations between in vitro cytotoxicity and crosslinked dermal sheep collagens. *Journal of Biomedical Materials Research* **26**, 1091-1110, (1992).

188 Huang-Lee, L. L. H., Cheung, D. T. & Nimni, M. E. Biochemical changes and cytotoxicity associated with the degradation of polymeric glutaraldehyde derived crosslinks. *Journal of Biomedical Materials Research* **24**, 1185-1201, (1990).

189 Simmons, D. M. & Kearney, J. N. Evaluation of collagen cross-linking techniques for the stabilization of tissue matrices. *Biotechnology and Applied Biochemistry* **17**, 23-29, (1993).

190 Jayakrishnan, A. & Jameela, S. R. Glutaraldehyde as a fixative in bioprostheses and drug delivery matrices. *Biomaterials* **17**, 471-484, (1996).

191 Schmidt, C. E. & Baier, J. M. Acellular vascular tissues: natural biomaterials for tissue repair and tissue engineering. *Biomaterials* **21**, 2215-2231, (2000).

192 Skotak, M., Noriega, S., Larsen, G. & Subramanian, A. Electrospun cross-linked gelatin fibers with controlled diameter: the effect of matrix stiffness of proliferative and biosynthetic activity of chondrocytes cultured *in vitro*. *Journal of Biomedical Materials Research Part A* **95A**, 828-836, (2010).

193 Barnes, C., Pemble, C., Brand, D., Simpson, D. & Bowlin, G. Cross-linking electrospun type II collagen tissue engineering scaffolds with carbodiimide in ethanol. *Tissue Engineering* **13**, 1593-1605, (2007).

194 Buttafoco, L., Kolkman, N., Engbers-Buijtenhuijs, P., Poot, A., Dijkstra, P. *et al.* Electrospinning of collagen and elastin for tissue engineering applications. *Biomaterials* **27**, 724-734, (2006).

195 Panzavolta, S., Gioffrè, M., Focarete, M. L., Gualandi, C., Foroni, L. *et al.* Electrospun gelatin nanofibers: Optimization of genipin cross-linking to preserve fiber morphology after exposure to water. *Acta Biomaterialia* **7**, 1702-1709, (2011).

196 Kim, M. S., Jun, I., Shin, Y. M., Jang, W., Kim, S. I. *et al.* The development of genipin-crosslinked poly(caprolactone) (PCL)/gelatin nanofibers for tissue engineering applications. *Macromolecular Bioscience* **10**, 91-100, (2010).

197 Sisson, K., Zhang, C., Farach-Carson, M., Chase, D. & Rabolt, J. Evaluation of cross-linking methods for electrospun gelatin on cell growth and viability. *Biomacromolecules* **10**, 1675-1680, (2009).

198 Su, Y. & Mo, X. Genipin crosslinked gelatin nanofibers for tissue engineering. *Journal of Controlled Release* **152, Supplement 1**, e230-e232, (2011).

199 Zhang, S., Huang, Y., Yang, X., Mei, F., Ma, Q. *et al.* Gelatin nanofibrous membrane fabricated by electrospinning of aqueous gelatin solution for guided tissue regeneration. *Journal of Biomedical Materials Research Part A* **90A**, 671-679, (2009).

200 Kim, S., Heo, D., Lee, J., Kim, J., Park, S. *et al.* Electrospun gelatin/polyurethane blended nanofibers for wound healing. *Biomedical Materials* **4**, 044106 (044111pp), (2010).

201 Biazar, E. & Keshel, S. H. Unrestricted somatic stem cells loaded in nanofibrous scaffolds as potential candidate for skin regeneration. *International Journal of Polymeric Materials and Polymeric Biomaterials* **63**, 741-752, (2014).

202 Chong, E., Phan, T., IJ, L., Zhang, Y., Bay, B. *et al.* Evaluation of electrospun PCL/gelatin nanofibrous scaffold for wound healing and layered dermal reconstitution. *Acta Biomaterialia* **3**, 321-330, (2007).

203 He, W., Yong, T., Teo, W., Ma, Z. & Ramakrishna, S. Fabrication and endothelialization of collagen-blended biodegradable polymer nanofibers: potential vascular graft for blood vessel tissue engineering. *Tissue Engineering* **11**, 1574-1588, (2005).

204 Venugopal, J. & Ramakrishna, S. Biocompatible nanofiber matrices for the engineering of a dermal substitute for skin regeneration. *Tissue Engineering* **11**, 847-854, (2005).

205 Heydarkhan-Hagvall, S., Schenke-Layland, L., Dhanasopon, A., Rofail, F., Smith, H. *et al.* Three-dimensional electrospun ECM-based hybrid scaffolds for cardiovascular tissue engineering. *Biomaterials* **29**, 2907-2914, (2008).

206 Zhang, Y., Ouyang, H., Lim, C., Ramakrishna, S. & Huang, Z. Electrospinning of gelatin fibers and gelatin/PCL composite fibrous scaffolds. *Journal of Biomedical Materials Research Part B: Applied Biomaterials* **72B**, 156-165, (2005).

207 Ravichandran, R., Venugopal, J., Sundarrajan, S., Mukherjee, S. & Ramakrishna, S. Poly(glycerol sebacate)/gelatin core/shell fibrous structure for regeneration of myocardial infarction. *Tissue Engineering, Part A* **17**, 1363-1373, (2011).

208 Yoo, H. S., Kim, T. G. & Park, T. G. Surface-functionalized electrospun nanofibers for tissue engineering and drug delivery. *Advanced Drug Delivery Reviews* **61**, 1033-1042, (2009).

209 Casper, C., Yang, W., Farach-Carson, M. & Rabolt, J. Coating electrospun collagen and gelatin fibers with perlecan domain I for increased growth factor binding. *Biomacromolecules* **8**, 1116-1123, (2007).

210 Ma, Z., He, W., Yong, T. & Ramakrishna, S. Grafting of gelatin on electrospun poly(caprolactone) nanofibers to improve endothelial cell spreading and proliferation and to control cell orientation. *Tissue Engineering* **11**, 1149-1158, (2005).

211 Li, M., Mondrinos, M., Chen, X., Gandhi, M., Ko, F. *et al.* Co-electrospun poly(lactide-*co*-glycolide), gelatin, and elastin blends for tissue engineering scaffolds. *Journal of Biomedical Materials Research* **79A**, 963-973, (2006).

212 Yilgor, E., Ekin Atilla, G., Ekin, A., Kurt, P. & Yilgor, I. Isopropyl alcohol: an unusual, powerful, ‘green’ solvent for the preparation of silicone–urea copolymers with high urea contents. *Polymer* **44**, 7787-7793, (2003).

213 Lin, W.-H. & Tsai, W.-B. In situ UV-crosslinking gelatin electrospun fibers for tissue engineering applications. *Biofabrication* **5**, 035008, (2013).

214 George, S. C. & Thomas, S. Transport phenomena through polymeric systems. *Progress in Polymer Science* **26**, 985-1017, (2001).

215 Reinhart, C. T. & Peppas, N. A. Solute diffusion in swollen membranes. Part II. Influence of crosslinking on diffusive properties. *Journal of Membrane Science* **18**, 227-239, (1984).

216 Zha, Z., Teng, W., Markle, V., Dai, Z. & Wu, X. Fabrication of gelatin nanofibrous scaffolds using ethanol/phosphate buffer saline as a benign solvent. *Biopolymers* **97**, 1026-1036, (2012).

217 Sarkar, D., Yang, J.-C. & Lopina, S. Structure-property relationship of L-tyrosine-based polyurethanes for biomaterial applications. *Journal of Applied Polymer Science* **108**, 2345-2355, (2008).

218 Skarja, G. & Woodhouse, K. Synthesis and characterization of degradable polyurethane elastomers containing an amino acid-based chain extender. *Journal of Biomaterials Science, Polymer Edition* **9**, 271-295, (1998).

219 Skarja, G. A. & Woodhouse, K. A. Structure-property relationships of degradable polyurethane elastomers containing an amino acid-based chain extender. *Journal of Applied Polymer Science* **75**, 1522-1534, (2000).

220 Han, J., Chen, B., Ye, L., Zhang, A.-Y., Zhang, J. *et al.* Synthesis and characterization of biodegradable polyurethane based on poly(ε-caprolactone) and L-lysine ethyl ester diisocyanate. *Frontiers of Materials Science in China* **3**, 25-32, (2009).

221 Spaans, C., de Groot, J., Dekens, F. & Pennings, A. High molecular weight polyurethanes and a polyurethane urea based on 1,4-butanediisocyanate. *Polymer Bulletin* **41**, 131-138, (1998).

222 Gautam, S., Dinda, A. K. & Mishra, N. C. Fabrication and characterization of PCL/gelatin composite nanofibrous scaffold for tissue engineering applications by electrospinning method. *Materials Science and Engineering: C* **33**, 1228-1235, (2013).

223 Powell, H. M. & Boyce, S. T. Engineered human skin fabricated using electrospun collagen-PCL blends: morphogenesis and mechanical properties. *Tissue Engineering, Part A* **15**, 2177-2187, (2009).

224 Zhang, Y. Z., Feng, Y., Huang, Z. M., Ramakrishna, S. & Lim, C. T. Fabrication of porous electrospun nanofibres. *Nanotechnology* **17**, 901, (2006).

225 Kwon, I. K. & Matsuda, T. Co-electrospun nanofiber fabrics of poly(l-lactide-co-ε-caprolactone) with type I collagen or heparin. *Biomacromolecules* **6**, 2096-2105, (2005).

226 Feng, B., Tu, H., Yuan, H., Peng, H. & Zhang, Y. Acetic-acid-mediated miscibility toward electrospinning homogeneous composite nanofibers of GT/PCL. *Biomacromolecules* **13**, 3917-3925, (2012).

227 Zheng, R., Duan, H., Xue, J., Liu, Y., Feng, B. *et al.* The influence of gelatin/PCL ratio and 3-D construct shape of electrospun membranes on cartilage regeneration. *Biomaterials* **35**, 152-164, (2014).

228 Guan, J., Sacks, M., Beckman, E. & Wagner, W. Biodegradable poly(ether ester urethane)urea elastomers based on poly(ether ester) triblock copolymers and putrescine: synthesis, characterization and cytocompatibility. *Biomaterials* **25**, 85-96, (2004).

229 Guan, J., Sacks, M., Beckman, E. & Wagner, W. Synthesis, characterization, and cytocompatibility of elastomeric, biodegradable poly(ester-urethane)ureas based on poly(caprolactone) and putrescine. *Journal of Biomedical Materials Research* **61**, 493-503, (2002).

230 Konig, G., McAllister, T. N., Dusserre, N., Garrido, S. A., Iyican, C. *et al.* Mechanical properties of completely autologous human tissue engineered blood vessels compared to human saphenous vein and mammary artery. *Biomaterials* **30**, 1542-1550, (2009).